Title
Flow and sediment transport disturbance caused by dams

Permalink
https://escholarship.org/uc/item/87p8w8kv

Author
Li, Tingyu

Publication Date
2021

Peer reviewed|Thesis/dissertation

Flow and sediment transport disturbance caused by dams

By

TINGYU LI
DISSERTATION

Submitted in partial satisfaction of the requirements for the degree of

DOCTOR OF PHILOSOPHY

in

Hydrologic Sciences

in the

OFFICE OF GRADUATE STUDIES

of the

UNIVERSITY OF CALIFORNIA

DAVIS

Approved:

_____

Gregory B. Pasternack, PhD, Chair

_____

Peng Gao, PhD

_____

Samuel Sandoval Solis, PhD

Committee in Charge

2021

i

有志者

事竟成

ABSTRACT

A large number of dams and hydropower plants have been built in mountain regions due to the rich water resources and high potential energy. As a consequence, flow regulation associated with dams has led to profound changes to the intertwined hydrologic, ecologic, and geomorphic functioning of rivers. Understanding the effect of dams on the interaction between hydrologic, ecologic, and geomorphic is critical for river management that aims to maximize a range of potential benefits. Therefore, my Ph.D. research proposed to investigate basic and applied scientific questions about two important disturbances caused by dams on mountain rivers-hydropeaking and reservoir sedimentation.

Hydropeaking is defined as rapid variations in power production by hydroelectric plants as a consequence of varying electricity generation and fluctuations in demand in the electricity market. In Chapter 1, public hourly flow data in the state of California was used to reveal the diversity of hydropeaking flow. To process a large amount of data and extract their hydrologic features, an open-source algorithm, Hydropeaking Events Detection Algorithm, was developed. Integrated clustering analysis was applied and identified four underlying hydropeaking patterns.

Chapters 2 and 3 moved beyond pure statistical analysis to mechanistic observation and modeling of hydro-morphologic interactions in dam-regulated mountain rivers. Both studies investigated hydraulic and sediment transport regimes upstream of two concrete-arch dams. Chapter 2 exploratively studied hydrologic controls associated with current flow operations in a small dam. A new supplementary reservoir sedimentation management strategy based on water transfer was proposed for small dams. Chapter 3 applies flow convergence routing theory backward to

redistribute sediment erosion upstream of the dam. Topographic steering and flow convergence routing was found to be able redistribute sediment erosion pattern and keep sediment away from the key structure.

ACKNOWLEDGMENTS

I would like to thank my dear boyfriend, Sheng Shen for a twelve-year-long accompany with endless support. Life was brightened after meeting you. You are the best friend to hang out with, the best peer to exchange ideas, and a harbor to heal all my depressions. I also want to thank all my family and friends, especially my parents for guiding me to be a good person and supporting me unconditionally.

TABLE OF CONTENTS

Page

LIST OF TABLES

CHAPTER 1.   REVEALING THE DIVERSITY OF HYDROPEAKING FLOW REGIMES

1.1   Abstract

Hydropeaking, a hydroelectricity generation strategy involving rapid changes to flow releases from dams in response to fluctuations in hourly-adjusted electricity markets has been widely applied due to its economic efficiency. However, these operational practices produce sub-daily flow fluctuations that pose substantial hazards to riverine ecosystems and human activities. To ascertain the downstream impacts of hydropeaking, features of hydropeaking have been analyzed with respect to ecologically relevant hydrologic variables. However, since studies aiming to characterize hydropeaking regime often require manual feature extraction, they are commonly limited to small temporal and spatial scales. Additionally, riverine ecologists have commonly treated hydropeaking as a broadly similar flow-alteration pattern regardless of the complexities of the electricity market and differences in the natural settings where it is applied. Therefore, this study sought to determine whether significantly different hydropeaking patterns exist on a regional scale, as revealed by temporal variations in hydropeaking over a long temporal scale (> five years). To fulfill this goal, a new algorithm, the Hydropeaking Event Detection Algorithm (HEDA), was developed in R to automate the characterization of hydropeaking flow regimes. Clustering analyses were conducted to explore the similarities and differences of hydropeaking regimes among 33 sites in numerous hydrologic regions of California. Four distinct classes of hydropeaking flow regimes were identified and distinguished by the duration and frequency of hydropeaking. Meanwhile, rate of change, amplitude and timing of hdyropeaking played less important roles in the classification.

1.2   Introduction

Hydropeaking operation is widely implemented due to the real-time electricity market mechanism and hydropower's ability to quickly respond to peak electricity demands (Moog 1993). Rapid flow fluctuation is one of the most significant disturbances of hydropeaking power plants and summarized as frequent, large and rapid flow fluctuations, occurring as one or several peaks per day with certain periodicity (Meile et al. 2010, Charmasson et al. 2011, N. LeRoy Poff 2016). Studies on hydropeaking started by comparing hydropeaking flow with natural flow to characterize the hydropeaking process, and to infer the critical condition when hydropeaking exceeds the ecological tolerance of river systems (Moog 1993, Poff et al. 1989, Young et al. 2011). These studies found that the magnitude, frequency, duration, timing and rate of change of hydropeaking significantly impact the age, growth, movement, migration, spawning and rearing of aquatic organisms (Resh et al. 1988, Harby et al. 2013, Anindito et al. 2019). For example, the relatively sudden flow decreases (rate of change-fall) can strand fish in isolated shallows and gravel-bar interstices as water level recedes (Hauer et al. 2017a, Hauer et al. 2017b, Melcher et al. 2017, Larrieu et al. 2020). Even though stranding may affect only a small portion of the fish population at a time, and may occur naturally, repeated flow fluctuations (frequency) can cause cumulative mortalities that can result in a significant fish loss (Young et al. 2011). Meanwhile, the ramping range (amplitude) of hydropeaking flow can partially explain the downstream displacement of both fish and macroinvertebrates (Thompson et al. 2010, Schülting et al. 2016). Riparian plants face both physiological and physical constraints because of the shifts between submergence and drainage, and erosion of substrates (Bejarano et al. 2018). Nevertheless, most studies set natural flow as the reference condition and treat hydropeaking broadly similarly, which ignores the

complexity of both power markets and natural settings (Haas et al. 2015, Lane et al. 2017). As a result, the general application in hydropeaking mitigation of these studies may be limited because each study can be site specific.

With an increasing understanding of the hydropeaking flow-ecology relationship, characterizing hydropeaking flow regimes systematically became an important topic. At the early stage, because of the availability of data and computation capability, only daily flow was used to evaluate hydropeaking-induced flow alteration which was found to mask features of hydropeaking flow. Further, sub-daily flow data are needed to properly assess hydropeaking-induced flow alteration and its ecological impacts (Baker et al. 2004, Meile et al. 2010, Zimmerman et al. 2010, Spurgeon et al. 2016). Sites with sub-daily data have elucidated some key differences among hydropeaking flow regimes. Beyond the general differences between natural flow and hydropeaking, the hydropeaking-induced flow variation was found to differ from site to site (Carolli et al. 2015, Greimel et al. 2016, Ashraf et al. 2018). In addition, flow alteration observed downstream of hydropeaking sites are strongly correlated with the magnitude and frequency of peaks (Bejarano et al. 2017). In the United States, McManamay (2015) found that peaking operations were the most prevalent type of hydropower operation based on extensive documentation mining, and identified three specific types of hydropeaking operations: peaking, intermediate peaking and run-of-river peaking. All these findings inspire this study, whose objective is to advance our fundamental understanding of hydropeaking regimes by conducting an explicit, data-driven analysis exploring the possible patterns and diversity among hydropeaking flow regimes.

Hydrologic classification is the process of systematically arranging streams into groups that are

3

most similar with respect to the characteristics or determinants of their flow regime (Olden et al. 2012). By identifying and categorizing dominant features (as revealed through a suite of hydrologic variables), hydrologic classification not only assists in describing the flow regimes at a regional scale but can also improve the predictive power and process basis of flow-ecology relationships. This ultimately leads to more effective environmental flow management with minimal data and resource requirements (Corduas 2011, Lane et al. 2018, Sergeant et al. 2020). Despite the marked value of hydrologic classification and rapidly growing computational power available to conduct it, limited hydrologic classification work on hydropeaking has been developed to characterize hydropeaking flow regimes at a regional scale (Palmer et al. 2005, Bergen et al. 2019, Reichstein et al. 2019). Part of the reason for this is that methods used to parse sub-daily hydropeaking flow are difficult to apply at a large spatial and temporal scale due to the frequent need to perform site pairing with gauging stations and feature extraction manually.

Approaches available for characterizing hydropeaking regimes have also constrained our understanding of hydropeaking-induced flow alteration. The Indicators of Hydrologic Alteration (IHA) and its derivatives have been used to characterize rapid flow fluctuations (Cushman 1985, Richter et al. 1996). However, when dealing with sub-daily flow records, IHA and its derivatives are incapable of capturing the temporal variation of the whole period because it requires manual feature extraction. To address this issue, wavelet transforms have been applied to extract the spectral pattern of hydropeaking flow by fully considering time-series variation at different temporal resolutions (Daubechies 1992, Zolezzi et al. 2009, Wu et al. 2015). Nevertheless, wavelet transforms can only be applied to one stream at a time and results are difficult to interpret in terms of ecological implications. To address limitations of these two approaches, a new method was

4

devised to integrate IHA into wavelet transform by replacing the original energy amplitude with the IHA index amplitude in the scale-averaged wavelet transform spectrum (Zolezzi et al. 2009). While this approach successfully fused the benefits of both these methods, their work is limited to the daily flow of an individual river. After that, an algorithm named COSH was developed to analyze the temporal variation of hydropeaking flow (Sauterleute et al. 2014). Unfortunately, even though COSH made an important advance in mining hydropeaking features automatically, it still requires iterative adjustments to thresholds to detect hydropeaking events for each river. These leaves open a gap for highly automated methods that can process a large number of records and the need for more basic science to handle extensive flow records with a high temporal resolution across a hydrologically diverse region.

In this study, our goal was to explore the diversity of hydropeaking flow regimes at a regional scale. To fulfill this goal, a new algorithm was developed to (1) distinguish hydropeaking flow from non-hydropeaking flow, and (2) automate hydropeaking regime characterization by treating flow records as Euclidean vectors and identifying peaking events by vector angle and magnitude. The application of a dynamic threshold consists of daily maximum and minimum flow prevented this algorithm from requiring iterative, manual adjustments for different time windows and river reaches. The algorithm was applied to 128 sites with sub-daily flow records in California and identified 33 sites with hydropeaking signals. Then, hydrologic classification was applied to the identified 33 sites to classify the broad range of hydropeaking process (governed by the electricity demand, power transmission lines, electricity price and natural site constraints) into several discrete categories. Two types of clustering analyses, hierarchical and fuzzy clustering, were used to provide a clear structural interpretation of data that sheds light on the underlying organized

patterns of hydropeaking flow while still considering the uncertainty of cluster membership.

1.1 **Material and methods**

1.1.1 **Study sites**

The study region comprises the state of California (425,000 km^2), a highly heterogeneous region with respect to physical and climatic characteristics that contains both the highest (4,418 m) and lowest (-86 m) points in the contiguous U.S. and extends from 32° N to 42° N latitude. A 600-km north-south-oriented mountain range, the Sierra Nevada, situated in eastern California provides large natural potential energy for hydropower facilities. California primarily exhibits a Mediterranean climate with cold and wet seasons (October-May), and warm and dry season (June-September). Many rivers with hydropower facilities have their source in high-altitude zones of the Sierra Nevada, where most precipitation in winter has historically been stored as snowpack, and runoff peaks during the spring snowmelt period. This combination of topography and climate makes California naturally suitable for year-round hydropower production due to the sustaining summer baseflow supplied by snowmelt.

California is a deregulated electricity market, which allows for the entrance of competitors to buy and sell electricity based on the hourly-variable electricity market demand, consisting of two major morning and evening peak demands on top of the baseload (Borenstein et al. 1995, Aghajanzadeh et al. 2019). The wholesale electricity market is comprised of distinct day-ahead and real-time markets in which the former one schedules the electricity production for the next day while the latter one is a spot market used to meet the last few increments of demand not covered in the former markets (CAISO 2016). Besides these two markets, ancillary services are to help maintain grid

stability and reliability by having hydropower plants generate electricity when unexpected events occurred (CAISO 2004). Hydropower is one of the important energy sources that can both undertake base load, peak load electricity generation and ancillary services (Key et al. 2012). In 2019, hydroelectric power plants accounted for 19 percent of the total in-state electricity generation in California based on the record of the California Energy Commission (CEC 2020).

A database of California hydropower plants was initially used to pair power facilities with gauging stations based on relevant documents and locations (CEC, 2018). All the available flow records (15-minute and hourly) were obtained from the U.S. Geological Survey (USGS, 2018) and through the California Data Exchange Center (CDEC, 2018) using two R packages ("dataRetrieval" and "CDECRetrieve"). For sites whose flow records were unavailable online, public data requests were made to local managers, though not all requests were answered. Using these approaches a total of 128 records were obtained.

1.1.2 Data analysis framework

This study had two objectives. The first objective (OBJ 1) was to automate hydropeaking events detection and feature extraction to enable data mining in a high temporal and spatial scale. The second objective (OBJ 2) was to explore the diversity of hydropeaking flow regimes in California with outputs from OBJ 1. A data analysis framework was developed to process flow record and identify classes of hydropeaking flow (Figure 1.1). To fulfill OBJ 1, Hydropeaking Event Detection Algorithm (HEDA) was developed (Details in section 1.1.4). To yield better performance, flow records were split into climatic dry and wet seasons because precipitation or snowmelt can disturb hydropeaking signals. Then, outputs of HEDA were used to locate gaging stations recording hydropeaking flow and extract hydrologic metrics. To fulfill OBJ 2, two types

of clustering analyses, hierarchical and fuzzy clustering, were conducted to explore data structure with seven independent hydrologic metrics of dry season dataset. Clustering analyses were heuristically determined with a combination of statistical interpretation, the examination of hydrographs, and documentation mining. Five important outcomes major outcomes (highlighted in grey rectangular in Figure 1.2) were investigated and are discussed herein.

OBJ1　　　　　　　　　　　　　　　　　　　　**OBJ2**
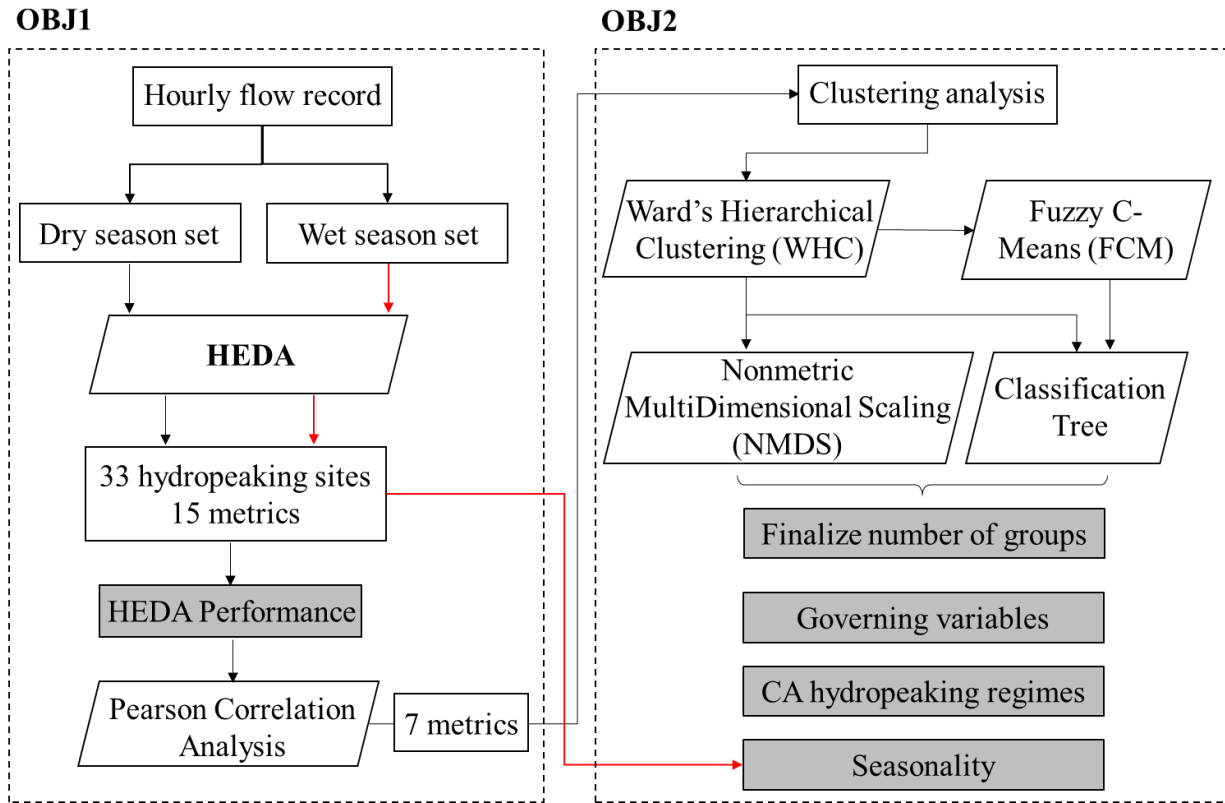
Figure 1.1. Data analysis frame of revealing the diversity of hydropeaking flow regimes.

1.1.3　Hydrologic variables

Five key dimensions of a hydrologic regime defined by Poff et al. (1997) were applied to analyze hydropeaking flow regimes. Fifteen ecologically meaningful flow metrics were then selected to represent these five dimensions (Baker et al. 2004, Meile et al. 2010, Bieri 2012, Bevelhimer et al. 2015) (Table 1.1). Each hydropeaking event is divided into base, rising, peak, and falling processes

(Figure 1.2). For each event, base flow is the minimum flow while peak flow is the maximum flow of a hydropeaking event. Rising and falling processes are the transition between base and peak flow. When two increases above a threshold magnitude are interspersed with a short period of no change, these two increases are counted as two rising processes (highlighted in dark grey in Figure 1.2). Daily and annual frequency of hydropeaking are the sum of rise and fall process per day and the number of days with hydropeaking per season/year respectively. One rise-fall cycle forms one hydropeaking event (highlighted in light grey in Figure 1.2) Timing is the date/time at which hydropeaking happens. Duration is the temporal length of rise/fall (D_{RC}) and peak (PK_{rtn}). Rate of change (RC) is the flow variation per unit time with a commonly used metric and Richards-Baker (RB) Index is a variability metric, where the impact of river size is eliminated by normalizing with Q_{ave}.
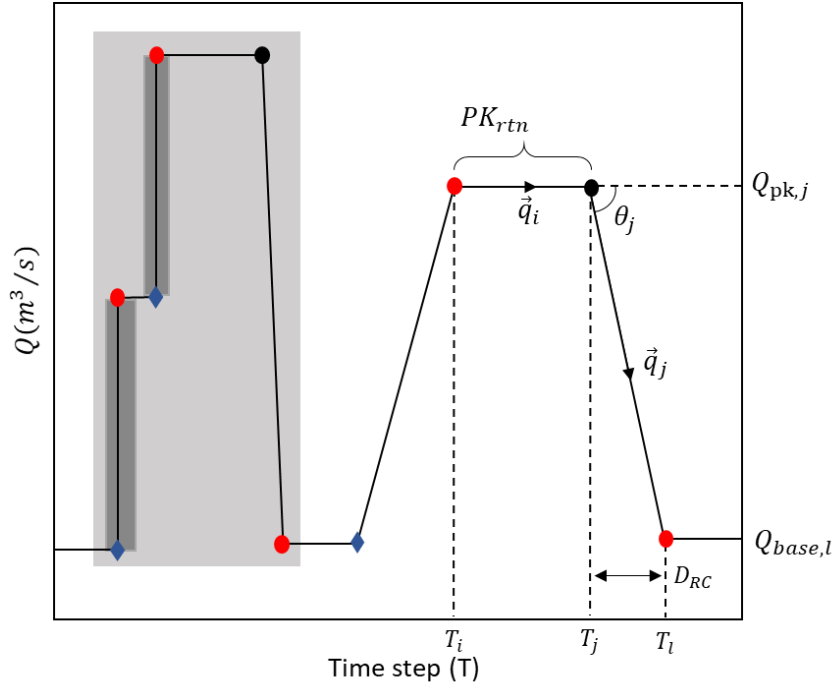
Figure 1.2. Events' definition and relevant values to calculate flow fluctuation parameters. Five hydropeaking events occur in the hydrograph. Vector angle (θ_j) is defined as the angle between two flow vectors ($\vec{q_i}, \vec{q_j}$).

Table 1.1. Hydrologic metrics derived from HEDA used in classification. Illustration was provided in Figure 1.2.

Variable	Metric	Metric Name	Symbol	Unit
Magnitude	$\dfrac{Q_{pk,i}}{Q_{ave}}$	Peaking discharge	Q_{peak}	-
	$\dfrac{Q_{base,l}}{Q_{ave}}$	Base flow	Q_{base}	-
	$\dfrac{\left|Q_{pk,j} - Q_{base,l}\right|}{Q_{ave}}$	Standardized amplitude	*St_{rg}	-
Frequency	Total number of rise and fall per day. One rise-fall cycle is one hydropeaking event.	Daily peaking number	PK_{no}	-
	Number of days has hydropeaking divided by the total number of days	Annual frequency	PK_{ratio}	-
Timing	Weighted value of time (1-24) hydropeaking happens per day.	Timing	**T_{max}	hr
Duration	$\left|T_i - T_j\right|$	Retention of peak	PK_{rtn}	hr
	$\left|T_j - T_l\right|$	Duration of rise/fall	*D_{RC}	hr
Rate of change	$\dfrac{\left|Q_{pk,j} - Q_{base,l}\right|}{\left[\left|T_j - T_l\right|Q_{ave}\right]}$	Flashness	*RB Index	hr⁻¹
	$\dfrac{\left|Q_{pk,j} - Q_{base,l}\right|}{\left|T_j - T_l\right|}$	Rate of Change	*RC	(m^3/s)/hr

*D_{RC}, RB Index, St_{rg} and RC are split into rise and fall processes and each process is calculated separately.

**The weighted average value of T_{max} instead of the median value was used because of the multi-modal distribution due to morning and evening peaks, which led median value fails to represent the most frequent value of timing. Therefore, T_{max} refers to the pattern of timing rather than the time hydropeaking happens. Q_{ave} is the average discharge of the whole period of each site.

1.1.4 Hydropeaking Event Detection Algorithm

To fulfill OBJ 1, a new algorithm, Hydropeaking Event Detection Algorithm (HEDA), was developed in R (R Core Team, 2021) to automate feature extraction of high-resolution hydropeaking flow with limited subjective decisions. HEDA consists of three modules: Data Preparation, Vector Angle, and Clean Noise (Figure 1.3). The first module, Data Preparation, starts with hourly flow records (15-minute records were converted to hourly records by taking the mean flow within the same hour) of the interest period (e.g., post-dam period) in CSV format. The flow record of each site is then split into dry (June-September) and wet (October-May) season datasets to optimize the performance of HEDA as hydropeaking tends to occur more frequently in the dry season while precipitation and snowmelt in other seasons can disturb the hydropeaking signals. Data smoothing strategies such as Gaussian filtering or locally estimated smoothing were not applied as these strategies (1) are unable to quickly process a large amount of data; (2) potentially mark peaking events as noise; and (3) degrade or destroy the peaking pattern (SI II). Instead, the flow record was smoothed with two steps. First, based on observation, intensive small fluctuations always occur at base and peaking discharge, thus flow records were truncated by 10th and 90th percentile of discharge during the whole period to remove these fluctuations (SI II). Second, flow variations ($\Delta q_i = Q_{i+1} - Q_i$) smaller than threshold X were assigned zero to avoid mischaracterizing small fluctuations as peaks due to measurement errors. Threshold X consists of a global (γ) and local static ($\alpha_1 * Q_{ave}$) threshold (Eq.1-1). The global threshold (γ) acted as a consistent standard to all the sites. Threshold values of γ was initialized based on the minimum rise/fall rate found in the literature (2.8 m³/s/hr) and finalized to be $\gamma = 1.1$ m³/s. The local static threshold ($\alpha_1 * Q_{ave}$) was a consistent standard to one site. The α_1 was assigned 0.03 by evaluating the range of Q_{ave} at 33 sites and the relative difference between all the thresholds ($T3_t$) used in

12

this study (SI II).

$$X = \max(\gamma, \ \alpha_1 * Q_{ave}) \tag{1-1}$$

The second module, Vector Angle, involves the identification of change points in flow time series (Figure 1.3). Among the flow record, consecutive data points (T_n, Q_n) and (T_{n+1}, Q_{n+1}) were treated as a Euclidean Vector $\overrightarrow{q_n}$ $(\Delta t_n, \ \Delta q_n)$, a quantity that has a magnitude and a direction. The magnitude of a vector is the distance between the two data point ($|\overrightarrow{q_n}| = \sqrt{(\Delta t_n)^2 + (\Delta q_n)^2}$ while direction is from its tail (T_n, Q_n) to its head (T_{n+1}, Q_{n+1}) (Figure 1.2). The vector angle (θ_{n+1}) between two continuous vectors $(\overrightarrow{q_n}, \overrightarrow{q_{n+1}})$ was used to identify change points instead of the first derivative of $q(t)$ to avoid excluding change points outside the range of the designated rise/fall rate ($\tan \theta = \Delta q_n / \Delta t_n$) can be excluded (Eq.1-2). The threshold value of θ was tested from 30° to 70° (70° was set based on the threshold of the minimum rise/fall rate (2.8m³/s/hr).) and finally set as 60° because it amounts to a rise/fall rate of 1.7m³/s/hr. This value was set to be lower than 2.8m³/s/hr which was used as a mitigation standard of hydropeaking the American river (SI II) (Young et al. 2011). After $q(t)$ with $\theta > 60°$ were identified, change points were grouped into four categories based on the symbol of Δq_{n+1} (+, 0, -) which separated hydropeaking processes into four groups (points 1-4 in Figure 1.3). Points 1 and 4 are always followed by a rising discharge while point 3 is followed by a falling discharge. Point 2 indicates the start of either a peak or base flow discharge. The sequence of point 2 followed by point 4 (base-flow pair) indicates base flow while the combination of point 2 and 3 (peak pair) indicates a peak discharge.

$$\theta_{n+1} = \cos^{-1}(\Delta t_n{}^2 * \Delta t_{n+1}{}^2 + \Delta q_n{}^2 * \Delta q_{n+1}{}^2) / \sqrt{\Delta q_n * \Delta t_n{}^2 + \Delta q_{n+1} * \Delta t_{n+1}{}^2} \tag{1-2}$$

In the Clean Noise module, three layers of correction (position, repetition and difference) clean change points identified incorrectly. In the position layer, change points are excluded if they occur

13

in the wrong position. For example, both point 3 and the peak pair represent the peaking discharge whose value (position) should be close to the daily maximum discharge. If the peaking discharge is close to the daily minimum discharge, change points are removed since they are in the wrong positions. The second layer, Repetition, cleans repeated points generated in the first layer. Before getting to the third layer, the first and second layers need to be repeated to make sure change points that violated the former two rules are removed. The last layer, Difference, evaluates whether Δq_i is large enough to be identified as a peaking event based on a daily amplitude threshold described below.
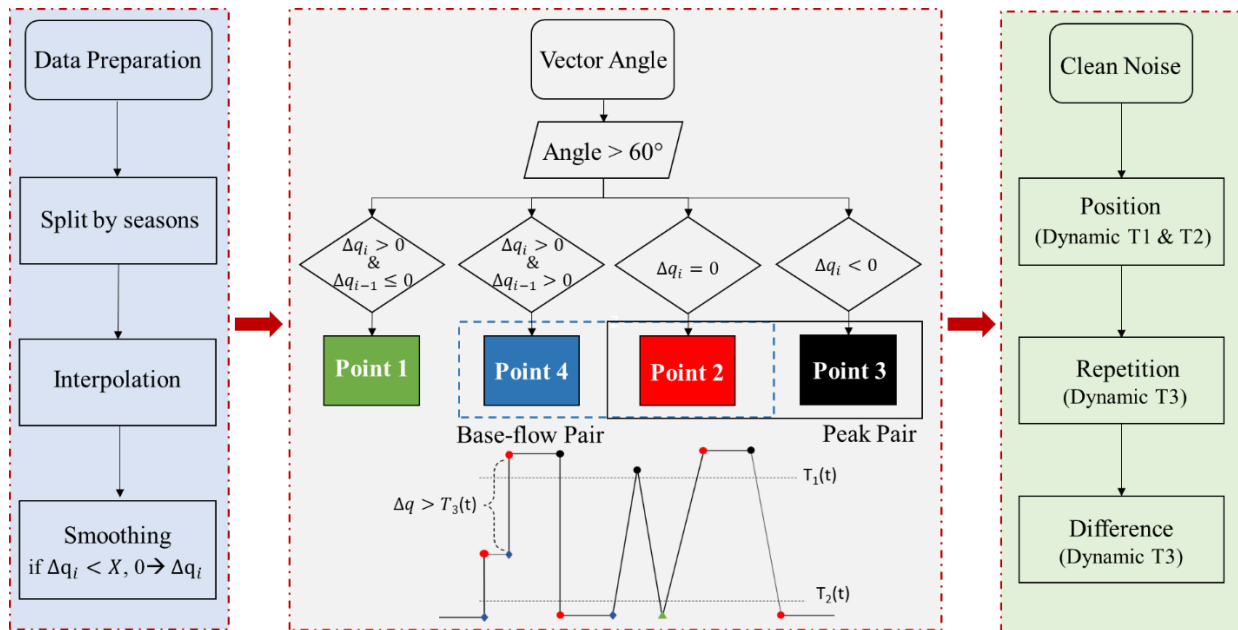
Figure 1.3. Schematic diagram showing the sequential steps of the HEDA.

Within the three layers, three thresholds were used, $T1(t)$, $T2(t)$, and $T3(t)$, (Eq.1-3, 1-4, 1-5 and Figure 1.3**Error! Reference source not found.**). In the position layer, two dynamic thresholds ($T1(t)$ and $T2(t)$) that were updated daily were used for each river to identify the relatively high and low discharge. The threshold value of high discharge was defined as the difference between

14

maximum daily flow ($Q_{max}(t)$) and 30% (α_2) of the daily maximum amplitude ($Q_{max}(t) -$ $Q_{min}(t)$) while that for low discharge was defined as the sum of daily minimum flow ($Q_{min}(t)$) and 30% (α_2) of the daily maximum amplitude. In the repetition and difference layers, $T3(t)$ was used as the standard to evaluate whether flow variation can be counted as a rise/fall process. $T3(t)$ consists of a local static threshold ($\alpha_3 * Q_{ave}$) and a dynamic threshold ($\alpha_4 * (Q_{max}(t) -$ $Q_{min}(t))$) that were updated daily for each river to reflect the evolvement evolution of climate, seasonality, and river size flow, all of which that are highly related to hydropower operation. To decide what fraction of Q_{ave} to be used, tests were run within a reference range (30%-100%) gained from literature with both Q_{ave} and amplitude available (Zimmerman et al. 2010, Hauer et al. 2012, Capra et al. 2017). Finally, 70% of Q_{ave} ($\alpha_3 = 0.7$) was selected as the threshold value because outputs of HEDA didn't change beyond this fraction. To identify different intensities of rise/fall process of each site, 50% of the daily maximum amplitude was used (SI II).

$$T1(t) = Q_{max}(t) - \alpha_2 * (Q_{max}(t) - Q_{min}(t)) \tag{1-3}$$

$$T2(t) = Q_{min}(t) + \alpha_2 * (Q_{max}(t) - Q_{min}(t)) \tag{1-4}$$

$$T3(t) = \max\left(\alpha_3 * Q_{ave} , \alpha_4 * (Q_{max}(t) - Q_{min}(t)) \right) \tag{1-5}$$

The performance of HEDA was assessed with visual examination, with 500 change points of each hydropeaking site plotted and visually checked. The error rate of HEDA was calculated by dividing the number of wrongly identified change points by 500.

1.1.5 Hydropeaking clustering

To fulfill OBJ2, outputs from HEDA of dry season dataset were analyzed with correlation analysis to select independent metrics for clustering analysis to explore the underlying diversity of hydropeaking flow regimes among the 33 sites. First, values of 15 metrics were transformed to

values between 0 and 1 by min-max normalization (Eq. 1-6) to remove scaling impact. A correlation matrix of fifteen flow metrics was created to identify and remove highly correlated metrics (SI I). Second, two types of clustering methods, hierarchical and fuzzy clustering, were used to explore the data structure from different perspectives. In the beginning, a hierarchical clustering analysis using Ward's algorithm (Ward's hierarchical clustering; WHC) (Ward, 1963) was used to make a preliminary assessment of hydropeaking patterns without any preconceived assumptions. The WHC started with the maximum cluster number (33 in this study), then reduced the number of clusters by merging them at the node with minimum merging cost, i.e. the least total within-cluster variance, from bottom to top. Then, Fuzzy c-means (FCM) clustering built on the WHC result was used to not only examine the clustering structure with the partitional-clustering algorithm but also the degree of membership (Bezdek 1973, 2013). Instead of assigning one site to one class each time, FCM assigned each site a cluster membership score, where being closer to the cluster center means a higher score. This provided more robust clustering against noise and outliers because low scoring sites have a reduced impact on the position of the cluster center (Kantardzic 2011). Also, presuming a soft boundary between clusters is more aligned with real-world hydropower operation since its underlying driving force is to maximize profit under constrained factors; thus, a powerhouse might use more than one operational mode.

$$Y'_i = \frac{Y_i - Y_{min}}{Y_{max} - Y_{min}} \tag{1-6}$$

The relative roles of hydropeaking metrics forming the data structure were analyzed next. Nonmetric multidimensional scaling (NMDS) (Clarke, 1993) was performed to visualize the hidden structure of the multivariate dataset in a reduced dimension (from seven to three dimensions). Principle component analysis was then built on NMDS to evaluate the relative

significance of the seven metrics on each axis. Box-and-whisker plotting was applied to illustrate relative differences in hydrologic metrics within and across the identified hydropeaking patterns. Finally, a classification and regression tree (CART) (Breiman 1984, De'ath et al. 2000) was used to identify the most explanatory hydrologic metrics in distinguishing hydropeaking patterns and their threshold values. The classification tree yielded a binary decision tree based on the proportion of presences and absences in the clusters. The splitting criterion was to maximize the homogeneity of the cluster and is defined by the Gini index measures the degree or probability of a particular variable being wrongly classified when it is randomly chosen. At each node, the selected feature/metric with the lowest Gini index was used to further split the tree. Euclidean distance was chosen as the distance measure. Ten-fold cross-validation was used to select tree size with the highest prediction accuracy.

Clustering validation was heuristically determined based on a combination of statistical analysis interpretation, the examination of hydrograph and documentation mining. First, potential numbers of clusters were identified based on the structure of the dendrogram and the Hartigan index (Hartigan 1975). Meanwhile, NMDS was used to visualize how potential clusters distinguish sites in a reduced dimension. The goal is to have clusters well separated from each other with the least overlapping areas. Second, site membership in clusters was analyzed and only those with a value > 50% were kept. Third, box-and-whisker plots and classification trees were also used to examine the performance of clustering. For reliable clustering, it is expected that metrics display a certain degree of difference between clusters, and classifiers trained by identified clusters can perform prediction reliably (cross-validation accuracy). Besides all the statistical interpretation, physical interpretation of the clusters was also conducted by checking hydrograph and historical

documentation of hydropower facilities. The goal of this heuristic refinement was not to make large adjustments to the purely statistical classification but to ensure that it was capturing real-world differences.

<div align="center">1.2 **Results**</div>

1.2.1 Identification of hydropeaking sites

Before attempting to use HEDA to identify hydropeaking sites, the performance of HEDA was assessed first (Figure 1.5) by applying it to sites where operation type is known (30 non-hydropeaking and 10 hydropeaking sites). HEDA worked effectively at distinguishing the non-hydropeaking flow from the hydropeaking flow. Compared with the hydropeaking flow, half of the non-hydropeaking flow sites obtained "NA" output (no value) for all metrics and the other half featured low PK_{ratio} (<5%) and PK_{No} (<0.9). Hydropeaking flow was defined as having high PK_{ratio} (10%-95%) and PK_{No} (>=1). Then, these criteria for PK_{ratio} and PK_{No} were employed as standards to identify sites using all flow records (128). Sites that met only one of the two standards (PK_{ratio} and PK_{No}) were double-checked with hydrographs and documentation about site operations. Consequently, 33 sites (site information in SI I) with a length of flow records at least five years were identified as hydropeaking sites and used for the following analyses (Figure 1.4).
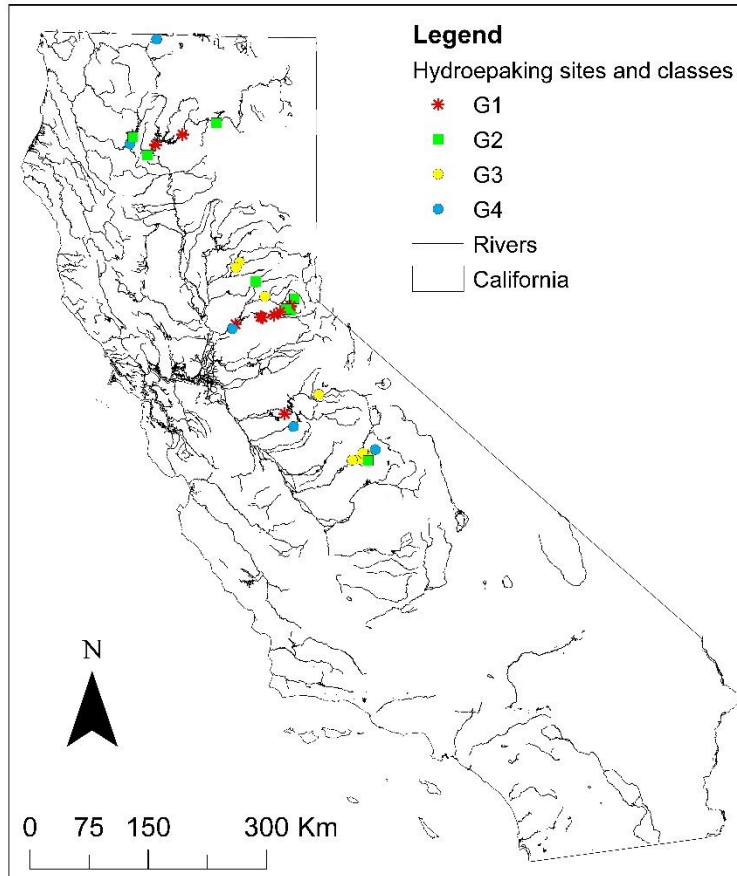
Figure 1.4. Map of hydropeaking sites identified by HEDA and classes identified by FCM, California, USA. An interactive map is available: https://ninalty.github.io/HPK_InteractiveMap/HPK_CA_InteractiveMap.html

Among the 33 hydropeaking sites, the average error rate of HEDA was 1% among sites with minimum and maximum values of 0% (six sites) and 2.8% (two sites), respectively. The incorrect change points were mainly caused by noisy segments of flow records from local agencies that did not perform sufficient quality assurance and quality control, yielding data that were too noisy even for manual identification (Figure 1.5A). As for other flow records, relatively small peaking events can be neglected when a mix of small and large peaking events occurred on the same day. The

19

large peaking discharge can make the upper bound of peaking ($T1(\text{t})$) too high for small peaking events to be detected. For example, in FOL site, the large peaking discharge is around 142 m^3/s while the small peaking discharge is around 71 m^3/s on the same day. Because of the large relative difference between hydropeaking events within that day, HEDA can only keep the large hydropeaking events but overlook the small ones (Figure 1.5B).
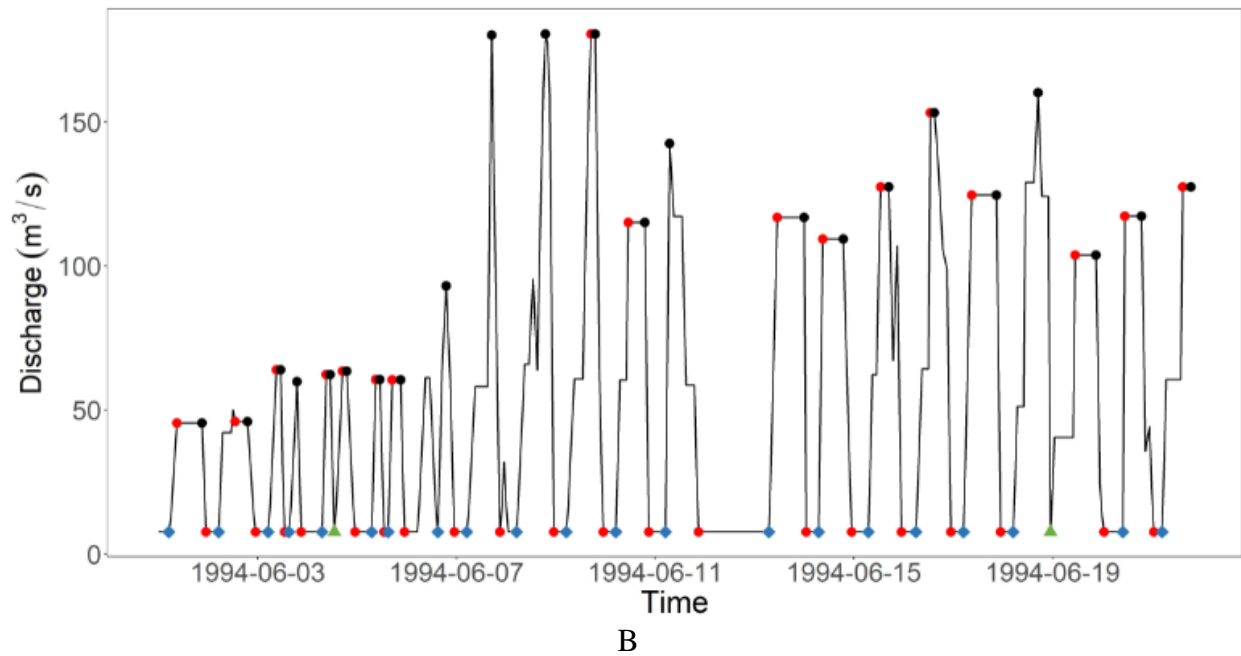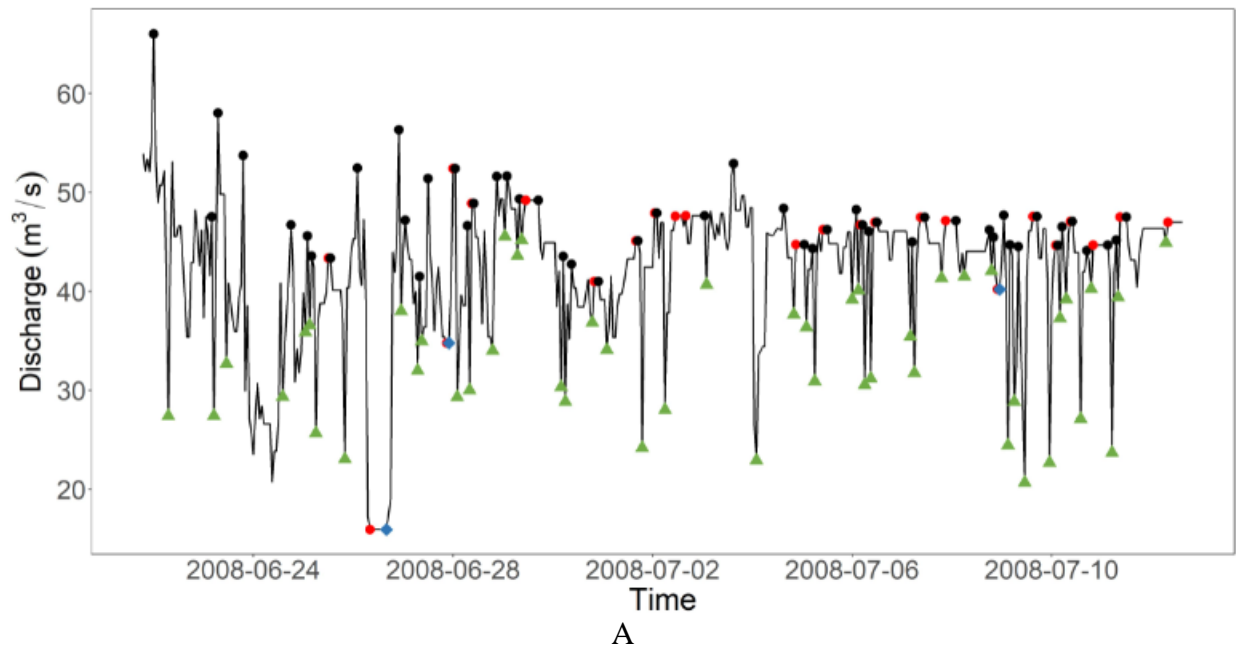
Figure 1.5. Hydrographs with 500 change points identified by HEDA in the dry season. A is streamflow below Big Creek Power House #3 recorded by gauge 11241800. B is streamflow below Folsom Lake outflow recorded by FOL.

1.2.2 Diversity of hydropeaking flow regimes

Outputs of HEDA (median values of 15 flow metrics) were further analyzed to reveal the diversity of hydropeaking flow regimes. Seven metrics were selected and regarded as uncorrelated (≤ 0.6). Even though PK_{ratio} is moderately related (0.69) to D_{RC} among the seven metrics, PK_{ratio} was still selected because it can provide the number of days that hydropeaking occurs during a certain period, such as summer in this case. As for the other six metrics, the correlation coefficients between them were all lower than that value and regarded as low enough to ignore the weak correlation between them. With a normalized subset of hydrologic metrics meeting statistical independence, WHC was first applied to illustrate the nested data structure of the 33 sites (Figure 1.6). The first split occurred at a distance of 2.8, distinguishing two clusters: one giant cluster and one small cluster – group four (G4). Subsequently, the tree split within the giant cluster and formed four big branches: group three (G2), group two (G3) and group one (G1) in sequence. All the subtrees continued to grow under each of the four branches. However, the internal clustering Hartigan index suggested that cutting the dendrogram into four groups was the optimal option driven by strong breaks in D_{RC}, PK_{No} and PK_{ratio}. This conformed with preliminary analyses of data structure in the reduced dimensions (NMDS) and tree structure of the clustering dendrogram (Figure 1.7). To have four clusters, the tree was cut at a distance of 2, and 11 sites were clustered to G1, eight sites as G2, nine sites as G3 and four sites as G4. Clustering validity was also tested by applying heuristic clustering refinement procedures explained in Section 2.4. Clustering hydropeaking flow into four groups also allowed the relative hydrologic similarity/dissimilarity of different sites group displayed in the multivariate space of reduced dimensionality to be in well-defined sets (Figure 1.7). The performance of the classification tree reached a cross-validation accuracy of 79% (Figure 1.8).

22
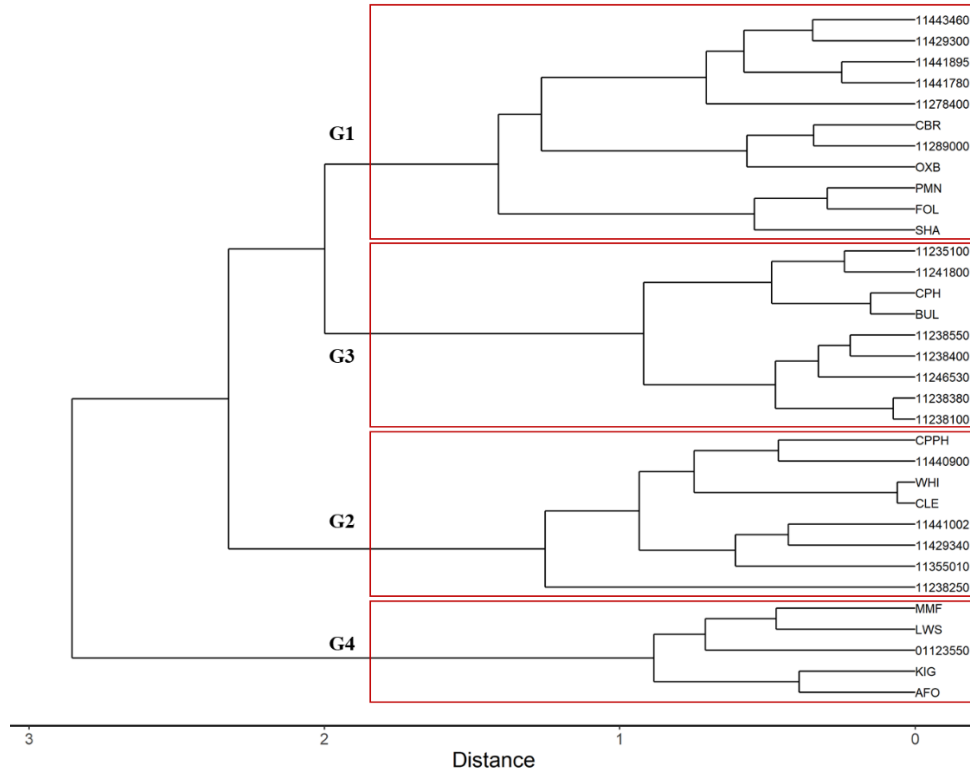
Figure 1.6. The hierarchical cluster diagram shows similarity/dissimilarity among 33 sites. Sites are indicated by either their USGS ID number or the CDEC 3-character ID.

To further evaluate clustering validity or uncertainty, FCM clustering was applied to assess the strength of WHC by knowing the membership value of each site in the identified groups. The fuzzification parameter (m) is a weighting parameter controlling the degree of fuzziness in the process of clustering. When m=1, the partitioning is 'hard' (probability of members to the designated cluster is one), as m increases the membership assignments of the clustering become fuzzier (members have evenly distributed probability in all clusters). Even though no theoretical or computational evidence distinguishes an optimal m, for most data sets, $1.25 \leq m \leq 3$ gives good results (Bezdek et al. 1984, Güler et al. 2004, Ross 2005). Based on trials and sensitivity testing in this study, it appeared that m = 1.3 resulted in clustering that was neither too fuzzy nor too hard.

From the membership matrix (Table 1.2), sites were assigned to the cluster of membership value > 0.5. Compared with WHC, assigning the same cluster number to FCM generated a similar clustering structure with only two sites clustered to different groups. Site 11278400 and OXB were moved from G1 to G3 and G2 by FCM. Site OXB had a weak membership in all the groups.

Table 1.2. FCM Membership Matrix of hydropeaking patterns. Bold numbers indicate group membership selected.

Sites	Group	Membership value			
		G1	G2	G3	G4
11278400	G3	0.40	0.04	0.54	0.01
11289000	G1	0.50	0.39	0.10	0.01
11355010	G2	0.10	0.86	0.03	0.00
11429300	G1	0.96	0.02	0.03	0.00
11429340	G2	0.04	0.94	0.02	0.00
11440900	G2	0.00	0.99	0.00	0.00
11441002	G2	0.06	0.94	0.00	0.00
11441780	G1	0.98	0.02	0.01	0.00
11441895	G1	1.00	0.00	0.00	0.00
11443460	G1	0.99	0.00	0.00	0.00
11238100	G3	0.00	0.00	1.00	0.00
11238380	G3	0.00	0.00	0.99	0.00
11238400	G3	0.00	0.00	1.00	0.00
11241800	G3	0.00	0.00	1.00	0.00
11246530	G3	0.00	0.00	1.00	0.00
11238550	G3	0.00	0.00	1.00	0.00
11235100	G3	0.00	0.00	1.00	0.00
01123550	G4	0.00	0.03	0.02	0.95
11238250	G2	0.16	0.74	0.08	0.02
AFO	G4	0.00	0.00	0.00	1.00
BUL	G3	0.03	0.00	0.97	0.00
CBR	G1	0.94	0.01	0.05	0.00
CLE	G2	0.01	0.99	0.00	0.00
CPH	G3	0.09	0.01	0.90	0.00
CPPH	G2	0.00	1.00	0.00	0.00
FOL	G1	0.94	0.05	0.01	0.00
KIG	G4	0.00	0.00	0.00	1.00
LWS	G4	0.00	0.00	0.00	1.00
MMF	G4	0.00	0.00	0.00	1.00
OXB	G2	0.17	0.38	0.32	0.13
PMN	G1	0.98	0.00	0.01	0.00
SHA	G1	0.92	0.04	0.03	0.01
WHI	G2	0.01	0.99	0.00	0.00

1.2.3 Clustering validity and relative significance of hydrologic metrics

Clustering validation was heuristically evaluated by exploring the data structure in a reduced dimension and analyzing the relative significance of the hydrologic metrics of each group. The three-dimensional NMDS ordination reached a stress value of 0.085 with a non-metric coefficient of determination of 0.99 between observed dissimilarity and ordination distance (Figure 1.7) which both indicate a good ordination with little risk of drawing false inferences (McCune et al. 2002). In the reduced dimensionality, a clear cut exists along the first axis showing five sites that belonged to G4 were well apart from the majority on the right side. Sites gathered on the right spread widely along the second axis and had a small overlapping area between G1 and G3. The three principal component axes (PCAs) resulting from the NMDS ordination explained 74% of the variance in the data with loadings of 0.65 for PK_{ratio}, -0.78 for PK_{rtn} and -0.65 for PK_{no} for PCA-1, PCA-2 and PCA-3 respectively. Besides PK_{rtn}, D_{RC} ranked the second highest (0.60) loadings for PCA-3. These analyses led to the conclusion that PK_{ratio} was the principle metric that distinguished G4 from the other three groups while PK_{rtn}, PK_{no} and D_{RC} together explained the separation of G1, G2 and G3.
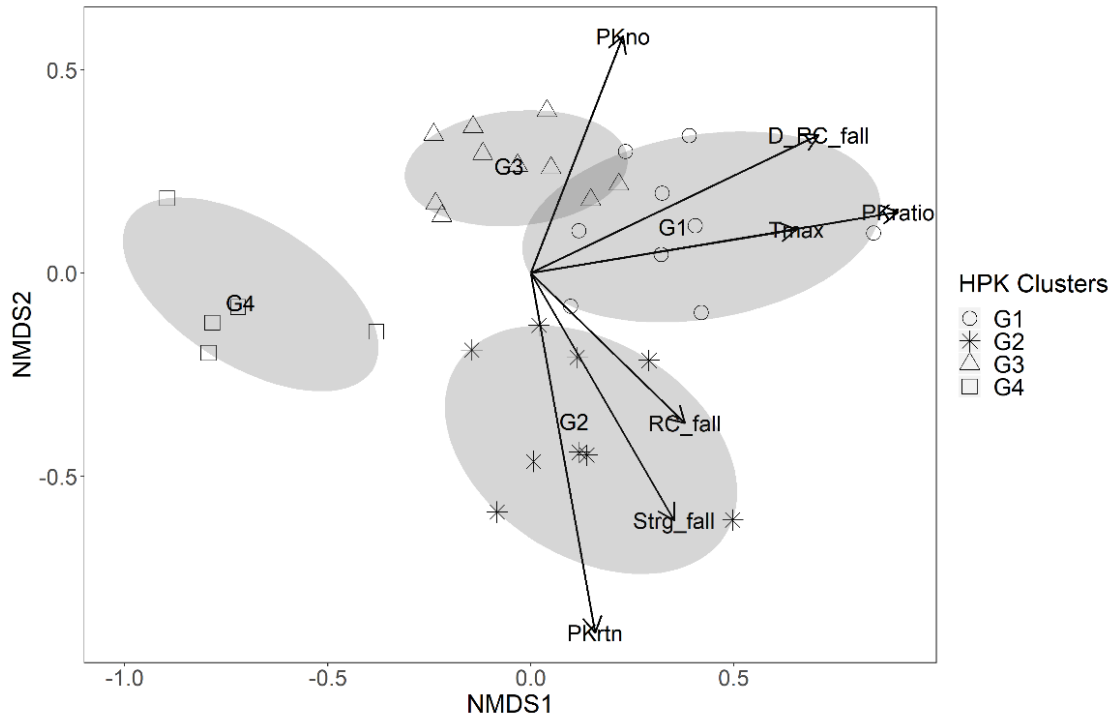
Figure 1.7. Results from non-metric multidimensional scaling.

Classification tree and box-and-whisker plots were used to identify the most explanatory hydrologic metrics distinguishing hydropeaking patterns and their threshold values. These provided potential ranges of metric values expected for each hydropeaking pattern. The classification tree model built on WHC determined three principle metrics and the relative strength to be as follows: PK_{no} (2.6), PK_{ratio} (46%) and PK_{rtn}(4.5) (Figure 1.8). The classification tree model built on FCM determined three principle metrics and their relative strength to be as follows: PK_{no} (2.6), D_{RC} (3.5), and PK_{ratio} (46%). The classification tree built on WHC and FCM both correctly classified 94% of the sites. Ten-fold cross-validation of the prediction was 79% (WHC) and 82% (FCM). Box-and-whisker plots illustrated relative differences in hydrologic metrics within and across the four identified hydropeaking groups (Figure 1.9). G1 had the highest D_{RC}

27

and PK_{ratio} which implied G1 features a relatively slow rise/fall process and frequent peaking operations across a year. G2 had the highest PK_{rtn}, RC, and St_{rg} implying that this group has a long-lasting peaking status, with a rapid fluctuations with large variations in magnitude. G3 stood out from other groups as having the highest PK_{no} but relatively low values of other metrics compared with the former two groups. G4 has the fewest hydropeaking features, with low values of all the hydrologic metrics. G1 and G2 have similar values of T_{max} while G4 has the lowest value of T_{max} and G3 ranked between them.

(A)   (B)
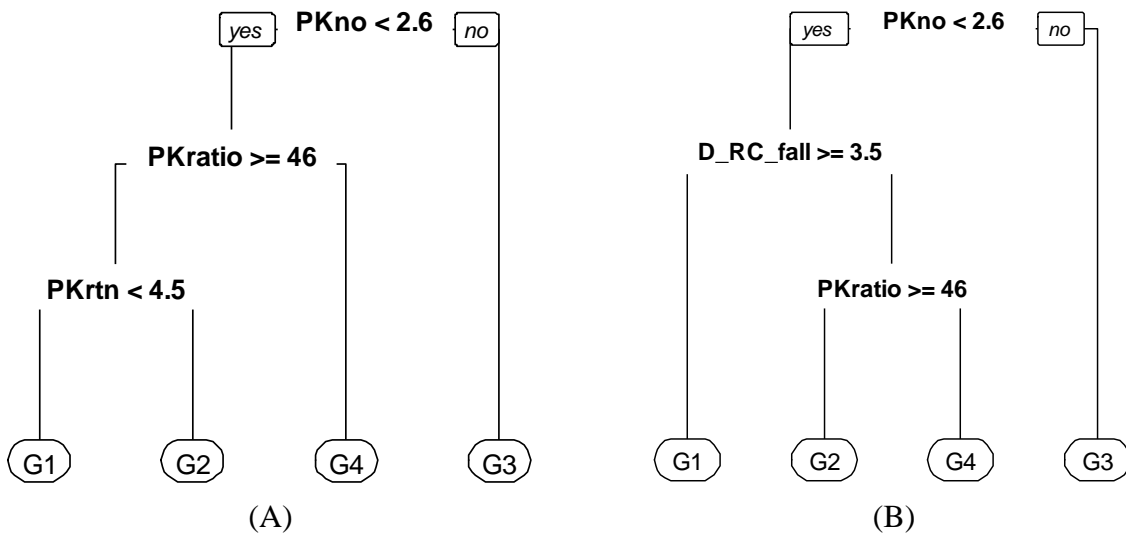
Figure 1.8. CART classification trees indicating primary attributes and their threshold values of distinguishing hydropeaking groups trained by WHC (A) and FCM (B).
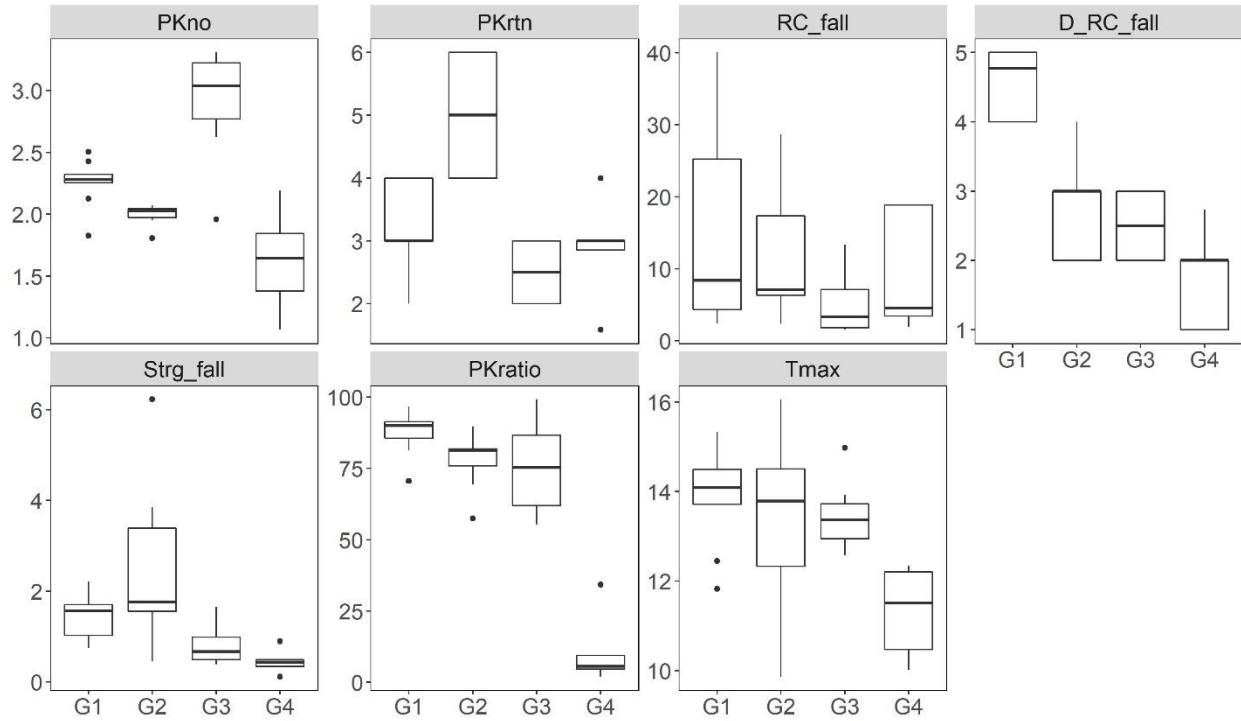
Figure 1.9. Box-and-whisker plot of normalized hydrologic metrics used in the FCM clustering analysis.

1.3 Discussion

1.3.1 HEDA performance

Instead of using the first derivative of discharge with time, treating consecutive points in a flow record as a Euclidean vector and detecting change points with vector angle and magnitude boosted the computational efficiency by avoiding over-detecting change points. In addition, the application of static and dynamic thresholds automatically adjusts the threshold over time and across sites. Thus, it requires minimal subjective input and iterative adjustment. The only subjective decisions that have been made are the four weighting coefficients α_1, α_2, α_3 and α_4. Their values were assigned based on the overall performance and reference range found in the literature, but they are open to user adjustments. All these features make HEDA stand out from other approaches for its

capability of distinguishing sites with and without hydropeaking and automating the feature extraction of hydropeaking flows.

Even though HEDA initially was not developed to distinguish hydropeaking flow from non-hydropeaking flow, it successfully distinguished the two types of flow with PK_{ratio} and PK_{No}. This is a very useful function because manually pairing the location of gauges to powerhouses is extremely time-consuming. Besides known hydropeaking sites, HEDA could identify hydropeaking sites by starting with flow records instead of with documentation – which is useful in regions of the world where getting this documentation can be quite difficult or in places where actual operations deviate from stated ones. With HEDA, users can finish this process within ten minutes by importing all the sub-daily flow record of a site into HEDA. Furthermore, HEDA successfully captured major hydropeaking events and filtered noises through the whole study period (five to thirty years) of 33 sites with a low error rate (Figure 1.5), thus enabling the extraction of hydrologic features automatically. Automating feature extraction of sub-daily flow on a large spatial scale opens infinite possibilities for scientific analysis, such as applications for a high-frequency sampling of many other types of flow alterations and the development of flow-ecology relationship.

1.3.2   Variables governing hydropeaking classification

NMDS and two types of clustering analyses were applied to explore the diversity of hydropeaking flow regimes. Together they delineated 33 hydropeaking sites into four distinct groups, providing meaningful information about differences in hydropeaking regimes in California. NMDS and WHC assisted in interpreting the similarity/dissimilarity between sites and finalized the number of clusters. FCM clustering further investigated the data structure and found a reliable membership

30

value of the clustering. The finalized classification built on WHC and FCM were examined by classification trees with ten-fold cross-validation. Even though both WHC and FCM generated similar clustering structures, the classification tree built on FCM had a higher accuracy of prediction than that on WHC. As for variables that govern the classification of hydropeaking, frequency and duration of peaking events were identified by classification trees. PK_{no}, PK_{ratio}, and PK_{rtn} distinguished the four classes G1-G4 in the classification tree built on WHC while PK_{no}, D_{RC} and PK_{ratio} distinguished G3, G4, G2 and G1 in the classification tree built on FCM. In both trees, daily number of peaking events (PK_{no}) is the principal metric distinguished G3 from the other three groups. The annual frequency (PK_{ratio}) was the principal metrics distinguished G4 from the other two interpreted from results of PCA and classification tree built on WHC. Meanwhile, the structure of classification tree built on FCM indicated that G4 also featured rise/fall process with a lower duration. As for G1 and G2, duration of peaking and rise/fall distinguished these two groups from each other. The magnitude, rate of change and timing were not identified as principal metrics that differentiated the four groups from each other which indicates that these features of hydropeaking events are similar among all hydropeaking sites. However, the governing variables might change in different regions.

1.3.3 California hydropeaking regimes

Four representative hydrographs of the identified groups/patterns were created for California (Figure 1.10). They highlight the role of hydropeaking intensity in differentiating these four regimes. G1 has the strongest hydropeaking intensity due to high values in all metrics except the peaking retention and standardized amplitude. G2 ranks the second strongest peaking regime with long-lasting peaking retention ($\geq$ 5 hr) and highest amplitude (two to four times mean annual discharge). Compared with G1, G2 represents a hydropeaking pattern that peaks less frequently

31

but with a relatively longer peak each time due to the high peaking retention. These two groups describe hydropower plants with large generation capability or reservoirs which allows them to handle major hydropeaking tasks. In G3, all metrics values are smaller than those of the former two groups, but this group had the highest number of daily peaking events. This indicates G3 represents hydropower plants that conduct hydropeaking more frequently on a daily basis but with lower magnitude and duration. Its relatively low annual frequency of peaking might imply that this group is not responsible for the major hydropeaking source of energy in California. G4 represents the weakest peaking intensity. Even though its PK_{ratio} is extremely low ($\leq 41\%$), the value of PK_{No} and PK_{rtn} strongly suggests that hydropeaking regulation still exists. This is an interesting group because its weak hydropeaking features are caused either by environmental restriction or the type of powerhouse. For example, the environmental restriction has been applied to Nimbus Dam (gauge AFO) to reduce steelhead trout stranding (Young et al. 2011). Thus, the downstream flow recorded by AFO still displays the peaking pattern but with a lower magnitude, frequency, and rate of change. The Merced Falls powerhouse (gauge MMF) is a run-of-the-river facility using water downstream of an impoundment. The impoundment's release capability limits its capability of generating strong peaking flow (McManamay 2017).
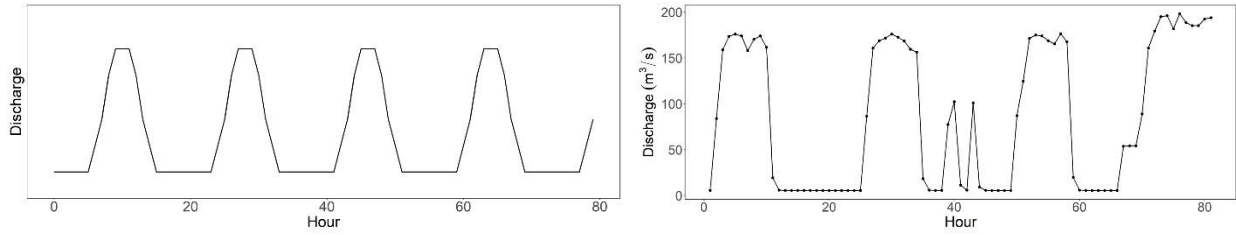
G1 Frequent hydropeaking
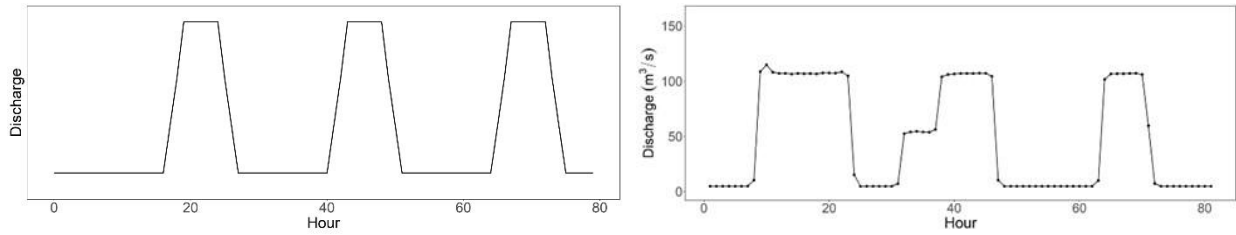
G2 Large hydropeaking
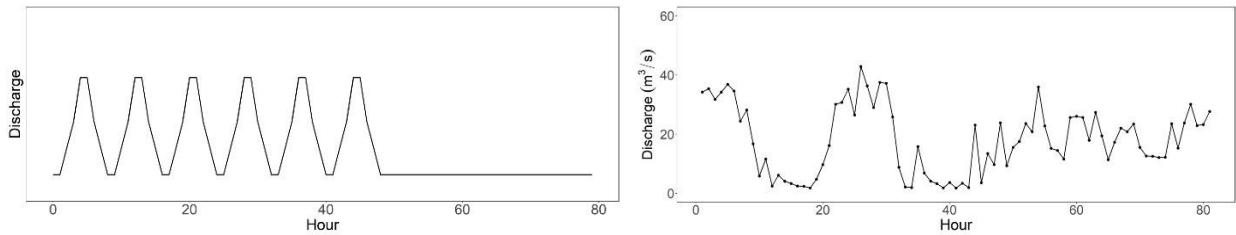
G3 Supplementary hydropeaking
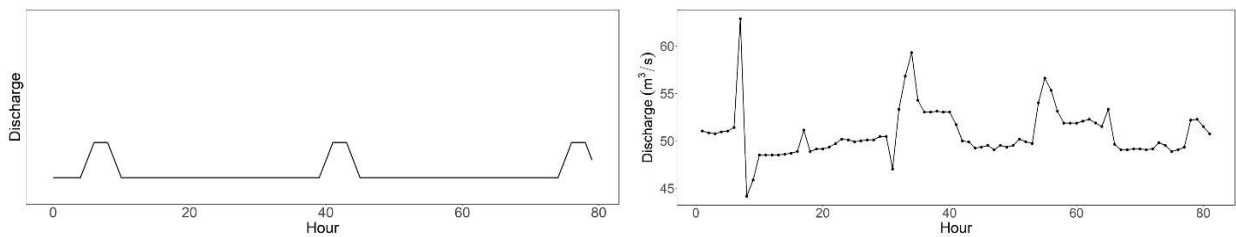
G4 Regulated hydropeaking

Figure 1.10. Representative hydrograph of the identified hydropeaking classes (left) and site member of each class (right; G1 gauge PMN; G2 gauge WHI; G3 gauge BUL; G4 gauge AFO).

In G3 and G4, the typical morning and night timing pattern was not obvious. G3 features hydroelectricity generation mainly for ancillary services which were built for maintaining grid stability and reliability when unexpected events happened. G4 features those regulated hydropeaking flow. Flow alteration in G4 consists of hydropeaking flow and environmental flow for aquatic ecosystem and river channel. Therefore, these two factors disturbed the timing of hydropeaking in G3 and G4 respectively.

1.3.4   Seasonality of California hydropeaking flow regimes

The seasonality of hydropeaking was assessed in terms of the variation of hydropeaking operations between the wet and dry seasons that comprise the annual cycle of the Mediterranean climate in California. Another prominent feature of this climate is pronounced interannual precipitation variability. Thus, we also examined differences in hydropeaking between years with above- and below-normal precipitation. The dry season of the two representative years was selected as the reference season. Representative drought and non-drought years were set to be 2014 and 2017 separately due to the availability of data (SI 1).

Generally, the annual frequency of hydropeaking in dry season was higher than that in wet season. The difference in annual frequency of hydropeaking between dry and wet season was over 10% in G1 (10%), G2 (13%) and G3 (17%) while was negligible (1%) in G4. These results indicated that sufficient water availability during wet season allows hydropower facilities to generate electricity constantly while hydropeaking operations are much more intensive in dry season due to the scarcity of water. In addition, the annual frequency of hydropeaking in the dry season is positively related to hydropeaking frequency in wet season indicated by the uncrossed lines of two seasons (Figure 1.11). That to say sites that tend to conduct hydropeaking frequently in dry season are

more likely to have high annual frequency of hydropeaking in wet season. As for the variance of hydropeaking between different types of years, the non-drought year had a lower annual frequency of hydropeaking operation than that in drought year for all groups. And the difference between them followed the similar pattern identified in the comparison of different seasons. The annual frequency of hydropeaking in drought year was 12%, 7% and 10% higher than that in non-drought year in G1, G2 and G3 respectively. Meanwhile, the hydropeaking signals almost disappeared in G4.
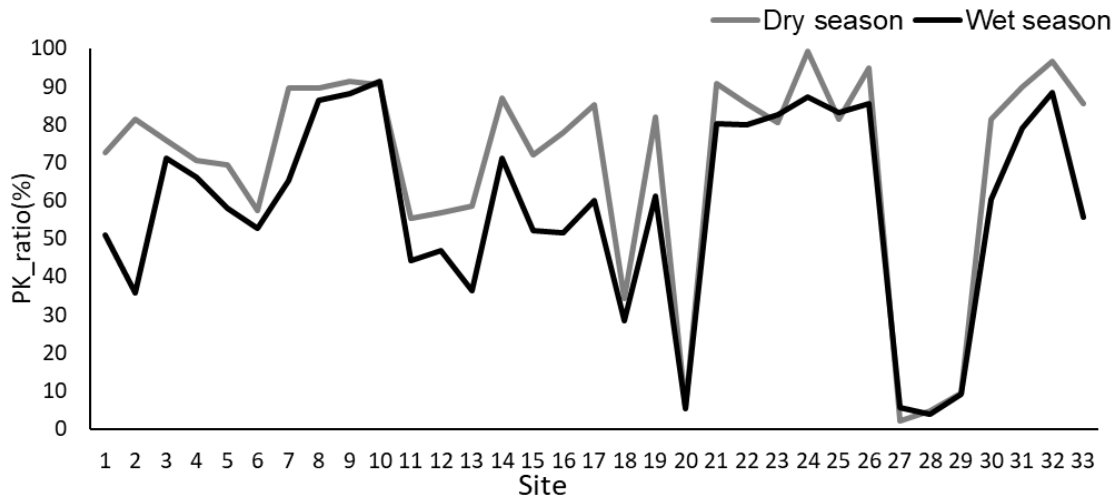
Figure 1.11. Annual frequency of hydropeaking during dry and wet seasons.

1.3.5 Uncertainty of the classification

Three types of uncertainties exist in this study: the uncertainty in knowledge about the operation of hydropower facilities, that caused by the method, and that associated with input data. As for operation uncertainty, because the underlying driving force of hydropower operation is to maximize profit; thus, more than one operation mode might be conducted by one powerhouse. Fuzzy classification was applied to explore the proportion of different types of hydropeaking at one site. Even though four distinct groups of hydropeaking were revealed, three sites have more

than one dominant type of hydropeaking (OXB, 11278400 and 1128900). For example, gauge OXB had an even membership in both G2 (38%) and G3 (32%) which indicated that two dominant types of hydropeaking exist. Gauge 11278400 also had an even membership in G1 (40%) and G3 (54%) which indicated that two types of hydropeaking jointly occurred. Methodological uncertainty originated from threshold values, especially the annual mean flow-based threshold (X and $T3_t$). In addition, seasonal flow-normalization was recommended for future research. Even though thorough tests were conducted and coefficients of annual mean flow were selected due to the stable outputs of HEDA, it is possible that the generality of HEDA cannot capture some details of the hydropeaking flow regime of an individual river. Therefore, it is highly recommended to adjust these coefficients if the study site is a single river (Table 1 in SI II). Input data uncertainty arose from the scarcity of sub-daily flow records, particularly for streamflow, penstock flow and reservoir outflow. Reservoir outflow and penstock flow record the most original flow regime of hydropeaking flow which can be used to infer the operation of facilities while streamflow records the degraded hydropeaking pattern which is valuable to the study of flow-ecology relationships.

1.4 Conclusions

In this study, a new method (HEDA) has been developed in R statistical software to automate hydropeaking feature extraction with minimal subjective decisions, adjustments, and iterations. This allows for an analysis of hydropeaking flow at a large temporal and spatial scale. Then, hierarchical and fuzzy clustering analyses were used to explore and discover hydropeaking patterns in California, using seven ecologically relevant hydrologic metrics computed by HEDA. Four hydropeaking patterns have been identified: Frequent (G1), Large (G2), Supplementary (G3), and Regulated hydropeaking (G4). G1, frequent hydropeaking, is characterized by long rise/fall

processes of an individual peaking event ($\geq$ 3.5 hr) but has the highest annual frequency ($\geq$ 80%). Its long duration of rise/fall process with consistent rate of change indicates these sites are more likely to occur in large rivers while the highest annual frequency of hydropeaking can pose hydropeaking-induced flow alterations to the aquatic system constantly. G2, large hydropeaking, is characterized by long-lasting peaking retention ($\geq$ 5 hr) and a large range of flow amplitude. The reduction of the annual frequency of hydropeaking is compensated by increasing the duration of peaking. The reduced annual frequency might reduce the impacts of hydropeaking but the increased flow amplitude can offset this relief to the downstream aquatic systems. G3, supplementary hydropeaking, has the highest frequency of daily peaking events but with a lower magnitude and duration of the individual peaking event. G4, regulated hydropeaking, has the lowest peaking signals among the four groups due to constraints of environment and facilities. G3 has the third strongest impact on the aquatic systems mainly due to its low frequency while G4 should have the least impacts. The four hydropeaking flow regimes were identified from raw time-series flow records are dominant hydropeaking flow regimes for their associated facilities, and it is possible that facilities adopt more than one type of hydropower operations.

As for the relative significance of flow-alteration metrics, the duration and frequency of hydropeaking are principal variables governing the classification. Additionally, the magnitude, rate of change and timing of hydropeaking play less important roles in differentiating hydropeaking flow regimes. By analyzing the seasonality of hydropeaking, it is found that hydropeaking is more frequently conducted in the dry season and in drought years. However, sites having strong peaking flow regimes in the dry season tend to have strong hydropeaking in wet season. Finally, this study not only provides a valuable tool to help the community to sample high-

37

frequency flow alteration on a large spatial and temporal scale but also created a data analysis framework that can also be used worldwide to explore the underlying process especially in regions where documentations of hydropower operation are not well documented. Moreover, the classification of hydropeaking flow provides important insights into the patterns of hydropeaking flow regimes, which is difficult to gain by only knowing the operation modes. Meanwhile, having hydropeaking flow regimes classified into several groups simplified the problem and offers new opportunities to improve the understanding of the flow-ecology relationship. As for the future study, the flow-ecology relationship in the setting of hydropeaking flow and the spatial distribution of the classification are highly encouraged.

1.3   References

AASHTO, I., 2005. A summary of Existing Research on Low-Head Dam Removal Projects. Transportation Research Board (TRB).

Abu-Aly, T.R., Pasternack, G.B., Wyrick, J.R., Barker, R., Massa, D. and Johnson, T., 2014. Effects of LiDAR-derived, spatially distributed vegetation roughness on two-dimensional hydraulics in a gravel-cobble river at flows of 0.2 to 20 times bankfull. Geomorphology, 206, pp.468-482.

Annandale, G.W., 2018. Reservoir sedimentation management: A sustainabledevelopment challenge. IAHR.

Atkinson, E., 1996. The feasibility of flushing sediment from reservoirs.

Barker, J.R., Pasternack, G.B., Bratovich, P.M., Massa, D.A., Wyrick, J.R. and Johnson, T.R., 2018. Kayak drifter surface velocity observation for 2D hydraulic model validation. River Research and Applications, 34(2), pp.124-134.

Blum, M.D. and Törnqvist, T.E., 2000. Fluvial responses to climate and sea‐level change: a review and look forward. Sedimentology, 47, pp.2-48.

Chow, V.T., 1959. Open-channel hydraulics. McGraw-Hill civil engineering series.

Csiki, S. and Rhoads, B.L., 2010. Hydraulic and geomorphological effects of run-of-river dams. Progress in Physical Geography, 34(6), pp.755-780.

Curtis, J.A., Flint, L.E., Alpers, C.N. and Yarnell, S.M., 2005. Conceptual model of sediment processes in the upper Yuba River watershed, Sierra Nevada, CA. Geomorphology, 68(3-4), pp.149-166.

East, A.E., Pess, G.R., Bountry, J.A., Magirl, C.S., Ritchie, A.C., Logan, J.B., Randle, T.J., Mastin, M.C., Minear, J.T., Duda, J.J. and Liermann, M.C., 2015. Reprint of: Large-scale dam removal on the Elwha River, Washington, USA: River channel and floodplain geomorphic change. Geomorphology, 246, pp.687-708.

ESSA. 2019. River Bathymetry Toolkit (RBT). https://portal.opentopography.org/tools/viewTool?toolId=81. (Assessed 01 2019).

Fripp, J., Morris, G., Hajimirzaie, S. and Hoeft, C.C., 2020, May. Sedimentation and Small Dams. In World Environmental and Water Resources Congress 2020: Hydraulics, Waterways, and Water Distribution Systems Analysis (pp. 195-201). Reston, VA: American Society of Civil Engineers.

Garcia, M. ed., 2008, May. Sedimentation engineering: processes, measurements, modeling, and practice. American Society of Civil Engineers.

Grantham, T.E., Viers, J.H. and Moyle, P.B., 2014. Systematic screening of dams for environmental flow assessment and implementation. BioScience, 64(11), pp.1006-1018.

Grill, G., Lehner, B., Thieme, M., Geenen, B., Tickner, D., Antonelli, F., Babu, S., Borrelli, P., Cheng, L., Crochetiere, H. and Macedo, H.E., 2019. Mapping the world's free-flowing rivers. Nature, 569(7755), pp.215-221.

Horne, A., Webb, A., Stewardson, M., Richter, B. and Acreman, M. eds., 2017. Water for the environment: From policy and science to implementation and management. Academic Press.

Ho, M., Lall, U., Allaire, M., Devineni, N., Kwon, H.H., Pal, I., Raff, D. and Wegner, D., 2017. The future role of dams in the United States of America. Water Resources Research, 53(2), pp.982-998.

Hotchkiss, R. H. 1990. Reservoir sedimentation and sediment sluicing: experimental and numerical analysis.

Jarrett, R.D., 1992. Hydraulics of mountain rivers. Channel flow resistance: Centennial of Manning's formula, pp.287-298.

Julien, P.Y., 2010. Erosion and sedimentation. Cambridge university press.

Kibler, K.M., 2017. The Hydraulic size Of A Dam: A metric Indicating potential hydrologic impact For storage And diversion.

Kjaran, S.P., Hólm, S.L. and Myer, E.M., 2004. Lake circulation and sediment transport in Lake Myvatn. Aquatic Ecology, 38(2), pp.145-162.

Kouassi, K.L., Kouame, K.I., Konan, K.S., Angulo, M.S. and Deme, M., 2013. Two-dimensional numerical simulation of the hydro-sedimentary phenomena in Lake Taabo, Côte d'ivoire. Water resources management, 27(12), pp.4379-4394.

Kondolf, G.M., Gao, Y., Annandale, G.W., Morris, G.L., Jiang, E., Zhang, J., Cao, Y., Carling, P., Fu, K., Guo, Q. and Hotchkiss, R., 2014. Sustainable sediment management in reservoirs and regulated rivers: Experiences from five continents. Earth's Future, 2(5), pp.256-280.

Li, T. and Pasternack, G.B., 2020, August. Reservoir sedimentation management with upstream sediment remanipulated. In River Flow 2020: Proceedings of the 10th Conference on Fluvial Hydraulics (Delft, Netherlands, 7-10 July 2020) (p. 355). CRC Press.

Liro, M., 2015. Gravel-bed channel changes upstream of a reservoir: The case of the Dunajec River upstream of the Czorsztyn Reservoir, southern Poland. Geomorphology, 228, pp.694-702.

Liro, M., 2016. Development of sediment slug upstream from the Czorsztyn Reservoir (southern Poland) and its interaction with river morphology. Geomorphology, 253, pp.225-238.

Liro, M., 2019. Dam reservoir backwater as a field-scale laboratory of human-induced changes in river biogeomorphology: A review focused on gravel-bed rivers. Science of the Total Environment, 651, pp.2899-2912.

Liro, M., Ruiz-Villanueva, V., Mikuś, P., Wyżga, B. and Castellet, E.B., 2020. Changes in the hydrodynamics of a mountain river induced by dam reservoir backwater. Science of The Total Environment, 744, p.140555.

Lisle, T.E., Nelson, J.M., Pitlick, J., Madej, M.A. and Barkett, B.L., 2000. Variability of bed mobility in natural, gravel‐bed channels and adjustments to sediment load at local and reach scales. Water Resources Research, 36(12), pp.3743-3755.

Minear, J.T. and Kondolf, G.M., 2009. Estimating reservoir sedimentation rates at large spatial and temporal scales: A case study of California. Water Resources Research, 45(12).

Morris, G.L. and Fan, J., 1998. Reservoir sedimentation handbook: design and management of dams, reservoirs, and watersheds for sustainable use. McGraw Hill Professional.

Murray, A.B., 2003. Contrasting the goals, strategies, and predictions associated with simplified numerical models and detailed simulations. Geophysical Monograph-American Geophysical Union, 135, pp.151-168.

NID, 2021. National Inventory of Dams. https://nid.sec.usace.army.mil/ (Accessed 03 2021).

Palmieri, A., Shah, F. and Dinar, A., 2001. Economics of reservoir sedimentation and sustainable management of dams. Journal of environmental management, 61(2), pp.149-163.

Pasternack, G.B., Bounrisavong, M.K. and Parikh, K.K., 2008. Backwater control on riffle–pool hydraulics, fish habitat quality, and sediment transport regime in gravel-bed rivers. Journal of Hydrology, 357(1-2), pp.125-139.

Pasternack, G.B. and Hopkins, C.E., 2017. Near-census 2D model comparison between SRH-2D and TUFLOW GPU for use in gravel/cobble rivers. Davis (CA): University of California at Davis. Prepared for Yuba County Water Agency.

Pasternack, G.B., 2020. River Restoration: Disappointing, Nascent, Yet Desperately Needed.

Person, E., 2013. Impact of hydropeaking on fish and their habitat (No. BOOK). EPFL-LCH.

Queen, R., 2018. Morphodynamic modeling of flow and sediment transport over low-head, Run-of-River dams. Hydropower Foundation.

Randle, T., Kimbrel, S., Collins, K., Boyd, P., Jonas, M., Vermeeren, R., Eidson, D., Cooper, D., Shelley, J., Juracek, K. and Fripp, J., 2017. Frequently asked questions about reservoir sedimentation and sustainability. Subcommittee on Sedimentation, National Reservoir Sedimentation.

Roads, J.O., Chen, S.C., Guetter, A.K. and Georgakakos, K.P., 1994. Large-scale aspects of the United States hydrologic cycle. Bulletin of the American Meteorological Society, 75(9), pp.1589-1610.

Shields Jr, F.D., 2009. Do we know enough about controlling sediment to mitigate damage to stream ecosystems?. Ecological Engineering, 35(12), pp.1727-1733.

Schleiss, A.J., 2018. The challenge of restoring dynamics by river engineering: where to find the truth about river flow-in the computer, in the lab or in the field?. In 9th International conference on fluvial hydraulics River Flow 2018 (No. POST_TALK).

Schwindt, S., Pasternack, G.B., Bratovich, P.M., Rabone, G. and Simodynes, D., 2019. Hydro-morphological parameters generate lifespan maps for stream restoration management. Journal of environmental management, 232, pp.475-489.

Skelton, G. 2017. California's reservoirs are filled with gunk, and it's crowding out room to store water. Los Angeles Times. https://www.latimes.com/politics/la-pol-sac-skelton-silt-california-dams-20170306-story.html (Acessed 03 2021).

Thorne, C., Hey, R. and Newson, M., 2005. Applied fluvial geomorphology for river engineering and management. John Wiley and Sons Ltd.

Toone, J., Rice, S.P. and Piégay, H., 2014. Spatial discontinuity and temporal evolution of channel morphology along a mixed bedrock-alluvial river, upper Drôme River, southeast France: Contingent responses to external and internal controls. Geomorphology, 205, pp.5-16.

USACE 2015. US Army Corps of Engineers. Dredging and Dredged Material Management.

Viviroli, D., Weingartner, R. and Messerli, B., 2003. Assessing the hydrological significance of the world's mountains. Mountain research and Development, 23(1), pp.32-40.

WBM. 2018. TUFLOW Classic/HPC User Manual Build 2018-03-AD. *WBM Oceanics Australia*.

Wilcock, P.R., Kondolf, G.M., Matthews, W.G. and Barta, A.F., 1996. Specification of sediment maintenance flows for a large gravel‐bed river. Water Resources Research, 32(9), pp.2911-2921.

Yang, G., Bowling, L.C., Cherkauer, K.A. and Pijanowski, B.C., 2011. The impact of urban development on hydrologic regime from catchment to basin scales. Landscape and Urban Planning, 103(2), pp.237-247.

CHAPTER 2. RESERVOIR OPERATIONS REDISTRIBUTE SEDIMENT IN SMALL MOUNTAIN RESERVOIRS

2.1 Abstract

Reservoir sedimentation management has become an important topic to large dams in the United States due to their historical design, current age, and increased environmental regulation. Less attention has been paid to small dams in remote mountains even though they are facing a more urgent sedimentation problem due to their relatively small storage. This study aimed to explore the relation between reservoir operations and sediment redistribution in a small dam's backwater zone to seek potential alternative solutions to flushing and excavation. Mindful timing and magnitude adjustment of water transfer, involving water diverted across watersheds by tunnels, through a reservoir was hypothesized to strategically redistribute sediment erosion for sites with water transfer/diversion facilities in the main channel. For a study site in the north-central Sierra Mountains of California, sediment erosion within the backwater zone increased by > 100% by turning the water transfer to the maximum quantity, which is 12 times higher than mean annual discharge. With reservoir stage drawdown, the increment of sediment erosion was further increased by > 50% compared with water-transfer-only scenarios. Upstream inflow with daily flow occurrence of 5-25% was found to be the optimal hydrologic condition for water transfer. These results indicated that water transfer optimization is a promising strategy to redistribute deposited sediment downstream of a dam with appropriate stage drawdown or to prevent sediment migration through a reservoir.

2.2 Introduction

Mountain rivers are defined as rivers located in a high-relief, high-elevation physiographic region with slope $\geq$ 0.002 m/m (Jarrett 1992) and a mean elevation above sea level $\geq$ 1000 m (Viviroli et al. 2003). Many dams have been built in these regions due to their rich water resources and high potential for energy (Person 2013, Grantham et al. 2014). Nowadays, water and sediment transfers by rivers are impeded by 91,457 dams in the Unites States (NID, 2021). About 93% of the dams are small dams, defined as a collection of low-head dams, run-of-the-river dams and any other dam whose height does not exceed 15 m (AASHTO 2005). Many small dams were placed in rivers as a way to transfer water for irrigation, municipal water supply and then for electricity generation to increase the grid reliability and the renewable energy portfolio (Csiki et al. 2010, Grantham et al. 2014). As a consequence, flow regulation associated with dams has led to changes intertwining hydrologic, ecologic, and geomorphic functioning of rivers, including upstream and downstream effects (Schleiss 2018, Grill et al. 2019). Reservoir sedimentation is always one of the critical challenges small dams face, as many of them fill up much faster with sediment given that they can be higher up in a catchment where sediment yield is higher and they have smaller total volume. Small dams also vary far more than large dams in terms of their wide dispersal across landscape positions, yielding a greater range of management issues and environmental concerns (Ho et al. 2017, Fripp et al. 2020, Li et al. 2020).

Reservoir sedimentation is the term used to describe the process of erosion, entrainment, transportation, deposition and compaction of sediment carried in the reservoir upstream of a dam

(Morris et al. 1998, Julien 2010). This sedimentation process has been ascribed to the backwater effect, the impact of the newly formed hydraulic base level on the upstream reach, including reduced flow velocity and increased water depth. Backwater is the water profile with a flow depth higher than the normal and critical flow depths (Chow 1959). In fluvial geomorphology, it is also defined as the water profile with flow depth higher than the average flow depth in the reservoir because the normal and critical flow depths of a natural river are difficult to calculate (Liro 2019). Due to the reduced flow velocity, more incoming coarse sediment tends to deposit at the reservoir head and then the focal point of deposition migrates upstream (Hotchkiss 1990). The primary sedimentation impact is storage loss that impairs water supply, hydropower and flood control (Garcia 2008). The secondary effect is associated with key locations in the reservoir, such as low-level valves and diversion tunnels that need to be kept free of sediment to maintain environmental flow regimes below dams and to provide water transfer among different reservoirs.

The array of reservoir sedimentation management strategies has been divided into three categories: (1) reduce sediment yield from the contributing watershed; (2) minimize sediment deposition in the reservoir; and (3) increase or recover reservoir volume (Kondolf et al. 2014). Hydraulic and mechanical excavation are two strategies widely used to reduce deposited sediment (Schleiss et al. 2016, Annandale et al. 2018). Hydraulic excavation involves adjusting flow operation based on the natural flow regime to maximize sediment transport, including flushing of deposited sediment with stage drawdown. Flushing is the management strategy mostly applied to small mountain reservoirs with hydraulic size (ratio of reservoir storage capacity to mean annual discharge) less than 0.02 (Atkinson 1996). Nevertheless, its impact to the downstream ecosystem and the resizing and clogging of low-level outlets limits its implementation (Kondolf et al. 1996). Mechanical

excavation removes accumulated sediments by heavy equipment or hydraulic pumps on barges with intakes (USACE 2015). This strategy requires expensive hauling and storage of removed material, which can also raise further challenges and constraints.

Reservoir storage recovery strategies have been primarily applied to large dams due to their profound effects on the riverine ecosystem (East et al. 2015). Relatively little is known about the status and consequences of small dams because the cost to study them can be higher than the cost of removing the dam (Skelton, 2017, Queen 2018). For small dams that still function but are harmed by excessive sedimentation, this study asks whether a better management strategy for protecting key dam functions could be tailored based on the current understanding of reservoir sedimentation and hydrologic operations. To seek solutions for the above question, this study explored possible management strategies of small mountain reservoirs that are part of a complex network of tunnels, diversions, canals, and facilities in a mountain region. How a water transfer/diversion, storage, and release network across watersheds is operated could significantly exacerbate or ameliorate reservoir sedimentation. For example, in a drought year with no floods, what if the energetic water transfers were to mobilize sediment in a reservoir's backwater zone to deposit at a designated location of concern, such as in front of a key low-elevation outlet; or what if remobilization opens a significant amount of "accommodation space" (Blum et al. 2000) in the reservoir to enable future flood deposits to fill up that space?

The overall goal of this study was to evaluate sediment erosion potential under different reservoir operations for small dams in confined mountain rivers, and how water transfers might help accelerate or mitigate reservoir sedimentation by redistributing deposited sediment. A diversion

dam (dam height < 15 m) in the Yuba River catchment in north-central California, USA served as the testbed to represent small dams usually having a hydraulic size below 0.01 (Kibler, 2017). Water transfer is proposed to be a supplementary strategy to sediment flushing. Three specific objectives were established to address the overall goal: (i) investigating the baseline sediment dynamism affected by the anthropogenic interventions beyond a small dam's blockage impact, (ii) estimating how altered water transfer scenarios could aid sediment management with exploratory simulations, and (iii) evaluating the optimal hydrologic conditions for water transfer.

2.2.1 Scientific questions and hypotheses

To achieve the objectives aforementioned, three questions were made to analyze impacts of water transfer and joint impacts of water transfer and stage drawdown on the sediment erosion as well find the optimal range of hydrologic conditions and explain the mechanistic sequence of hydrodynamics trigged by water transfer (Table 2.1). Specifically, water transfer is hypothesized to be a potential strategy that can increase sediment erosion in a small reservoir and transport sediment to a designated area. Stage drawdown is hypothesized to be the prerequisite of water transfer. Because upstream inflow and WSE are correlated, the joint effect of water transfer and stage drawdown on sediment erosion is hypothesized to be limited to a certain range of hydrologic conditions. Therefore, an optimal range of hydrologic conditions for the proposed strategy was conjectured to exist. Additionally, backwater effects are hypothesized to be a critical underlying governing mechanism of reservoir sediment dynamism. It is hypothesized that eroded area will increase and move towards (or down) the reservoir if the length of the backwater zone shrinks.

Table 2.1. List of scientific questions about impacts and applications of the proposed flow operation.

Question ID	Questions
Qt1	How is sediment erosion affected by water transfer?
Qt2	How is sediment erosion affected by the interplay of water transfer and water surface elevation?
Qt3	Optimal hydrologic conditions for water transfer?

2.3   Material and methods

2.3.1   Experimental design

To answer scientific questions using hypothesis testing, five scenarios were designed (Table 2.2). To infer sediment erosion in regular reservoir operation for representative grain sizes of focus, 18 flow events (Table 1 in supplementary material I) were simulated for five representative grain sizes (1, 3, 8, 32, and 64mm) in scenario S1. To simplify the analyses of scenarios S2-S5, one representative grain size was selected based on the sensitivity analysis. Three out of 18 flow events were selected to simulate sediment transport in the base, medium and high flow regime. Comparison between S1, S2 and S3 were to answer Qt1. Comparisons between S3 to S5 were to answer Qt2 and Qt3.

Table 2.2. Exploratory modeling scenarios.

Scenario	Name of scenario	Design conceptualization
S1	Current flow operation	S1 is the reference scenario.
S2	Low water transfer	Water transfer was reduced to 10% of the original tunnel flow.
S3	High water transfer	Water transfer discharge was set to the maximum level ($24.4 \text{ m}^3/\text{s}$).
S4	Water transfer and stage drawdown I	Adjusting water transfer discharge and WSE jointly. WSE was reduced by one-third of the adjustable range of WSE (difference between the flood and minimum WSE).
S5	Water transfer and stage drawdown II	WSE was reduced by two-thirds of the adjustable range of WSE.

2.3.2 Data analysis framework

To evaluate sediment dynamism, spatially explicit bed shear stress and flow depth rasters were used to describe scour potential (independent of sediment supply), the location(s) where sediment erosion would happen relative to key infrastructure, and the longitudinal extent of backwater effects (Figure 2.1). Three test metrics, the areal percentage of unstable river bed (section 2.3.5.1), sediment transport distance (section 2.6.2) and longitudinal extent of backwater effects (section 2.6.3) were computed and used to address the questions and hypotheses.
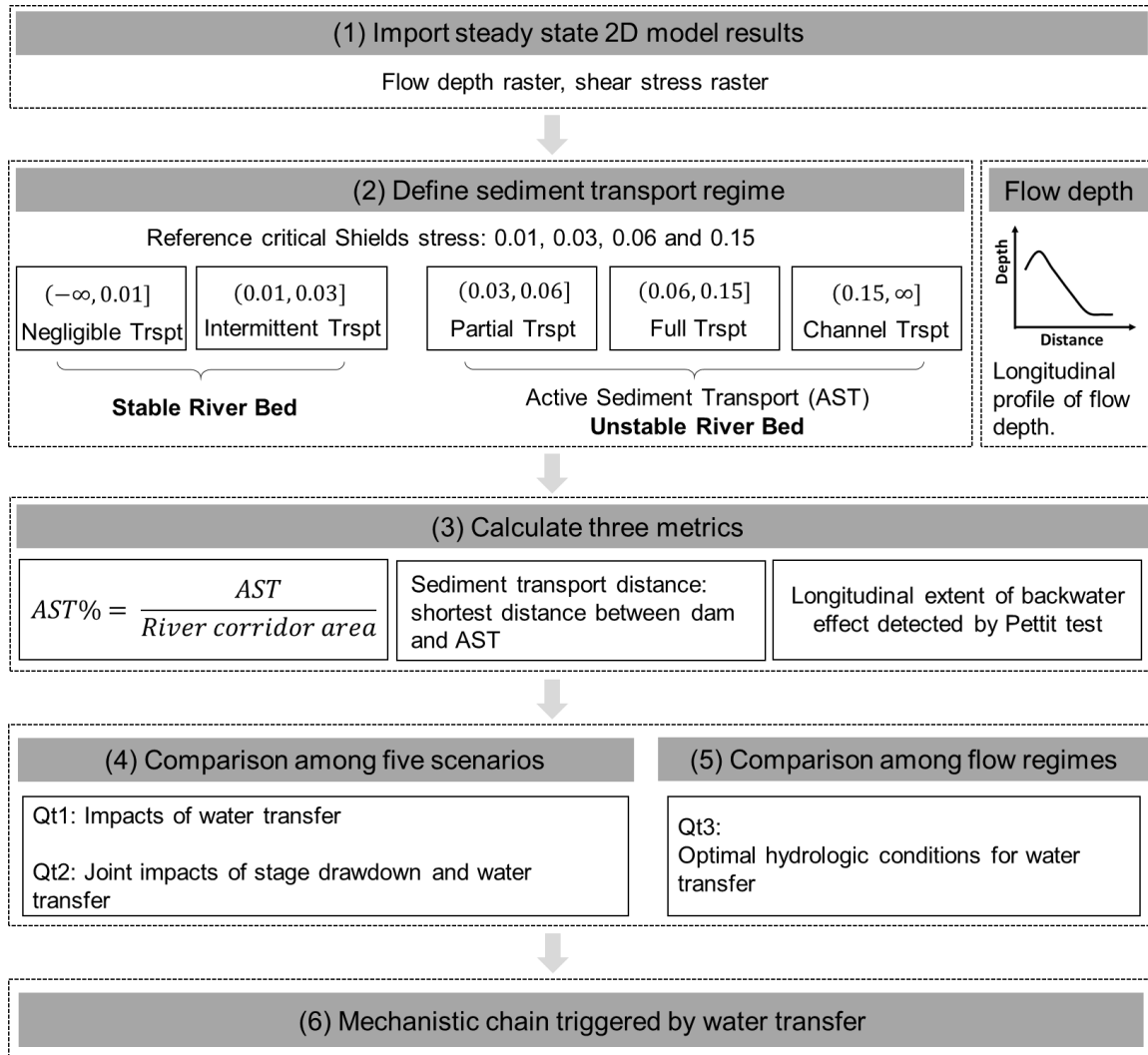
Figure 2.1. Data analysis framework developed in this study.

2.3.3 Study site

In-channel sediment supplies and hillslope processes (mass wasting and land-surface erosion) are the primary sources of ongoing sediment contribution in the Yuba River basin (Curtis et al. 2005). Most in-channel supplies are attributed to legacy materials from hydraulic gold mining with erosion in upland tributaries. As a consequence, LCD experiences excessive sediment deposition leading to impairment of operations for environmental flow releases. The study reach length affected by LCD (~ 0.5 km) was selected based on the distribution of subaerial gravel-bar

deposition (Figure 2.2). From upstream to downstream, the extent of the backwater zone was evident in a channel boundary transition from bedrock to the onset of bar deposition. Therefore, upstream where bar deposition transitioned to bedrock was deemed to be free of significant backwatering.
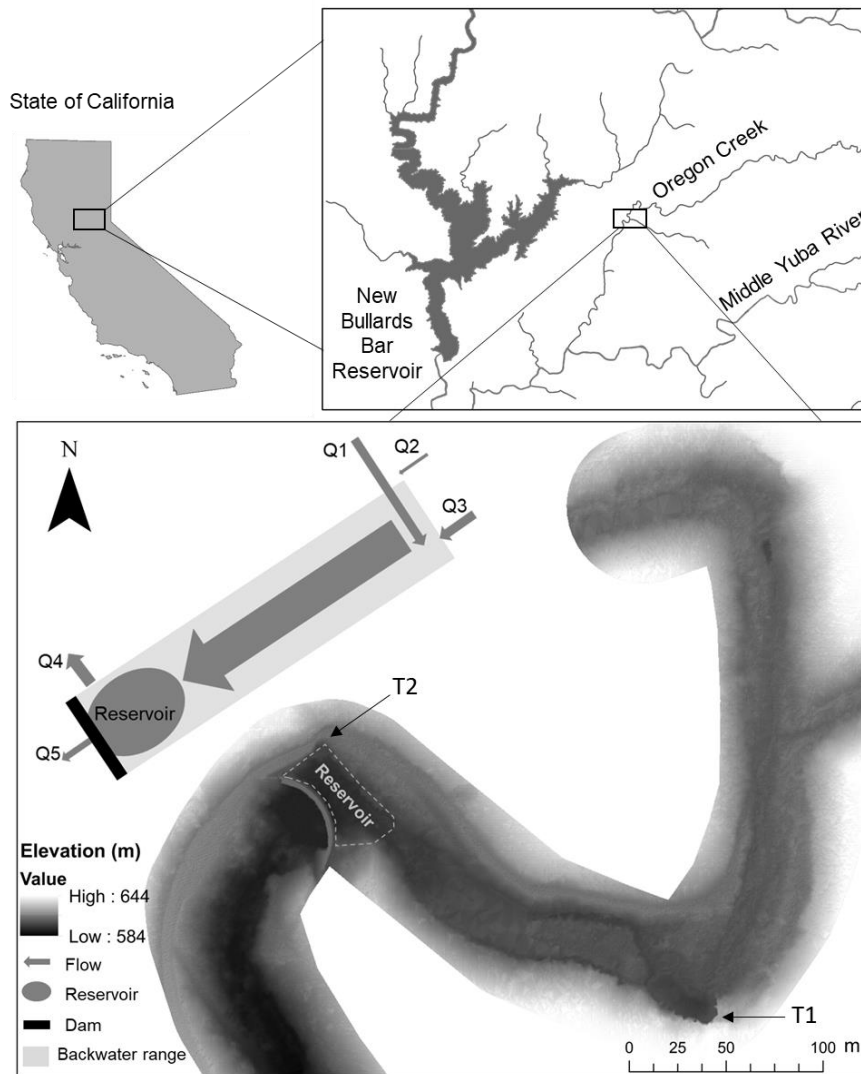
Figure 2.2. Yuba River catchment showing the path of the Middle Yuba River and its tributary Oregon Creek. The study reach was detailed by the digital elevation model (DEM). Next to the DEM is a simplified hydrologic schematic diagram of inflows (Q1, Q2, and Q3, Table 3.) and outflows (Q4 and Q5, Table 3).

50

Log Cabin Dam (LCD) is a 32-m-radius and 12-m height concrete arch diversion dam in a remote mountain canyon, located 6.4 km upstream from Oregon Creek's confluence with the Middle Yuba River (Figure 2.3). The mean annual flow of Oregon Creek is 2 m^3/s. Over half of the time (69%), Oregon Creek had zero flow (summer and fall). Winter floods driven by atmospheric rivers regularly flow over the dam with a strong downstream current. Two diversion tunnels are operated near LCD. Lohman Ridge Diversion Tunnel (T1) conveys a maximum flow of 24.4 m^3/s from Middle Yuba River to Oregon Creek. T1 transfers water 12 times larger than the discharge that Oregon Creek carries. Camptonville Tunnel (T2) conveys 31 m^3/s water from Oregon Creek to New Bullards Bar Reservoir (YWA, 2012). Inflow to LCD consists of Oregon Creek flow, Grizzly Creek flow and the outflow from T1 (Table 2.3).

Figure 2.3. Log Cabin Dam. A: Low-Level outlet in LCD site (Diameter: 1.5 m). B: fish outlet for the environmental flow release.

Table 2.3. Log Cabin Dam USGS gauges. Location of gauges are marked in Figure 2.3.

Gage name	USGS	Symbol	Date
Oregon Creek	11409300	Q1*	NA
Grizzly Creek	NA	Q2*	NA
T1	11408870	Q3	
T2	11409350	Q4	2000-09-30 to 2018-09-30
Oregon Creek outflow	11409400	Q5	

*Q1 was estimated based on the mass conservation to match the date of the flow data used in the simulation. Grizzly Creek (Q2) is the only ungagged input. Area-weighted scaling was used to estimate water from Grizzly Creek (Roads et al. 1994, Yang et al. 2011).

2.3.4   2D Hydrodynamic Modelling

The LCD study area is in a confined canyon protected from wind fetch or waves (Figure 2.4). The maximum pool volume of LCD is 111,013 m^3 with a corresponding hydraulic size of 0.005. The density currents or other complex lake physical processes were assumed to be negligible. Tunnel inflow and outflow structures are on opposite sides of the river, potentially setting up a cross-channel sediment transport under some conditions. Reservoir sedimentation in the backwater zone shows lateral and longitudinal variability consistent with sediment redistribution during shallow flows. In light of these physical conditions, the decision was taken to apply a two-dimensional depth-averaged (2D) hydrodynamic model to evaluate both the lateral and longitudinal positioning of sediment erosion under different scenarios. A one-dimensional model would not have resolved the cross-channel hydraulics essential to addressing the study's questions. A three-dimensional model was not necessary in light of the relatively shallow depths of such a small reservoir and the

absence of wind-driving mixing (Kjaran et al., 2004, Kouassi et al., 2013).

2.3.4.1 Digital elevation model

A combination of airborne near-infrared Light Detection and Ranging (LiDAR) point cloud data from the OpenTopography website (2014 USFS Tahoe National Forest LiDAR dataset (8.9 pts/m^2)) and survey points mapped in October to November 2018 using a Leica TPS1100 robotic total station and Trimble R8 Real-Time Kinematic Global Positioning System unit were used to make a digital elevation model (DEM). The point density in areas covered by LiDAR or with little morphologic variability was 1pt/9m^2. In other areas, the point density was 1-1.5 pts/m^2. The unwadable reservoir was mapped by boat using a single-beam echosounder. An one-meter resolution DEM was produced using these points followed published procedures and with quality control/quality assurance measures taken (Barker et al. 2018).

2.3.4.2 Model parameters

The commercial software TUFLOW HPC was used to simulate steady-state lateral and longitudinal hydraulics. TUFLOW HPC is an explicit solver parallelized across multiple computational cores for the full 2D Shallow Water Equations, including a sub-grid scale eddy viscosity model (WBM 2018). A computational mesh was built with one-meter grid size. The computational domain started 0.5 km upstream and ended at LCD. The default TUFLOW Smagorinsky viscosity was used for turbulence closure with a coefficient value of 0.5 and a constant value of 0.005 m^2/s. Oregon Creek has little aquatic vegetation but its banks are heavily covered (> 50%) by riparian vegetation, especially willows. Therefore, vegetated surface roughness was assigned using a Manning's n of 0.24 based on Abu-Aly et al. (2014). As for the unvegetated surface roughness, due to the L-shape channel geometry, Oregon Creek has an abrupt

53

variation in grain size from gravel to sand/clay. Thus, a spatially distributed Manning's n was used to represent flow resistance caused by gravel (0.04) or sand/clay (0.02) substrate.
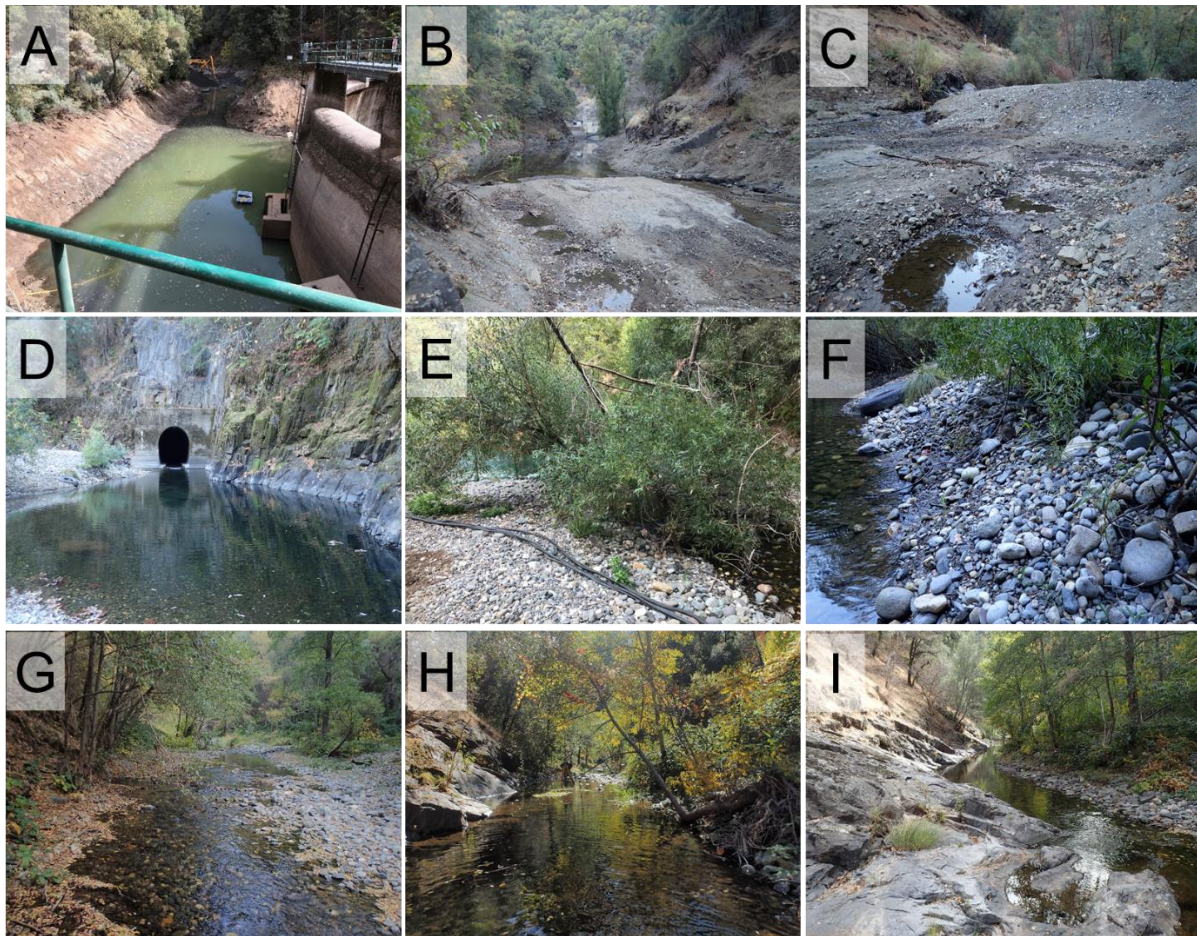
Figure 2.4. Photo collection of substrates. Letter A to I refers to the sequencing of views from at the dam (A) to further upstream (I).

2.3.4.3 Steady-state flow simulations

Steady-state flow simulations of in-channel flows (not floods) were used to evaluate how sediment would respond to different water transfer schemes under a constant volume of water with sediment load it is capable of carrying, and thus to know what type of flow events can obtain the designated level and magnitude of sediment erosion. Steady-state flow simulation was selected because water

transfers tend to be operated over many days, holding relatively steady in all the flow regimes.

Eighteen flow events, ranging from the lowest to highest flow, were simulated in the regular reservoir operation scenario (table 1 in supplementary material I). Three representative flow events out of 18 flow events were selected for scenario 2 to 5. To select representative flow events, spearman correlation and flow frequency analysis were applied to infer the relationship between inflows, outflows and WSE, and the recurrence rate of upstream flow separately. The high correlation coefficient (>0.8) between upstream flow and WSE implied that LCD tended to pond more water when the upstream inflow increased. Meanwhile, the correlation coefficients between other inflows and outflows were all below 0.3, indicating a relatively weak relationship. On the basis of daily flow recurrence from 1970 to 2000, the upstream flow regime was categorized into: base flow [25%, 70%], medium flow [5%, 25%], high flow [1%, 5%] and flood regimes [$-\infty$, 1%] separately from which three representative flow events were selected. The corresponding breakpoints for the four flow regimes were 1.56, 7.65, and 21.24 m^3/s. The flood regime was not considered because WSE tends to constantly reach the spillway elevation (601 m) due to the excessive inflow, which makes WSE adjustment impossible.

Given the remote and extremely hazardous conditions in the river during even modest flows, most model validation was infeasible except for comparing modeled and observed water surface elevations at the dam crest. Comparing WSE is in fact the common strategy for validating lake/reservoir hydrodynamic models, if any validation is done at all (Kouassi et al., 2013; Castillo et al. 2015). As a result, the study is in the realm of scientific exploration and not predictive forecasting with high certainty, using the uncertainty terminology and concepts of Murray (2003).

In addition, TUFLOW HPC is a well-developed model that has been extensively validated for use in Yuba River (Pasternack et al. 2017, Schwindt et al. 2019).

Table 2.4. Representative steady-state flow events of the three flow regimes.

Flow regime	WSE (m)	Q1 (m³/s)	Q2 (m³/s)	Q3 (m³/s)	Q4 (m³/s)
Base flow	600	0.3	0.1	21.5	21.4
Medium flow	600	6.3	1.2	16.5	23.3
High flow	600	18.0	3.4	6.8	27.6

2.3.5 Test metrics

2.3.5.1 Sediment erosion capability

To infer the scour capability of water to the deposited sediment, bed shear stress (Eq. 2-1) was first converted into non-dimensional shear stress (Shields stress, Eq. 2-2) to make results comparable across all scenarios. Instead of calculating a specific sediment transport rate, the local Shields stress (τ^*) values were categorized into sediment transport regimes defined by Lisle et al. (2000) where values of $\tau^* < 0.01$ correspond to negligible transport, $0.01 < \tau^* < 0.03$ correspond to intermittent entrainment, $0.03 < \tau^* < 0.06$ corresponds to partial transport (Wilcock et al., 1996), $0.06 < \tau^* < 0.15$ corresponds to full transport, and $\tau^* > 0.15$ corresponds to channel alteration. The use of groupings significantly reduces uncertainty and simplifies the prediction target, because the exact value from the 2D model does not matter, only the assignment of the correct group label. Intermittent transport indicated disturbances exist to the substrate of benthic organisms, but not necessarily to sediment movement. Partial transport implies some over-ample and over-exposed

56

particles of a given size on the bed surface area are active while others of the same size are immobile. Full transport implies a consistent 'conveyor belt' of sediment transport along the bed, up to two grains thick. Channel alteration transport indicates an increased scour potential compared with that in full transport, possibly with riverbed reconfiguration.

To further simplify erosion analysis and increase the likelihood of predictive success, partial, full and channel alteration transport regimes were grouped into a single active sediment transport regime (AST). Area covered by AST was referred to as an unstable riverbed. The normalized-areal coverage of AST (Ast, Eq. 2-3) was used as the test metric to evaluate the scour capability of water. Meanwhile, area covered by negligible and intermittent transport regimes were assumed to be stable riverbed.

$$\tau_b = \rho g V^2 n^2 \Big/ h^{1/3} \qquad (2\text{-}1)$$

$$\tau^* = \tau_b \Big/ (\rho_s - \rho_w) g d \qquad (2\text{-}2)$$

$$A_{st} = \frac{(A_p + A_f + A_c)}{TA_{s1}} * 100\% \qquad (2\text{-}3)$$

where ρ_w is water density, ρ_s is bed particle bulk density, d is the representative grain size. A_p, A_f, A_c are the areal coverage of partial, full and channel alteration regimes respectively. A_{st} is the areal coverage of AST normalized by the maximum total wet area in S1 (14,985 m^2). $A_{st} = 100\%$ means that the whole channel is unstable while the minimum $A_{st} = 0\%$ means that the whole channel is stable. This approach evaluates sediment transport capacity of water, so it is independent of sediment supply. It is reporting the potential for what could happen to sediment in the study area.

57

2.3.5.2 Shortest distance between AST and T2

The second test metric characterizes the shortest distance between AST and T2. The sediment transport distance was defined as the shortest distance between T2 and the cross-section with an AST coverage $\leq 50\%$. To calculate the AST coverage within each cross-section, 102 cross-sections along the centerline of the corridor were created by River Bathymetry Toolkit (ESSA 2019). The maximum wet area in S1 and bank extended from that to where the vegetation started to intensively occur were delineated as the river corridor based on its definition (Thorne et al. 2005). The percentage of AST coverage within each cross-section was calculated by dividing AST coverage by the area of the cross-section.

2.3.5.3 Longitudinal extent of backwater effect

The Pettit test allowed for automatic detection of the location of a change in river hydrodynamics along the longitudinal river profile (Liro et al. 2020). This test previously detected homogeneous river sections with regard to active channel width (Toone et al. 2014), morphological channel changes (Liro 2015) and in-channel sedimentation (Liro 2016). It assumes a sequence of random values X_1, X_2, to X_T has a change point at τ if X_t for $t = 1,\ 2$, to τ has a common distribution function $F_1(x)$, X_t for $t = \tau + 1$ to T has a common distribution function $F_2(x)$ and $F_1(x) \neq F_2(x)$. The null hypothesis (H_0) is defined by the stationarity of the series, i.e. no change (or T=n). The H_0 is tested against the alternative hypothesis H_a defined by a change. Let t be the rank and K_T the nonparametric statistic:

$$U_{t,T} = \sum_{i=1}^{t} \sum_{j=t+1}^{T} sign(X_i - X_j) \tag{2-4}$$

$$K_T = \max_{1 \leq i \leq T} |U_{t,T}| \tag{2-5}$$

For a given scenario, the averaged flow depth of a given flow event was calculated for consecutive river cross-sections represented a data series which was analyzed with the test to identify the location of a change disrupting its homogeneity.

2.4   Results

The design of scenarios and selection of representative grain size were made based on the understanding of sediment erosion in the regular reservoir operation. Therefore, sediment erosion pattern in the baseline scenario was analyzed first. As for the other four scenarios, results were analyzed separately for the whole channel and backwater zone.

2.4.1   Sediment erosion in regular reservoir operation

The areal percentage of AST of five grains can be summarized into two groups by grain size of eight mm. When the grain size was smaller than eight mm, around 50% of the study reach was occupied by unstable river bed. When the grain size was larger than that, around 70% of the river bed was stable. Spatially, the longitudinal A_{st} indicates grains smaller than eight mm passed through the backwater zone and entered the reservoir in all simulated flow events, while most of the large grains (> 8mm) would stop near the river bend (T1) except for relatively low WSE (Figure 2.5). Therefore, three mm was selected as the representative grain size used in the other four scenarios.
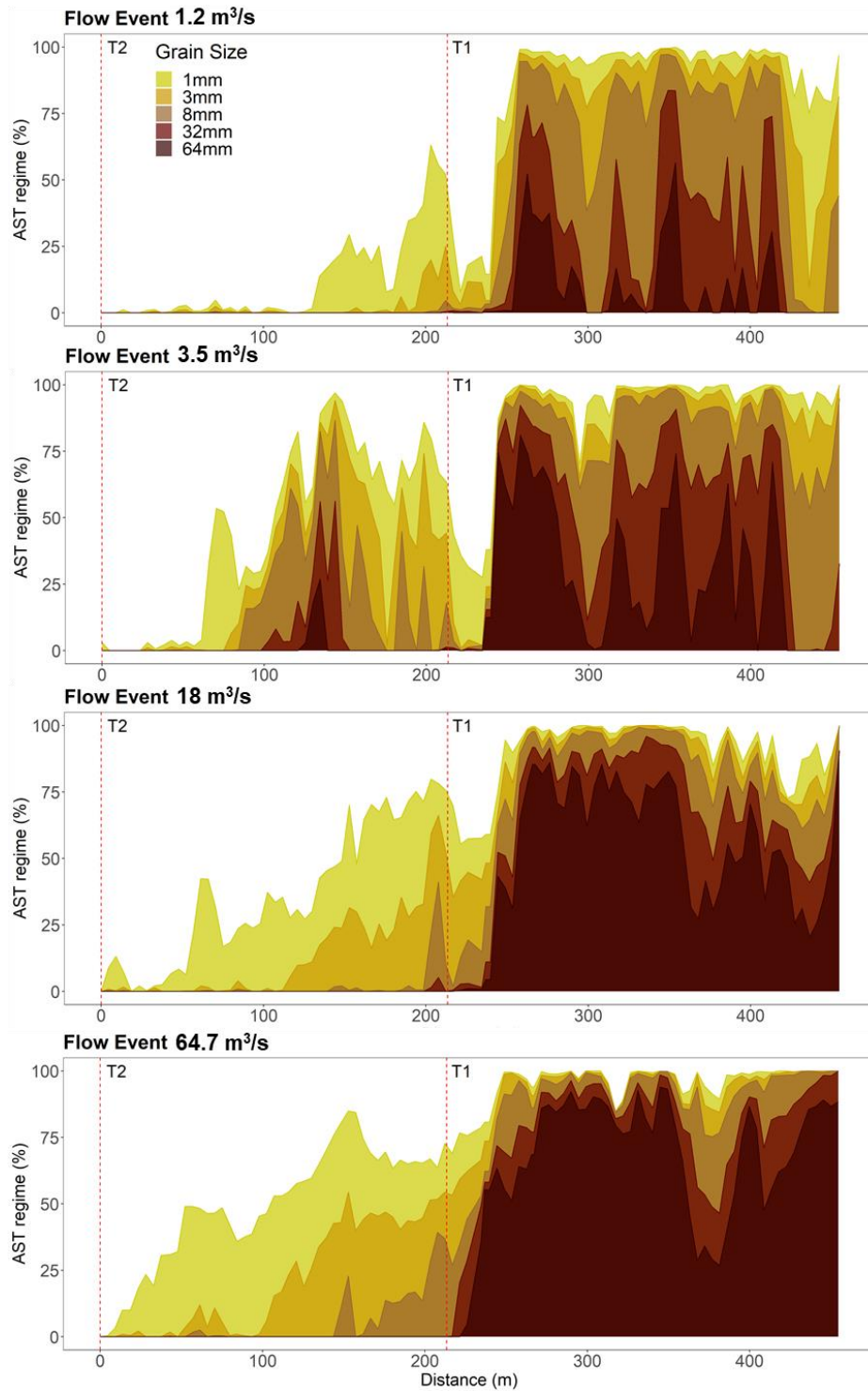
Figure 2.5. Longitudinal variation of AST regime from upstream (457 m) to T2 (0 m) in S1. T1 is

Lohman Ridge Tunnel. T2 is the position of Camptonville Tunnel.

In the 18 simulated flow events, the spatial distribution of AST in the reference scenario exhibited three modes (M1, M2 and M3) and were jointly controlled by the upstream inflow (Q1+Q2), tunnel flow (Q3) and water surface elevation (WSE) (Figure 2.7). In M1, AST mainly occurred upstream of T1 when no water transfer conducted. The A_{st} in the upstream of T1 was positively related to the magnitude of upstream flow. In M2, not only the upstream but also area downstream of T1 had AST. The reduced WSE freed space for the upstream flow and tunnel flow and thus allowed sediment to be eroded downstream of T1. In addition, the pathway of AST was always constrained within the side channel. In M3, the whole channel was fully activated. M3 occurred in the flood regime which always has a WSE reaching the spillway height (601 m). In this circumstance, even though the backwater effect was the strongest, upstream flow was strong enough to transport sediment into the reservoir.
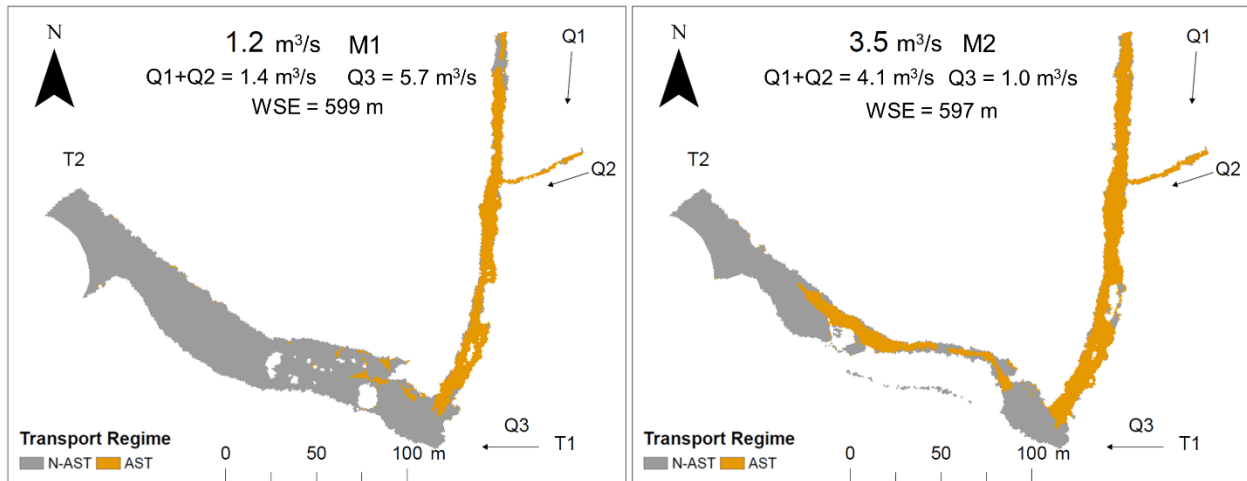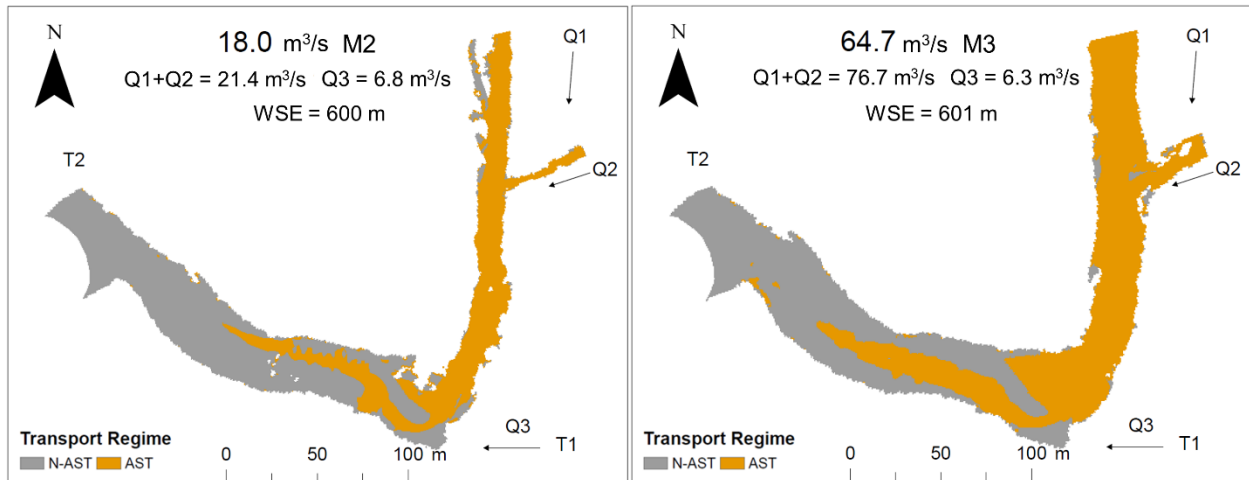
Figure 2.6. Spatial distribution of the sediment transport regimes in S1. Q1 is the Oregon Creek, Q2 is Grizzly Creek flow, Q3 is flow out of Lohman Ridge Tunnel (T1).

Transitions among the three modes were primarily controlled by upstream flow and WSE. Both M1 and M2 occurred in non-flood flow events. The transition between M1 and M2 was controlled by the joint effect of WSE and upstream flow. M1 was formed because the high WSE stopped upstream flow from entering the impounded area while the tunnel water was weak. With the same magnitude of upstream inflow, lowering WSE switched M1 to M2. Meanwhile, the transition between M2 and M3 was controlled by the upstream flow. As long as upstream flow reached the magnitude that water can fill the reservoir, M3 will occur no matter whether the tunnel was turned on or not.

2.4.2 Sediment erosion pattern in the whole channel

2.4.2.1 Water transfer

Adjusting tunnel operation had limited impacts on sediment erosion along the whole channel (Figure 2.8 and Figure 2.9). In water-transfer scenarios (S2 and S3), AST coverage increased along

with upstream inflow. The highest A_{st} in both S2 and S3 occurred in high flow regime (S2: 23%; S3: 27%) and the lowest A_{st} was in the base flow regime (S2 and S3: 3%). In addition, the variance of A_{st} caused by water transfer was negatively related to upstream inflow. For example, compared with A_{st} in S1, reducing water transfer discharge by 10% of the original discharge caused negligible impacts on A_{st} in S2. The A_{st} was increased by less than 8% in S2 across all three flow events. Compare S3 with S2, turning on the tunnel water to its maximum level increased A_{st} by 14%, 24% and 18% in the three flow regimes respectively.
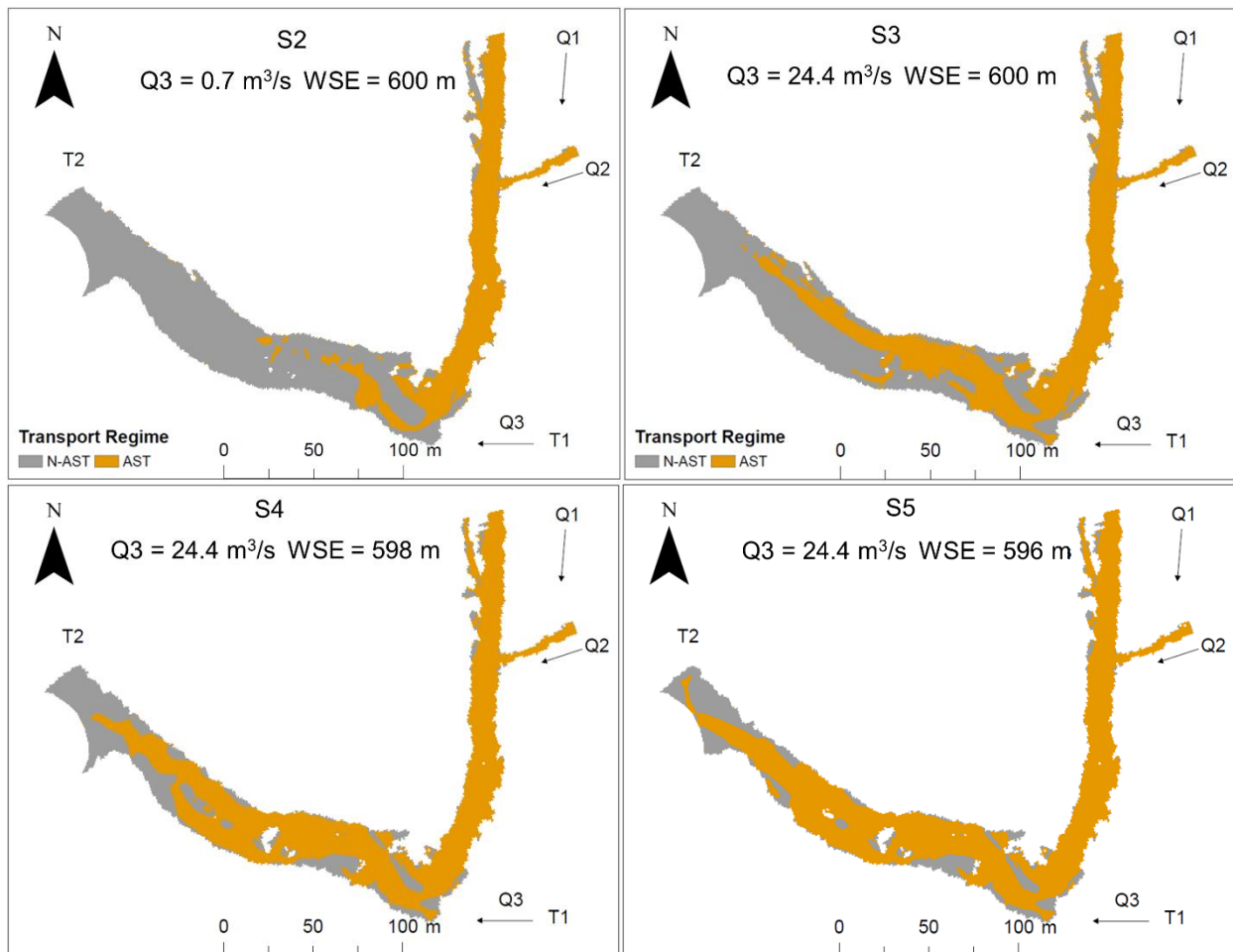
Figure 2.7. Spatial distribution of the sediment transport regimes of high flow regime (flow event 18 m³/s) from S2 to S5. Q3 is out of Lohman Ridge Tunnel (T1).
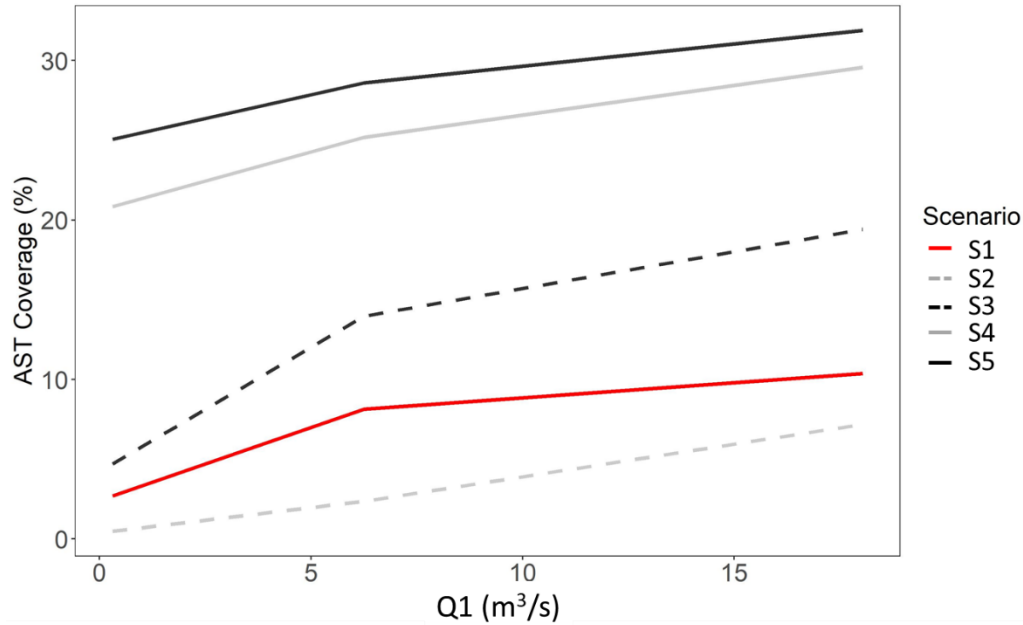
Figure 2.8. Areal percentage of AST of seven scenarios in the downstream of T1.

2.4.2.2 Water transfer with stage drawdown

Different from water transfer, lowering WSE can erode more deposited sediment across the whole channel and further increase A_{st} from water transfer scenarios (Figure 2.8). A_{st} in both S4 and S5 ranked the top two among all scenarios. In S4, 17, 32 and 42% of the study reach was covered by AST in base, medium and high flow regimes respectively. In S5, 21, 36 and 46% of the study reach was covered by AST. Compared with S3 which has the maximum water transfer discharge, stage drawdown increased AST coverage by 419, 63 and 55% of A_{st} in S3 from base to high flow regimes. Continue to reduce WSE increased A_{st} by 29, 12 and 9% of A_{st} in S5 compared with that in S4.

2.4.3 Sediment erosion pattern within backwater zone

2.4.3.1 Water transfer

Adjusting water transfer through tunnel operations had a much stronger impacts on sediment erosion within the backwater zone (downstream of T1) than in the whole channel. In S2, AST coverage was reduced below 12% of the downstream area and ranked the lowest among all scenarios (Table 2.5). As for the relative variance of A_{st} caused by water transfer, compared with S1, lowering water transfer discharge by 10% of its original condition reduced downstream A_{st} by 81, 70 and 31% in base, medium and high flow regime respectively. Meanwhile, increasing water transfer discharge from a low point (S2) to the maximum tunnel capacity (S3) increased A_{st} by 840, 483 and 169% in base, medium and high flow regime respectively.

As for the shortest distance between AST cross section and T2, adjusting water transfer discharge can change this distance. Specifically, increasing water transfer discharge reduced the shortest distance while decreasing water transfer discharge increased the distance. From the base to high flow regime, the shortest distance was 75 (343 m), 49 (224 m) and 32% (146 m) in S2 while 45 (206 m), 20 (91 m) and 13% (59 m) of the study reach in S3. Compared with S1, reducing water transfer discharge (S2) increased the shortest distance by 13% (58 m) of the length of study reach on average. Compare S3 with S2, increasing water transfer discharge from the low point to the maximum level decreased shortest distance by 30, 29 and 19% of the study reach.

Table 2.5. The coverage of AST in the T1 downstream.

Scenario	A_{st}		
	0.3 m³/s	6.3 m³/s	18 m³/s
S1	4.4%	13.3%	17.1%
S2	0.8%	3.9%	11.8%
S3	7.7%	23.0%	31.8%
S4	34.1%	41.4%	48.6%
S5	41.2%	46.9%	52.4%

2.4.3.2 Water transfer with stage drawdown

Compared with water transfer adjustment, reducing WSE significantly increased the areal coverage of unstable river bed. A_{st} in S4 and S5 ranked the top two among the five scenarios. The lowest and highest A_{st} was 31% and 39% in S4, and 37% and 46% in S5 respectively (Table 2.5). Compared with that in S1, A_{st} was increased by 670% in base flow regime and 185% in high flow regime respectively in S4. Compared with S3, reducing WSE increased A_{st} by 343%, 80% and 53% from base to high flow regime respectively in S4. Compare S5 with S4, further lowering WSE one-third of the adjustable range increased A_{st} by 210%, 130% and 8% from the base to high flow regimes.

The joint adjustment also had a strong impact on the shortest distance compared to water transfer alone. For example, even in the base flow regime, reducing WSE reduced shortest distance from 206 m (45% of the study reach) (S3) to 40 m (9% of the study reach) (S4). In the other two flow regimes, AST occurred in the vicinity of T2 in S4 (31 m, 7% of the study reach). Compared with

S3, stage drawdown made the shortest distance in S4 160 m, 80 m and 48 m (35, 17 and 10% of study reach) shorter from base to high flow regime, respectively. Further reducing WSE in S5 reduced the distance to zero in all flow regimes. Compared with S4, the shortest distance was shortened by 40 m, 12 m and 12 m (9, 7 and 7% of study reach).

2.4.3.3   Longitudinal extent of backwater effect

In S1, S2 and S3, the extent of backwater effect stopped 218 m upstream of T1 near where T2 locates in all three flow regimes (Figure 2.9). These findings indicate that adjusting tunnel operation will not change the extent of backwater effect. That to say, increasing water transfer discharge to its maximum level will not extend backwater effect. As for S4 and S5, the break point of backwater effect also occurred in the vicinity of T1 in base and medium flow regimes. However, in high flow regime of S4 and S5, the break point occurred farther upstream (S4: 355 m; S5: 373 m) of T1. This result was counterintuitive since the longitudinal extent of backwater effect was expected to shrink due to the reduced WSE in both S4 and S5 (Fig. 9). One potential reason might be the backwater effect was too weak to be correctly identified due to the reduced downstream WSE and increased upstream WSE according to the increased upstream inflow (S6: 103 m; S7:87 m). Therefore, the break point was manually located where the variation of flow depth became relatively flat.
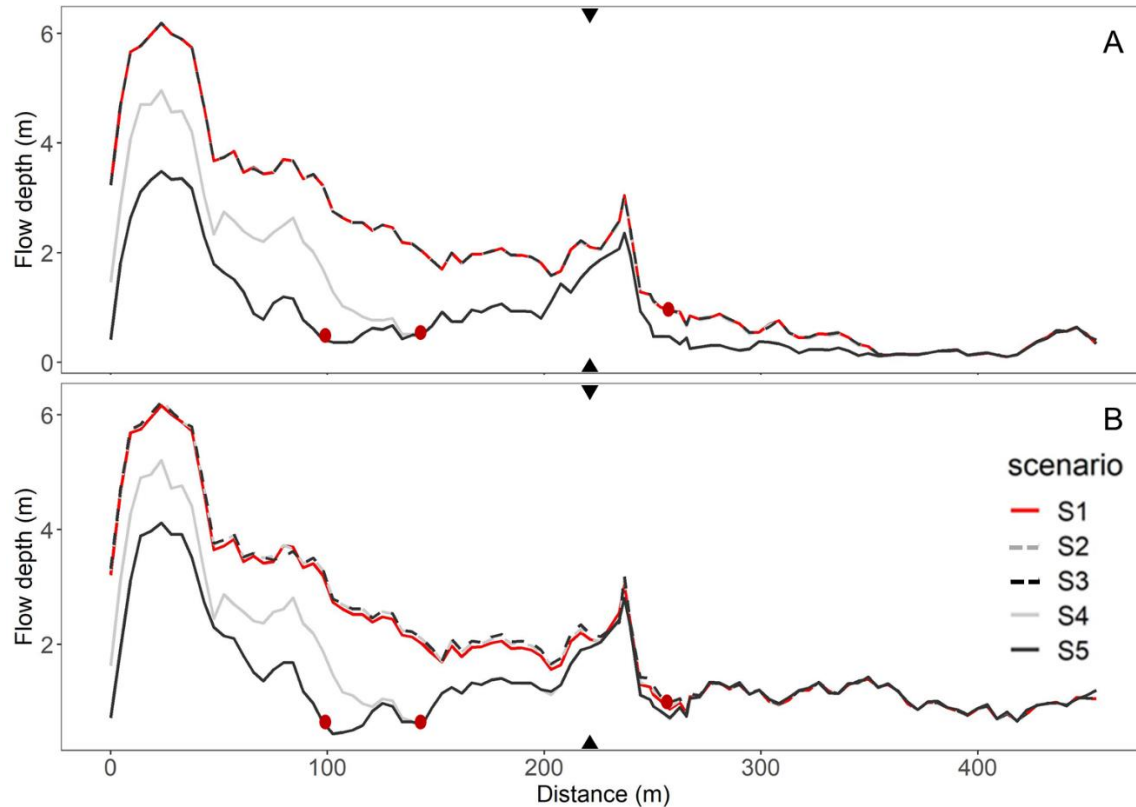
Figure 2.9. Longitudinal profile of water surface elevation and bed elevation. Distance = 0 m indicates the location of T2. Distance = 457 m is the upstream. Black triangle is the location of T1. Red circles are change points detected by pettitt test. A is base flow regime (0.3 m³/s). B is high flow regime (18 m³/s).

2.5   Discussion

Sediment erosion capacity was analyzed in the whole channel and T1 downstream, respectively. It was found that water transfer had limited impacts on the sediment erosion in the whole channel because of its exclusive impact on T1 downstream. T1 upstream was highly erosive due to channel confinement. Therefore, discussion on impacts of water transfer and stage drawdown on sediment erosion in the following part mainly focused on the T1 downstream.

2.5.1 Question 1: Impacts of water transfer

Adjusting water transfer discharge had a significant impact on sediment erosion within the backwater zone. The coverage of unstable river bed is positively related to the water transfer discharge. Turning water transfer to its maximum capacity can increase the unstable river area by over 100% while shutting down it reduced the unstable river bed to the lowest. The range of variance of the unstable areal coverage was about 7% to 20% of the maximum wet area in S1. Besides mobilizing the deposited sediment, increasing water transfer discharge can erode sediment in the vicinity of low-level outlet while turning off water transfer move the active sediment erosion zone about 100 m (22% of the study reach) away from the low-level outlet. The range of variance in the distance was 20% to 30% of the study reach.

2.5.2 Question 2: Impacts of water transfer with stage drawdown

Stage drawdown was known to have significant impacts on sediment erosion and requested to be a prior action of sediment flushing. It was proved that stage drawdown was an important hydrologic factor affecting the performance of water transfer in this study. Compared sediment erosion in high water transfer scenario (S3), reducing WSE by one third of the adjustable flow depth increased the unstable riverbed area by at least 53 % in S4. Further lowering WSE by another one third of the adjustable flow depth increased the unstable riverbed area in S5 by over 60% compared with that in S4. Even tough unstable riverbed area in S5 ranked the highest, it did not necessarily mean reducing WSE to the lowest point can always increase sediment erosion efficiently. Compare the two stage drawdown scenarios (S4 vs S5), continuing to lower WSE in S5 increased the area of unstable riverbed by 21% on average. This variation was relatively small compared with variation caused (343%) by lowering WSE on top of water transfer (S3 vs S4). As

69

for the shortest distance between AST and T2, adjusting WSE and water transfer together shortened the distance within 50 m in all simulated events. This finding supported the study hypothesis that water transfer can act as a supplementary strategy to avoid too much stage drawdown.

2.5.3 Question 3: Optimal hydrologic conditions for water transfer

An optimal range of hydrologic condition was found for water transfer strategy based on the relative variance of unstable river bed coverage. The relative variance of unstable river bed area between scenarios was always found to be the highest in base flow events and lowest in high flow regime. For example, in the comparison between high and low water transfer scenarios, the highest variation (840%) occurred in base flow while the lowest occurred in high flow. This pattern existed in all comparisons among the five scenarios which indicates that base flow regime is the best hydrologic condition for water transfer. However, the break point of unstable river bed coverage implied that medium flow regime would be the optimal hydrologic condition instead (Fig. 8). The variance (slope of AST coverage) was steep between base (0.3 m^3/s) and medium (6.3 m^3/s) flow regime. Then it became relatively gentle between medium (6.3 m^3/s) and high (18 m^3/s) flow regime. Even though in base flow regime, water transfer can induce the highest variation of unstable river bed coverage, increase in the unstable area was small because the total inflow was not high enough to erode sediment. But as the upstream inflow kept increasing, the threshold value of sediment erosion was reached and the unstable area increasing rate was enhanced. Thus, medium flow regime is the optimal hydrologic condition for water transfer to mobilize sediment within the backwater zone.

2.6 Conclusions

This study experimentally tested the performance of water transfer in assisting the sedimentation management of sand and gravel fraction bedload within the backwater zone. Sediment transport regimes were divided into stable and unstable river bed by the reference value of non-dimensional shear stress 0.03. The areal coverage and location of unstable river bed were analyzed to evaluate the redistribution of deposited sediment triggered by water transfer. The extent of backwater effect was detected by the Pettit test to infer the mechanistic chain triggered by water transfer. The results found that water transfer is a potential strategy to redistribute the deposited sediment by increasing unstable area over 100% compared with low water transfer. WSE is the key factor that in affecting the performance of tunnel flow in transporting sediment. With stage drawdown, water transfer can further increase sediment erosion cover from the water transfer scenarios. The largest increment both occurred in the medium flow regime: unstable river area can be increased by over 300% by the joint adjustment strategy compared with water transfer only. We understand that the water transfer/diversion is based on a complex and delicate balance of many competing factors. This analysis in no way diminishes the importance of that, nor should it be perceived as any criticism about that. It merely attempts to evaluate whether sediment management may be part of the set of considerations in specifying the water transfer regime. Whether this supplementary strategy can be used still depends on the local conditions of dams.

2.7 References

AASHTO, I., 2005. A summary of Existing Research on Low-Head Dam Removal Projects. Transportation Research Board (TRB).

Abu-Aly, T.R., Pasternack, G.B., Wyrick, J.R., Barker, R., Massa, D. and Johnson, T., 2014. Effects of LiDAR-derived, spatially distributed vegetation roughness on two-dimensional hydraulics in a gravel-cobble river at flows of 0.2 to 20 times bankfull. Geomorphology, 206, pp.468-482.

Annandale, G.W., 2018. Reservoir sedimentation management: A sustainabledevelopment challenge. IAHR.

Atkinson, E., 1996. The feasibility of flushing sediment from reservoirs.

Barker, J.R., Pasternack, G.B., Bratovich, P.M., Massa, D.A., Wyrick, J.R. and Johnson, T.R., 2018. Kayak drifter surface velocity observation for 2D hydraulic model validation. River Research and Applications, 34(2), pp.124-134.

Blum, M.D. and Törnqvist, T.E., 2000. Fluvial responses to climate and sea‑level change: a review and look forward. Sedimentology, 47, pp.2-48.

Chow, V.T., 1959. Open-channel hydraulics. McGraw-Hill civil engineering series.

Csiki, S. and Rhoads, B.L., 2010. Hydraulic and geomorphological effects of run-of-river dams. Progress in Physical Geography, 34(6), pp.755-780.

Curtis, J.A., Flint, L.E., Alpers, C.N. and Yarnell, S.M., 2005. Conceptual model of sediment processes in the upper Yuba River watershed, Sierra Nevada, CA. Geomorphology, 68(3-4), pp.149-166.

East, A.E., Pess, G.R., Bountry, J.A., Magirl, C.S., Ritchie, A.C., Logan, J.B., Randle, T.J., Mastin, M.C., Minear, J.T., Duda, J.J. and Liermann, M.C., 2015. Reprint of: Large-scale dam removal on the Elwha River, Washington, USA: River channel and floodplain geomorphic change. Geomorphology, 246, pp.687-708.

ESSA. 2019. River Bathymetry Toolkit (RBT). https://portal.opentopography.org/tools/viewTool?toolId=81. (Assessed 01 2019).

Fripp, J., Morris, G., Hajimirzaie, S. and Hoeft, C.C., 2020, May. Sedimentation and Small Dams. In World Environmental and Water Resources Congress 2020: Hydraulics, Waterways, and Water Distribution Systems Analysis (pp. 195-201). Reston, VA: American Society of Civil Engineers.

Garcia, M. ed., 2008, May. Sedimentation engineering: processes, measurements, modeling, and practice. American Society of Civil Engineers.

Grantham, T.E., Viers, J.H. and Moyle, P.B., 2014. Systematic screening of dams for environmental flow assessment and implementation. BioScience, 64(11), pp.1006-1018.

Grill, G., Lehner, B., Thieme, M., Geenen, B., Tickner, D., Antonelli, F., Babu, S., Borrelli, P., Cheng, L., Crochetiere, H. and Macedo, H.E., 2019. Mapping the world's free-flowing rivers. Nature, 569(7755), pp.215-221.

Horne, A., Webb, A., Stewardson, M., Richter, B. and Acreman, M. eds., 2017. Water for the environment: From policy and science to implementation and management. Academic Press.

Ho, M., Lall, U., Allaire, M., Devineni, N., Kwon, H.H., Pal, I., Raff, D. and Wegner, D., 2017. The future role of dams in the United States of America. Water Resources Research, 53(2), pp.982-998.

Hotchkiss, R. H. 1990. Reservoir sedimentation and sediment sluicing: experimental and numerical analysis.

Jarrett, R.D., 1992. Hydraulics of mountain rivers. Channel flow resistance: Centennial of Manning's formula, pp.287-298.

Julien, P.Y., 2010. Erosion and sedimentation. Cambridge university press.

Kibler, K.M., 2017. The Hydraulic size Of A Dam: A metric Indicating potential hydrologic impact For storage And diversion.

Kjaran, S.P., Hólm, S.L. and Myer, E.M., 2004. Lake circulation and sediment transport in Lake Myvatn. Aquatic Ecology, 38(2), pp.145-162.

Kouassi, K.L., Kouame, K.I., Konan, K.S., Angulo, M.S. and Deme, M., 2013. Two-dimensional numerical simulation of the hydro-sedimentary phenomena in Lake Taabo, Côte d'ivoire. Water resources management, 27(12), pp.4379-4394.

Kondolf, G.M., Gao, Y., Annandale, G.W., Morris, G.L., Jiang, E., Zhang, J., Cao, Y., Carling, P., Fu, K., Guo, Q. and Hotchkiss, R., 2014. Sustainable sediment management in reservoirs and regulated rivers: Experiences from five continents. Earth's Future, 2(5), pp.256-280.

Li, T. and Pasternack, G.B., 2020, August. Reservoir sedimentation management with upstream sediment remanipulated. In River Flow 2020: Proceedings of the 10th Conference on Fluvial Hydraulics (Delft, Netherlands, 7-10 July 2020) (p. 355). CRC Press.

Liro, M., 2015. Gravel-bed channel changes upstream of a reservoir: The case of the Dunajec River upstream of the Czorsztyn Reservoir, southern Poland. Geomorphology, 228, pp.694-702.

Liro, M., 2016. Development of sediment slug upstream from the Czorsztyn Reservoir (southern Poland) and its interaction with river morphology. Geomorphology, 253, pp.225-238.

Liro, M., 2019. Dam reservoir backwater as a field-scale laboratory of human-induced changes in river biogeomorphology: A review focused on gravel-bed rivers. Science of the Total Environment, 651, pp.2899-2912.

Liro, M., Ruiz-Villanueva, V., Mikuś, P., Wyżga, B. and Castellet, E.B., 2020. Changes in the hydrodynamics of a mountain river induced by dam reservoir backwater. Science of The Total Environment, 744, p.140555.

Lisle, T.E., Nelson, J.M., Pitlick, J., Madej, M.A. and Barkett, B.L., 2000. Variability of bed mobility in natural, gravel‐bed channels and adjustments to sediment load at local and reach scales. Water Resources Research, 36(12), pp.3743-3755.

Minear, J.T. and Kondolf, G.M., 2009. Estimating reservoir sedimentation rates at large spatial and temporal scales: A case study of California. Water Resources Research, 45(12).

Morris, G.L. and Fan, J., 1998. Reservoir sedimentation handbook: design and management of dams, reservoirs, and watersheds for sustainable use. McGraw Hill Professional.

Murray, A.B., 2003. Contrasting the goals, strategies, and predictions associated with simplified numerical models and detailed simulations. Geophysical Monograph-American Geophysical Union, 135, pp.151-168.

NID, 2021. National Inventory of Dams. https://nid.sec.usace.army.mil/ (Accessed 03 2021).

Palmieri, A., Shah, F. and Dinar, A., 2001. Economics of reservoir sedimentation and sustainable management of dams. Journal of environmental management, 61(2), pp.149-163.

Pasternack, G.B., Bounrisavong, M.K. and Parikh, K.K., 2008. Backwater control on riffle–pool hydraulics, fish habitat quality, and sediment transport regime in gravel-bed rivers. Journal of Hydrology, 357(1-2), pp.125-139.

Pasternack, G.B. and Hopkins, C.E., 2017. Near-census 2D model comparison between SRH-2D and TUFLOW GPU for use in gravel/cobble rivers. Davis (CA): University of California at Davis. Prepared for Yuba County Water Agency.

Pasternack, G.B., 2020. River Restoration: Disappointing, Nascent, Yet Desperately Needed.

Person, E., 2013. Impact of hydropeaking on fish and their habitat (No. BOOK). EPFL-LCH.

Queen, R., 2018. Morphodynamic modeling of flow and sediment transport over low-head, Run-of-River dams. Hydropower Foundation.

Randle, T., Kimbrel, S., Collins, K., Boyd, P., Jonas, M., Vermeeren, R., Eidson, D., Cooper, D., Shelley, J., Juracek, K. and Fripp, J., 2017. Frequently asked questions about reservoir sedimentation and sustainability. Subcommittee on Sedimentation, National Reservoir Sedimentation.

Roads, J.O., Chen, S.C., Guetter, A.K. and Georgakakos, K.P., 1994. Large-scale aspects of the United States hydrologic cycle. Bulletin of the American Meteorological Society, 75(9), pp.1589-1610.

Shields Jr, F.D., 2009. Do we know enough about controlling sediment to mitigate damage to stream ecosystems?. Ecological Engineering, 35(12), pp.1727-1733.

Schleiss, A.J., 2018. The challenge of restoring dynamics by river engineering: where to find the truth about river flow-in the computer, in the lab or in the field?. In 9th International conference on fluvial hydraulics River Flow 2018 (No. POST_TALK).

Schwindt, S., Pasternack, G.B., Bratovich, P.M., Rabone, G. and Simodynes, D., 2019. Hydro-morphological parameters generate lifespan maps for stream restoration management. Journal of environmental management, 232, pp.475-489.

Skelton, G. 2017. California's reservoirs are filled with gunk, and it's crowding out room to store water. Los Angeles Times. https://www.latimes.com/politics/la-pol-sac-skelton-silt-california-dams-20170306-story.html (Acessed 03 2021).

Thorne, C., Hey, R. and Newson, M., 2005. Applied fluvial geomorphology for river engineering and management. John Wiley and Sons Ltd.

Toone, J., Rice, S.P. and Piégay, H., 2014. Spatial discontinuity and temporal evolution of channel morphology along a mixed bedrock-alluvial river, upper Drôme River, southeast France: Contingent responses to external and internal controls. Geomorphology, 205, pp.5-16.

USACE 2015. US Army Corps of Engineers. Dredging and Dredged Material Management.

Viviroli, D., Weingartner, R. and Messerli, B., 2003. Assessing the hydrological significance of the world's mountains. Mountain research and Development, 23(1), pp.32-40.

WBM. 2018. TUFLOW Classic/HPC User Manual Build 2018-03-AD. *WBM Oceanics Australia*.

Wilcock, P.R., Kondolf, G.M., Matthews, W.G. and Barta, A.F., 1996. Specification of sediment maintenance flows for a large gravel‐bed river. Water Resources Research, 32(9), pp.2911-2921.

Yang, G., Bowling, L.C., Cherkauer, K.A. and Pijanowski, B.C., 2011. The impact of urban development on hydrologic regime from catchment to basin scales. Landscape and Urban Planning, 103(2), pp.237-247.

CHAPTER 3. APPLYING FLOW COVERGENCE ROUTING TO REDISTRIBUTE SEDIMENT EROSION FOCI IN A DAM'S BACKWATER ZONE

3.1 Abstract

Despite studies showing that dams have significant effects on the sediment dynamics and evolution of a river upstream of a dam, the knowledge on relationships between river topography and sediment transport in a dam's backwater zone has been poorly applied in reservoir sedimentation management. This study investigated the potential of a sequence of engineered topographic constrictions and expansions, utilizing flow convergence routing theory, to redistribute sediment erosion foci in a dam's backwater zone. To test scientific ideas and engineering alternatives, the current topography of Our House Dam on the confined, mountainous Middle Yuba River, California was re-contoured into different scenarios. As most of the dam's backwater zone is filled with sediment (a common global problem), two-dimensional hydrodynamic modeling was useful for evaluating erosion patterns. The results found that high velocity concentrates near topographic constrictions, resulting in the topographic expansion functioning as a sediment-deposition buffer zone (with low velocity) away from the dam where the key valves are located and need to be kept free of sedimentation. As flow increases, the high-velocity zone will extend to the expansion area, then to the constriction close to the dam. The performance of topographic constrictions is flow dependent. Moderate in-channel flow (daily reccurrence of ~ 5-30%) was best for ponding sediment upstream, while high in-channel flow (reccurrence of 1-5%) was best for significant sediment erosion in the backwater zone.

3.2   Introduction

Reservoir sedimentation is the term used to describe the process of erosion, entrainment, transportation, deposition and compaction of sediment carried in the reservoir upstream of a dam (Morris et al. 1998, Julien 2010). This sedimentation process has been ascribed to the backwater effect, the impact of the dam's newly formed hydraulic base level on the upstream reach, including reduced flow velocity and increased water depth. Backwater is the water profile with the ponded flow depth higher than the normal and critical flow depth (Chow 1959). In fluvial geomorphology, it is also defined as the condition that the ponded flow depth is higher than the normal or average flow depth when the normal and critical flow depth is difficult to calculate (Liro 2019).

Starting from sediment dynamics, incoming coarse sediment (bedload) derives from upstream catchment and channel erosion. This material tends to deposit and form a delta at the head of the reservoir, while fine sediment deposits further downstream in the reservoir (Hotchkiss 1991). Delta deposits can progress in two directions (Shotbolt et al., 2005). Due to the growing sediment plug at the delta head, the leading edge of the backwater zone shifts upstream and the foci of coarse sediment deposition migrates upstream with it, increasing flood heights (Hotchkiss 1990). Meanwhile, coarse and fine sediment prograde down into the reservoir with hydraulic sorting downstream (Thornton et al, 1990). Delta growth into the reservoir reduces reservoir capacity, and eventually eliminates the capacity for flow regulation crucial for assuring reservoir functions of water supply, energy production, navigation, and flood control (Morris et al. 1998, Brandt 2000). Consequently, a variety of morphological adjustments are triggered, such as lateral river migration, channel deepening and widening, morphological evolution of channel bars and the grain-size

76

partitioning along the channel axis (Maselli et al. 2018). Feedbacks also exist between sediment dynamics and morphological adjustment (Coleman, 1976). The over-widened channel where there the large bars itself may act as a barrier to sediment transport from upstream (Hooke 2003, Fryirs 2013), and further sediment may be added to its tail resulting in the upstream extension of sedimentation zones in the river channel (Schumm et al., 1984, Fryirs, 2013).

Topographic steering is defined as morphological control of water depth, speed and direction (i.e. hydraulics) (Blanckaert 2010, Nelson et al. 2016). The term is used by some engineers to refer exclusively to a fluid mechanics phenomenon, but increasingly, geomorphologists and river restoration practitioners are adapting it to refer to a more literal concept in which topography associated with fluvial landforms and large bed elements steers water and controls its hydrodynamics. In this updated context, topographic steering occurs when the flow direction is controlled by immobile topographic features such as boulders, bedrock, hillslopes, canyon walls, and alluvial deposits (Brown and Pasternack, 2014). Materials in transport can be steered by the main flow direction and effectively pushed into immobile topographic features creating depositional forms, or deposits due to particle trapping (Brown et al. 2014).

Flow convergence routing (FCR) is a thoroughly-studied hydro-morphodynamic mechanism associated with topographic steering. Flow convergence relates to the fluid mechanism and routing relates to its sediment dynamics. According to this mechanism, locations of most concentrated flow (i.e. geometric constrictions or nozzles) at any discharge having the greatest potential to scour and route sediment through them (MacWilliams et al. 2006, Pasternack et al. 2018). In contrast, locations of least concentrated flow at any discharge (generally oversized cross-sections) have

flow divergence and the highest likelihood of sediment deposition at that flow. Most importantly, these locations of least and most concentrated flow (and the erosion and deposition they drive) can shift as a function of discharge, because fluvial landforms are often nested within other fluvial landforms with different topographic steering (Pasternack et al., 2018b). In fact, for a confined mountain river, Pasternack et al. (2021) found that there exists a threshold stage above which river topography dramatically changes from predominantly nozzle and oversized landforms to wide bar and constricted pool landforms. Flow convergence routing has been found to be a dominant process in confined and partially confined reaches of the Yuba River catchment, which is the where the site for this study is located (Sawyer et al., 2010; Strom et al., 2016; Gore et al., 2016; Pasternack et al., 2018; Pasternack et al, 2021), so it is well understood and locally relevant.

These ideas and questions present the possibility of a new way to mitigate reservoir sedimentation, especially where wholesale excavation is too expensive or infeasible, by re-contouring deposited sediment to control where and when sediment deposits. Increasingly, studies are using numerical experimentation to evaluate how topographic steering and FCR could be manipulated through mindful river design to control sediment transport and morphodynamics (Jackson et al. 2015, Brown et al. 2016, Anim et al. 2019). Further, the ideas of applying topographic controls have been implemented into real river restoration projects on the Napa River (EPA, 2020) and Dry Creek tributary of the Russian River (SW, 2020). Therefore, the purpose of this study was to use exploratory numerical modeling to test the potential for applying topographic constrictions for redistributing sediment erosion foci in a dam's backwater zone.

To achieve the study purpose, three scientific questions were posed to analyze impacts of

topographic constriction and stage drawdown on reservoir sediment erosion, the optimal range of hydrologic conditions, and the mechanistic sequence of hydrodynamics triggered by re-contouring (Table 3.1). The topographic control is a set of two topographic constrictions (aka "nozzle" landform, TPC1 & TPC2) and a topographic expansion (aka "oversized" landform) between constrictions (Figure 3.1). The terms nozzle and oversized come from the flow convergence routing (FCR) landform theory of Pasternack et al. (2018, 2021). According to theory, these two landform types are not naturally self-sustainable in the face of sediment dynamics, unless a nozzle is highly resistant to erosion, such as if its lithology is highly resistant bedrock. However, a nozzle can be engineered for persistence as a hard structure.
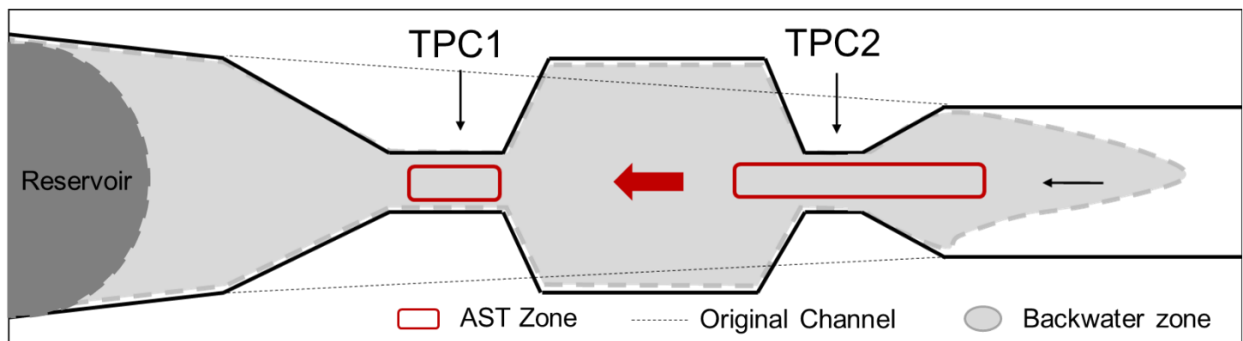
Figure 3.1. Conceptual configuration of topographic controls in a reservoir backwater zone.

Topographic steering of flow and FCR is hypothesized to be capable of manipulating the spatial distribution of sediment erosion in a reservoir to shift the foci of erosion away from critical dam infrastructure. Under this hypothesis, TPC2 ought to yield a convergent and accelerated flow at the head of a topographic expansion; which generates a hydraulic jet through and downstream of the constriction, causing erosion and making a new foci of sediment erosion. Therefore, TPC2 is assumed to accelerate flow and deliver more sediment to the oversized landform downstream of it. Meanwhile, TPC1 is hypothesized to have low possibility of transporting sediment because of

a lack of sediment supply routing through to it due to the upstream oversized landform. It serves as a backstop to sediment transport by backing water up into the oversized landform, thereby further enhancing the overall dynamism.

TPC performance is hypothesized to be sensitive to the downstream water surface elevation (WSE) imposed by the reservoir. Reducing WSE can reduce the ponding effect of the reservoir and thus increase sediment erosion in both TPC2 and the oversized landform. With more eroded sediment upstream, sediment erosion in TPC1 is hypothesized to increase. Increasing WSE can increase the ponding effect of the oversized landform and thus reduce sediment erosion in TPC2. By having less sediment transport to the oversized landform, sediment erosion near the dam can be reduced. Even though impacts of WSE adjustment can be independent of inflow to the extent that outflows can be manipulated to enforce the designated reservoir WSE, it can be no longer controllable beyond certain high flow. Therefore, the effectiveness of TPCs is hypothesized to be flow dependent. When the flow reaches certain range, the performance of TPC1 is hypothesized to act as an accelerator to increase sediment transport through/over the reservoir due to the submergence of TPC2.

Table 3.1. List of scientific questions about impacts and applications of the proposed strategies.

Question ID	Questions
Qt1	How do topographic controls affect foci of sediment erosion pattern?
Qt2	How does the topographic with WSE adjustment affect sediment erosion?
Qt3	Optimal hydrologic conditions for the topographic control to increase sediment erosion upstream of TPC1 or pond sediment upstream of TPC2?

3.3 Study site

In theory, the study questions could be answered with an entirely hypothetical set of topographic and hydrological scenarios (e.g. Brown et al., 2017), but it is often helpful to use a real- site with real, typical river management problems as a testbed (e.g. Wheaton et al., 2010). The study site used herein was the backwater zone upstream of Our House Dam (OHD), a 40-m-radius concrete arch dam located 19 km upstream of the confluence of Middle Yuba river and North Yuba River (Figure 3.2). The dam is 21 m high with a drainage area of 376 km^2 (YWA, 2017).

The catchment's climate is Mediterranean-montane, with warm, dry summers and cool, wet winters whose annual precipitation ranges from 500-2000 mm varying with elevation and aspect. Winter flood pulses often stem from narrow-banded atmospheric rivers that deliver localized, intense, high-magnitude precipitation (Ralph et al., 2006; Dettinger, 2011). The catchment also periodically experiences low-pressure systems and "bomb cyclones" that can deliver moderate to

heavy precipitation over an extended duration. Hydrologically, Middle Yuba River (MYR) is the only inflow to OHD (Figure 3.2). The mean annual flow of MYR is 8.8 m^3/s. Recent instantaneous flood peak discharges were 405 m^3/s in 2017, 501 m^3/s in 2006, and 779 m^3/s in 1997. Inflow at OHD is partially diverted to Oregon Creek through the Lohman Ridge Tunnel. Lohman Ridge Diversion Tunnel conveys a maximum flow of 24.4 m^3/s.

In-channel sediment supplies and hillslope processes (mass wasting and surface erosion) are the primary sources of ongoing sediment contribution in the Yuba River basin (Curtis et al. 2005). Most in-channel supplies are attributed to legacy materials from hydraulic gold mining with erosion in upland tributaries. Mining operations left large patches of unvegetated terrain with easily-erodible soils, but as throughout the Sierra Mountains, MYR also has other areas of deforestation, roads, land use, and wildfire causing higher sediment yields (Lewis et al., 2006; Litschert and MacDonald, 2009; Olsen et al., 2021). As a consequence, OHD experiences significant sediment deposition leading to impairment of operations for environmental flow releases.

The reach length affected by OHD (~ 1 km) was selected based on the distribution of subaerial gravel-bar deposition as an indicator of backwater extent (Figure 3.2). It is a confined riffle-pool channel whose bed sediment fines downstream from gravel/cobble at the entrance to sand/silt at the dam. The mean bed slope and width are 0.02 and 47 m, respectively. Hillsides are well vegetated, while the active riverbed is intermittently vegetated with willow species depending on the time since the last channel-altering flood.
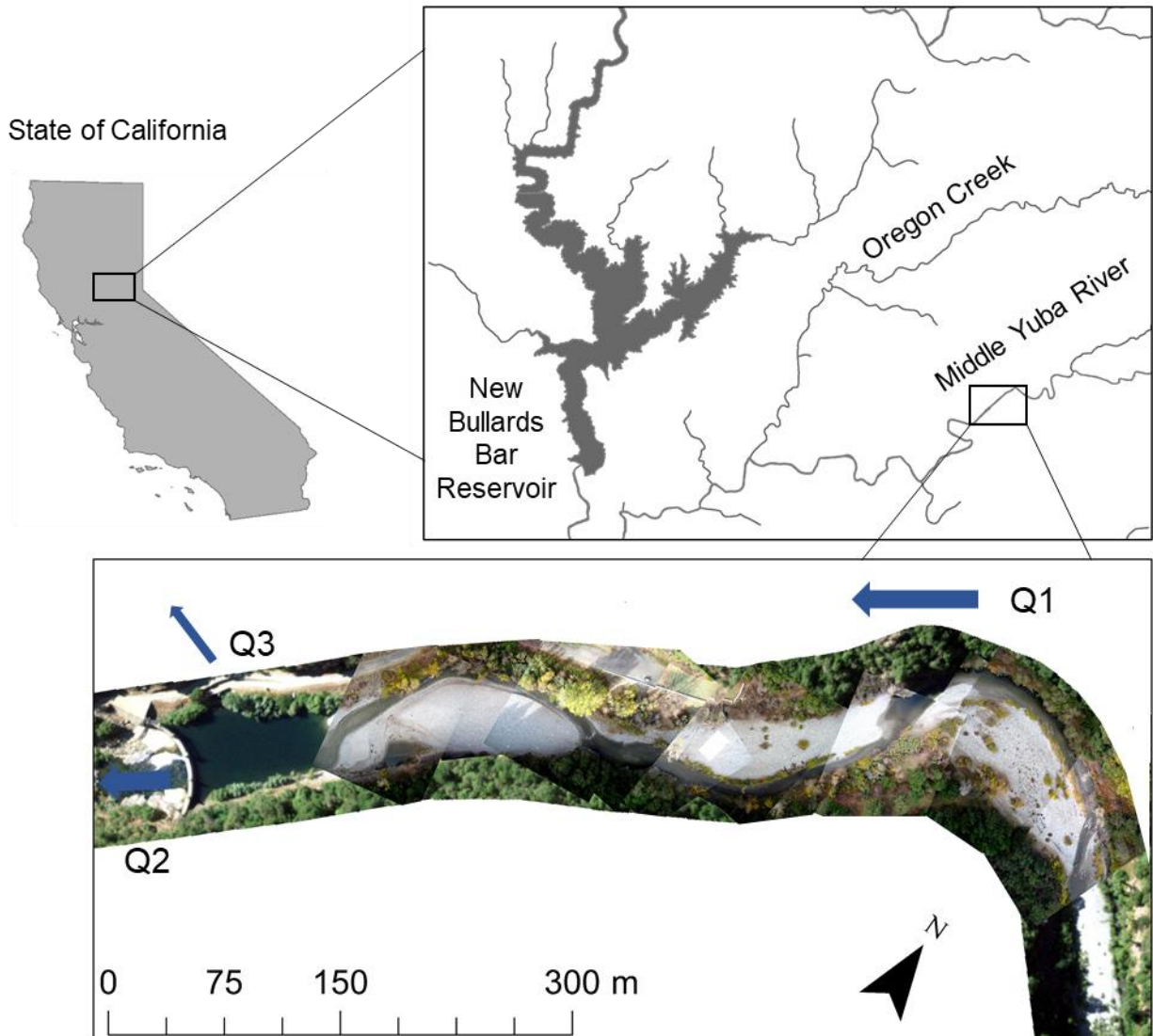
Figure 3.2. Map of California, USA with zoom of Yuba River catchment showing the path of the Middle Yuba River and a further zoom of the study reach. Q1 and Q2 are Middle Yuba River inflow and outflow, respectively. Q3 is water diverted through Lohman Ridge Tunnel (Table 3).

3.4   Material and methods

3.4.1   Experimental design

The section presents an overview of the experimental design to show how specific, tractable

scientific questions and their associated hypotheses (guided by a pre-existing mechanistic conceptualization) were tested, with details in subsequent methods sections. The design involved using an analytical and statistical framework (Figure 3.2) for comparing three topographic-hydrological scenarios (Table 3.2) using three test metrics. Each metric has a pre-established range of values indicating the physical mechanisms in question. Comparisons of test metrics between H1 and H2 were used to answer Qt1, while those between H2 and H3 were used to answer Qt2.Comparison of test metrics among different flows simulated for H1, H2, and H3 were used to answer Qt3.

In H3-1 and H3-3, reservoir WSE was reduced by 0.6 and 2.9 m, respectively, to evaluate how WSE adjustment affects the TPCs performance. In H3-2, WSE was increased by 0.3 m to evaluate the performance of TPCs with increased backwater effects. The minor WSE adjustment (-0.6 m and +0.3 m) was set because the average reservoir WSE was close to the spillway height. Reducing reservoir by 2.9m account for ¼ of the adjustable WSE range to evaluate how large adjustment affects TPCs performance. The adjustable WSE range is the difference between spillway height (619 m) and minimum WSE (607).

Table 3.2. Exploratory scenarios to answer study questions.

Scenario	Scenario name	Design conceptualization
H1	Original topography	The reference scenario based on recent topographic mapping and hydrological data.
H2	Topographic control	Two topographic controls (TPC1 & TPC2) were built into the study reach.
H3	Topo-hydro control	Three reservoir WSE scenarios were designed. H3-1 represents minor WSE reduction. H3-2 is the minor WSE increment. H3-3 is the large WSE increment.

To obtain a robust understanding of baseline hydraulics, two-dimensional (2D) hydrodynamic modeling (section 3.4.3) of H1 was performed for 18 flow events (Table 1 in supplementary material I) considering the response of five representative grain sizes (3, 8, 32, 64 and 119 mm) to predicted bed shear stress. To evaluate sediment dynamics, spatially explicit bed shear stress and flow depth rasters from 2D modeling were used to quantify scour potential (independent of sediment supply), the location(s) where sediment erosion would happen relative to key infrastructure, and the longitudinal extent of backwater effects (Figure 3.3). Three test metrics – the areal percentage of unstable river bed (section 3.4.4.1), sediment transport distance (section 3.4.4.2) and longitudinal extent of backwater effects (section 3.4.4.3) – were computed and used to address the questions and hypotheses (section 3.5).

(1) Import steady state 2D model results

Flow depth raster, shear stress raster

(2) Define sediment transport regime

Reference critical Shields stress: 0.01, 0.03, 0.06 and 0.15

| $(-\infty, 0.01]$ | $(0.01, 0.03]$ | | $(0.03, 0.06]$ | $(0.06, 0.15]$ | $(0.15, \infty]$ |
| Negligible Trspt | Intermittent Trspt | | Partial Trspt | Full Trspt | Channel Trspt |

Stable River Bed

Active Sediment Transport (AST)
Unstable River Bed

(3) Test metrics

$$AST\% = \frac{AST}{River\ corridor\ area}$$

Shortest distance between dam and AST

(4) H1 vs H2

Qt1: Impacts of topographic controls?

(5) H2 vs H3

Qt2: Joint Impacts of topographic controls with stage drawdown?

(6) Comparison among H1, H2 and H3 along with inflow

Qt3: Optimal hydrologic conditions for water transfer?

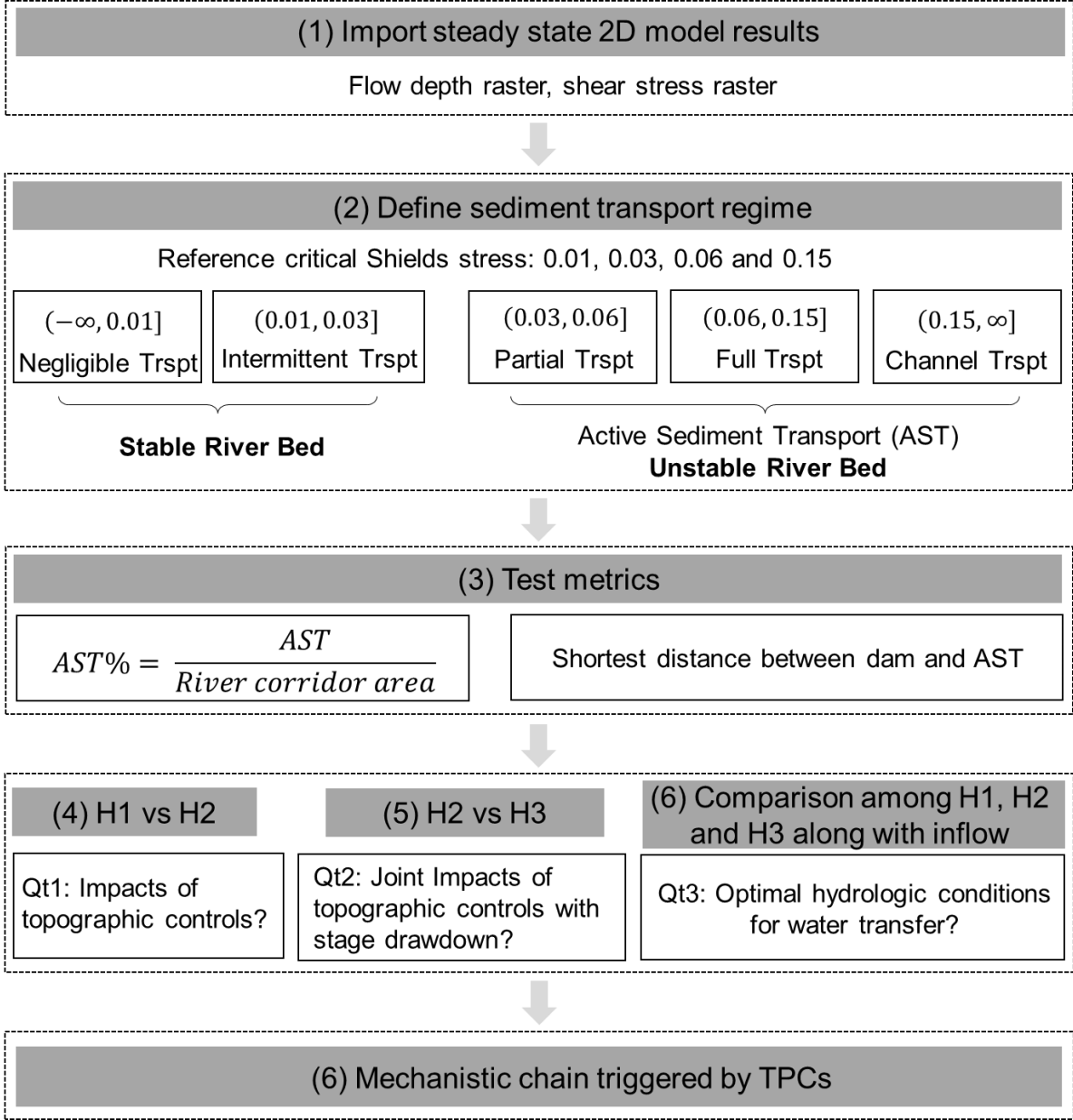**(6) Mechanistic chain triggered by TPCs**

Figure 3.3. Data analysis framework developed in this study.

3.4.2 Digital elevation models

A combination of airborne near-infrared Light Detection and Ranging (LiDAR) point cloud data from the OpenTopography website (2014 USFS Tahoe National Forest LiDAR dataset (11.6 pts/m^2)) and survey points mapped in October to November 2018 using a Leica TPS1100 robotic total station and Trimble R8 Real-Time Kinematic Global Positioning System unit were used to make a digital elevation model (DEM) of the study site. The point density in areas covered by LiDAR or with little morphologic variability was 1 pt per 9 m^2. In other areas, the point density was 1-1.5 pts per m^2. The unwadable reservoir was mapped by boat using a single-beam echosounder and RTK GPS. A one-meter resolution DEM was produced using these points followed published procedures and with quality control/quality assurance measures taken (Barker et al. 2018).

A synthetic topography with topographic controls (TPCs) were built on the original channel elevation (Figure 3.4B). The topographic control consists of two topographic constrictions (TPC1 & TPC2) and one expansion. To build TPCs on the river, the gross fill of sediment moved was 337,956 m^3, gross cut was 66,532 m^3, and net fill was 271,424 m^3. These values indicate that substantial additional material would need to be brought in to enable the re-contouring, which could be accomplished by simply waiting for more reservoir sedimentation to take place (Figure 1 in supplementary material I).

TPC1 was designed to be a very strong nozzle, with significant width reduction and bed elevation increase. River width at TPC1 was reduced to be 30% of the original wetted width at the highest flow (407 m^3/s) during the simulation period. The height of TPC1 was set to be the highest flow

depth (407 m^3/s) to have TPC1 not inundated by flows. In contrast, TPC2 involved a modest re-contouring emphasizing effects for low flows, instead of for all flows. The low-flow width of the riverbed at TPC2 was reduced to 40% of the original riverbed. The elevation on the left bank was increased by 3 m while the right bank was slightly elevated (1 m) due to the feature of topography. Between the two topographic constrictions, a natural topographic expansion exists. Its bed elevation was reduced by 3 m to mimic the condition when the deposited sediment is removed, and then that material could be used to build the TPCs instead of bringing in material from elsewhere.
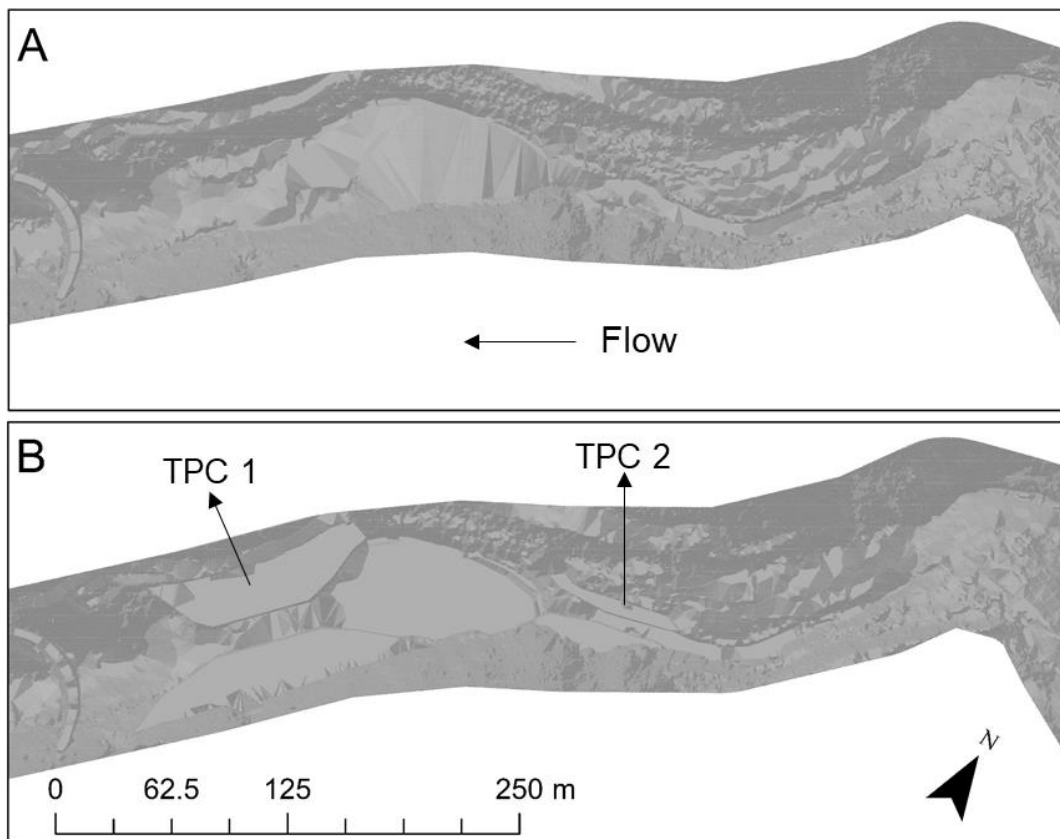

Figure 3.4. Digital elevation models (DEMs) used in the study. (A) is the existing 2018 river topography and (B) is a synthetic design that implements topographic constrictions (TPC1 and TPC2).

3.4.3   2D Hydrodynamic Modelling

The OHD study site is in a confined canyon protected from wind fetch or waves. It has no tributaries, so there is only a single predominant flow direction controlled by the river. Extensive sedimentation has filled the majority of the reservoir, yielding predominantly fluvial (not lacustrine) hydrodynamics. Density currents or other complex lake physical processes appeared to be negligible. Reservoir sedimentation and fluvial landforms in the backwater zone shows lateral and longitudinal patterning consistent with sediment redistribution during in-channel flows, not just infrequent, large floods. Further, the proposed topographic controls were designed for managing sediment during in-channel flows. In other words, it may be infeasible to use topographic re-contouring to control effects of floods, but it could save substantial money on expensive excavation, dredging, and flushing approaches, and protect critical infrastructure in many years.

In light of these physical conditions, a two-dimensional depth-averaged (2D) hydrodynamic model was used to evaluate both the lateral and longitudinal positioning of sediment erosion under the different scenarios. A one-dimensional model would not have resolved the cross-channel hydraulics essential to addressing the study's questions about sediment dynamics spatial patterns associated with topographic constrictions and expansions. A three-dimensional model was not necessary in light of valley confinement, modest depths compared to a lake, the absence of wind-driving mixing, and the lower discharges investigated (Kjaran et al., 2004, Kouassi et al., 2013).

Morphodynamic models are not used in this study because the physical processes of sediment transport are extremely complex and thus far numerical modelling to directly simulate sediment

transport is still under development. Besides, model-predicted sediment transport rates are still markedly different from measured ones (Yager et al., 2019), questioning the viability of morphodynamic modelling for management use. In addition, the scenarios studied here are exploratory, which makes it difficult to validate the results given the remote setting and flood flows. Therefore, A 2D hydrodynamic model was well suited to the OHD study of reservoir sediment management using artificial constrictions and expansions in a narrow canyon.

The commercial software TUFLOW HPC was used to simulate the steady-state lateral and longitudinal hydraulic field. TUFLOW HPC is an explicit parallelized solver for the full 2D Shallow Water Equations, including a sub-grid scale eddy viscosity model (WBM 2018). A one-meter resolution computational grid was built for the domain starting 1 km upstream and ending at OHD.

3.4.3.1 Model parameters

TUFLOW HPC requires turbulence closure and flow resistance parameters. The default TUFLOW Smagorinsky viscosity method was used for turbulence closure with a coefficient value of 0.5 and a constant value of 0.005 m^2/s, as these values have proven effective in validated 2D model studies in other reaches of the Yuba River. Because the majority of the OHD study site had gravel and cobble alluvial sediment and complex small bedforms, a global Manning's n value of 0.04 was used based on flow resistance assessments for 2D model studied of other reaches of the Yuba stream network (Figure 3.5).
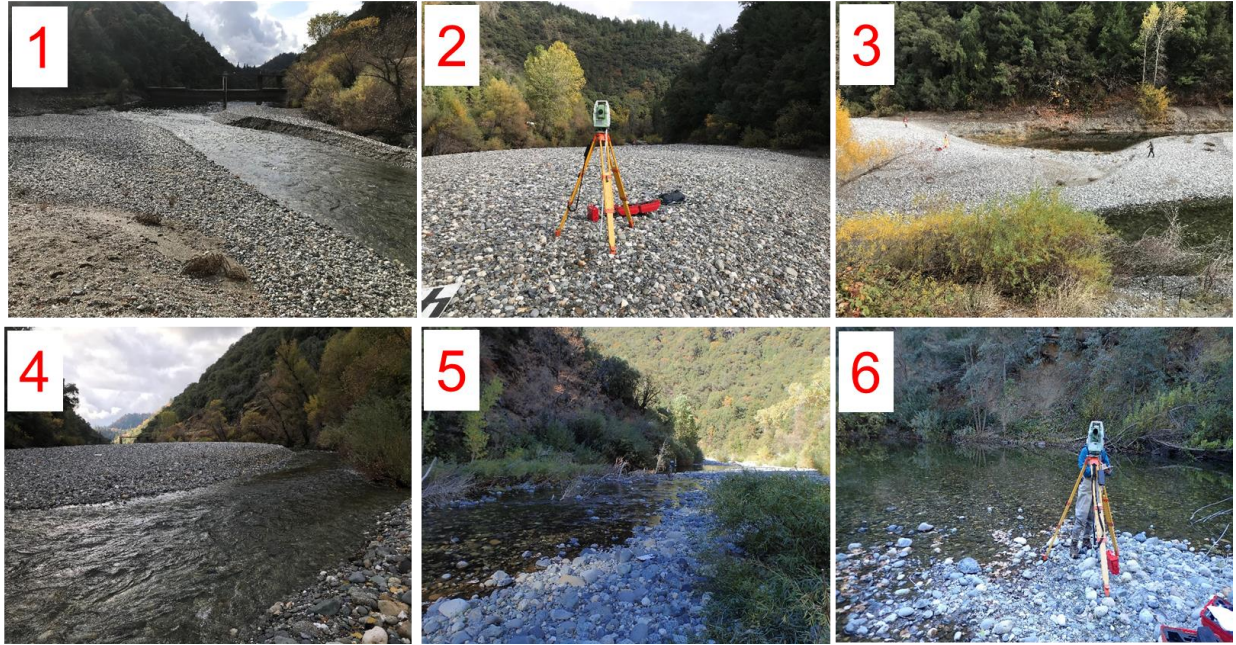
Figure 3.5. Photo collection of substrates. Number 1 to 6 refers to the orientation from downstream to upstream of the survey reach in OHD site.

3.4.3.2 Steady-state flow simulations

Steady-state flow runs of in-channel flows were simulated to evaluate how sediment would respond to different topographic controls under a constant flux of water with the sediment load it is capable of carrying, and thus to know what type of flow events can obtain the designated level and magnitude of sediment erosion. TUFLOW HPC is capable of simulating unsteady flows, but designing rising and falling limbs would add extra complexity to the study design beyond what is needed for addressing the study questions.

Eighteen operation flows were simulated in the reference scenario to understand baseline dynamics more thoroughly (Table 1 in supplementary material I). Out of those, four flows were selected to compare scenario H2 to H3 under a range of flow conditions (Table 3.3). Spearman correlation

was used to investigate the relationship among inflow, outflows (river and tunnel), and WSE. The high correlation coefficient (>0.7) between inflow and WSE indicated that OHD tended to pond water when the upstream inflow increased. Meanwhile, the correlation coefficients between inflow and the two outflows were all below 0.3, indicating a relatively weak relationship, so the role of the tunnel and river flow releases on mediating that relation was limited.

On the basis of daily flow recurrences between 1988 to 2018, the upstream flow regime was categorized into four ranges (Table 3.3) from which three representative in-channel flows were selected. Floods were not considered in this study, because during floods the reservoir's WSE reaches and exceeds the spillway crest elevation (619 m) due to the low storage capacity and buffering effect of the small reservoir that is largely filled in with sediment and given the excessive inflow. This makes realistic artificial WSE adjustment impossible, which precludes a key part of the experimental design. Further, the focus of this study is on management of sediment influx and redistribution within the reservoir during lower flows that necessitate expensive regular maintenance operations.

Table 3.3. Flow regime of steady state flow runs in OHD site.

Flow regime	Flow range (m^3/s)	frequency of daily occurrence	Selected flow event (m^3/s)
Low in-channel flow	[0, 8.5]	[30%, 70%]	2.5
Medium in-channel flow	(8.5, 31]	(5%, 30%]	9.4/17
High in-channel flow	(31, 85]	(1%, 5%]	83
Flood flow	(>85]	(−∞, 1%]	none

3.4.3.3 Model performance

Given the remote and extremely hazardous conditions in the river during even modest flows, most model validation was infeasible except for comparing modeled and observed water surface elevations at the dam crest. Comparing WSE is in fact the common strategy for validating lake/reservoir hydrodynamic models, if any validation is done at all (Kouassi et al., 2013; Castillo et al. 2015). As a result, the study is in the realm of scientific exploration and not predictive forecasting with high certainty, using the uncertainty terminology and concepts of Murray (2003). In addition, TUFLOW HPC is a well-developed model that has been validated for use in Yuba River (Pasternack et al. 2017, Schwindt et al. 2019).

3.4.4 Test metrics

The introduction presented a hypothesized hydro-morphodynamic mechanism that would be instituted by re-contouring the river. The modeling performed in this study is capable of characterizing how the rivers flow-dependent hydraulics ought to respond to the alternative

topographic steering. Rather than relying on a qualitative description of model output rasters to characterize the differences among scenarios H1, H2, and H3, this study implemented three specific test metrics that quantify the magnitude of difference among scenarios.

3.4.4.1 Sediment erosion capability

The purpose of the metric was to identify areas of active scour in each simulation. Because the hypothesized conceptual model of the TPCs functioning requires that active scour be focused in the vicinity of the TPCs, delineating scour areas in each scenario and comparing them among scenarios is a vital test of the hypothesis. The first step involved estimating where flow had the capability to scour sediment (and/or route sediment through without depositing) in the OHD backwater zone. Bed shear stress (Eq. 3-1) variable was converted into non-dimensional shear stress (Shields stress, Eq. 3-2) to make results comparable across all scenarios.

Next, instead of calculating a specific sediment transport rate, which can be highly uncertain, the local Shields stress (τ^*) values were categorized/aggregated into less uncertain sediment transport regimes defined by Lisle et al. (2000) where values of $\tau^* < 0.01$ correspond to negligible transport, $0.01 < \tau^* < 0.03$ correspond to intermittent entrainment, $0.03 < \tau^* < 0.06$ corresponds to partial transport (Wilcock et al., 1996), $0.06 < \tau^* < 0.15$ corresponds to full transport, and $\tau^* > 0.15$ corresponds to channel alteration. Intermittent transport indicated disturbances exist to the substrate of benthic organisms, but not necessarily to sediment movement, and there can even be deposition during this regime (Sawyer et al., 2010). Partial transport implies some over-ample and over-exposed particles of a given size on the bed surface area are active while others of the same size are immobile. Full transport implies a consistent 'conveyor belt' of sediment transport along

the bed, up to two grains thick. Channel alteration transport indicates an increased scour potential

compared with that in full transport, possibly with riverbed reconfiguration. Thus, 2D modeling is

only used to predict which regime a location is in, which is an easier goal than predicting sediment

transport rates explicitly.

Finally, to further simplify erosion analysis and reduce uncertainty, partial, full and channel

alteration transport regimes were added up and referred to as the active sediment transport regime

(AST). Area covered by AST was considered unstable riverbed. The normalized-areal coverage of

AST (A_{st}, Eq.3-3) was used as the test metric to evaluate flow scour capability throughout the

model domain, especially looking for its occurrence in the vicinity of the TPCs. Meanwhile, area

covered by negligible and intermittent transport regimes were assumed to be stable riverbed, and

likely areas for sediment deposition, which are hypothesized to occur in oversized landforms, such

as the one designed upstream of each TPC.

$$\tau_b = \rho g V^2 n^2 \big/ h^{1/3} \tag{3-1}$$

$$\tau^* = \tau_b \big/ (\rho_s - \rho_w) g d \tag{3-2}$$

$$A_{st} = \frac{(A_p + A_f + A_c)}{TA_{s1}} * 100\% \tag{3-3}$$

where ρ_w is water density, ρ_s is bed particle bulk density, d is the representative grain size.

A_p, A_f, A_c are the areal coverage of partial, full and channel alteration regimes respectively. A_{st}

is the areal coverage of AST normalized by the maximum total wet area in H1 (14,985 m^2). $A_{st} =$

100% means that the whole channel is unstable while the minimum $A_{st} = 0\%$ means that the

whole channel is stable. This approach evaluates sediment transport capacity of water, so it is

independent of sediment supply. It is reporting the potential for what could happen to sediment in

the study area.

3.4.4.2 Shortest distance between AST and dam

The purpose of the second metric was to identify the shortest distance between active scour area and dam infrastructure. Because the concern with reservoir sedimentation is that sediment eroded in the backwater zone will transport downstream and deposit in front of the sediment wedge, eventually impacting dam infrastructure- or outright depositing there if velocities are high enough to enable that. This metric evaluates how scenarios H2 and H3 affect the shortest distance, holding erosion further upstream.

The sediment transport distance was defined as the shortest distance between OHD and the cross-section with an AST coverage ≥ 40%. To calculate the AST coverage within each cross-section, 102 cross-sections along the centerline of the corridor were created using River Bathymetry Toolkit (ESSA 2019). The maximum wet area in H1 and bank extended from that to where the vegetation started to intensively occur were delineated as the river corridor based on its definition (Thorne et al. 2005). The percentage of AST coverage within each cross-section was calculated by dividing AST coverage by the area of the cross-section.

3.4.4.3 How questions were answered

To answer Qt1 about the impacts of topographic controls on the foci of sediment erosion, the variance in AST (Eq. 3-4) was estimated by dividing the difference of AST between H1 and H2 by AST in H1 (i in Eq. 3-4 is H2 in this case, reference scenario is H1). The AST variance value < 30% was assumed to be small impacts while > 60% was large impacts. Scenarios H1 and H2 were compared for the difference in the shortest distance between AST and the dam to evaluate

how the re-contouring force sediment erosion occurs in the TPCs and its upstream. Besides the location, the size, centroid and shape of AST were also used to evaluate the impact of TPCs on the pattern of sediment erosion with visual check.

$$\text{AST variance} = \frac{(\text{AST}_i - \text{AST}_{\text{reference}})}{\text{AST}_{reference}} * 100\% \tag{3-4}$$

Same protocol was followed to answer the Qt2 about impacts of topographic controls with WSE drawdown on the sediment erosion pattern. H2 was set to be the reference scenario. Comparison of AST between H2 and H3-1 was used to estimate how small WSE adjustment performed while between H2 and H3-3 to evaluate how the large WSE adjustment affected sediment erosion.

To answer the Qt3 about finding the optimal hydrologic conditions for the designed topographic controls, the AST of each simulated flow in H2 and H3 was compared with that in H1. The higher the AST variance is, the more efficient the adjustment is assumed. The flow with the highest AST variance was chosen as the optimal flow range.

3.5   Results

3.5.1   Sediment erosion with original topography

In the 18 simulated flow events, the distribution of sediment transport regimes in the existing topography displayed a spotty pattern in response to the presence of landform constrictions and large bed elements that impose topographic steering (Figure 6 and supplementary document II). Beginning at base flow, AST occurred mainly in riffle-pool units and secondarily at bedrock outcrops. As inflow increased, the areal percent of AST expanded upstream and downstream. When inflow was in the medium flow regime, independent AST patches coalesced, forming bar-shaped erosion zones along the river bends. When inflow was in the high flow regime, the bar-

shaped erosion zones coalesced making the entire river fully activated for sediment transport.
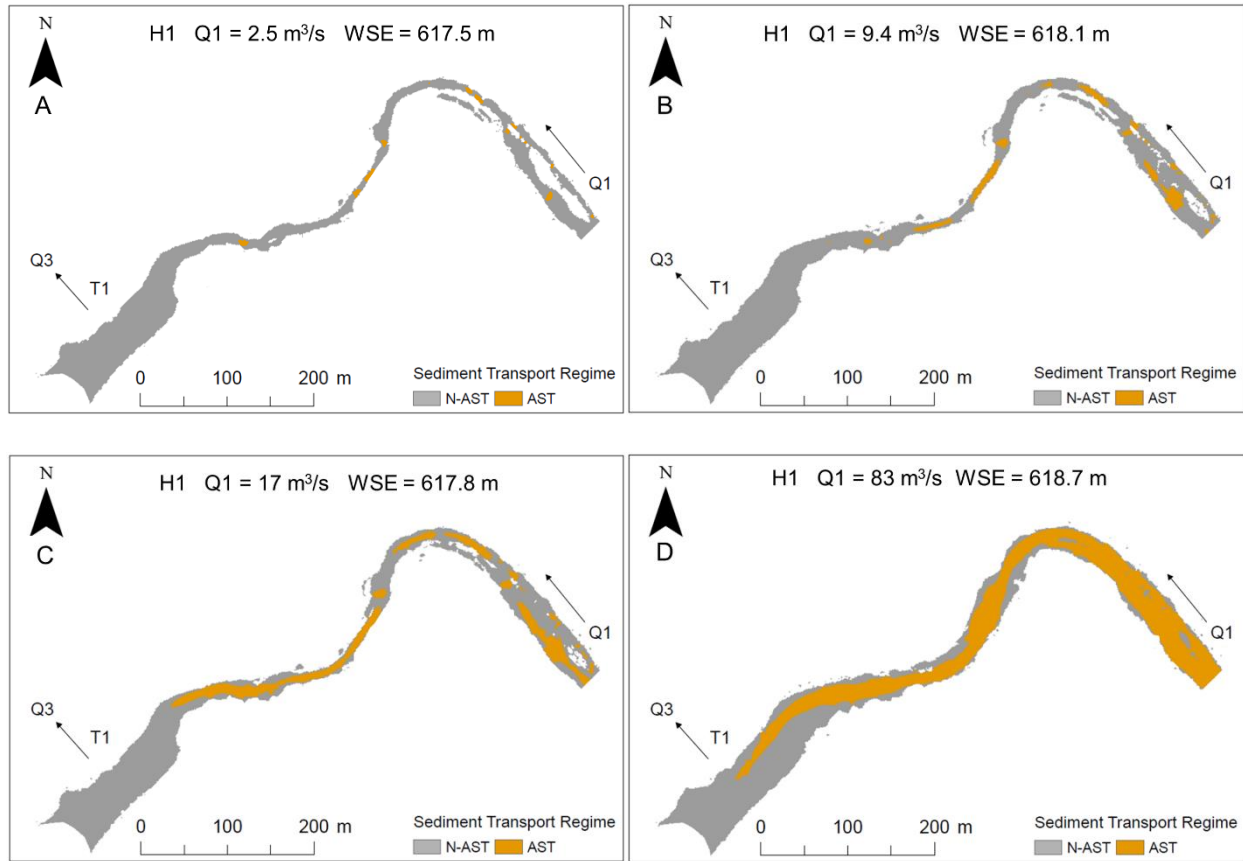
Figure 3.6. Spatial distribution of the sediment transport regimes in H1 of grain size 32 mm. Q1 is the Middle Yuba River inflow, Q2 is OHD outflow, Q3 is flow diverted through tunnel.

As for different grain sizes, the occurrence of sediment erosion patterns differed (Supplementary document II). For grain size $\leq$ 32 mm, the spotty pattern existed across all flow events, reflecting the greater sensitivity that lower bed shear stresses capable of moving smaller gravel sizes are widespread. The presence of large gravel bars throughout the backwater zone provides new terrain to submerge, yielding new AST areas with increasing discharge. For grain size > 32 mm, the river's capability of transporting coarse gravel was weak, except in the flood regime. Sensitivity analysis found that AST variation hit a break point at 32 mm (Figure.1 in supplementary document I). For

grains < 32 mm, less than 30% of the area was occupied by negligible transport regime, while those > 32 mm had negligible and intermittent transport regimes dominating the whole study reach (>50%); for those sizes, the channel alteration regime almost disappeared.

In addition, sediment with size ≤ 32 mm occurred more frequently in the reservoir while sediment > 32 mm stayed upstream (supplementary document II). For sediment < 32 mm, the shortest distance between AST and dam ranged from 0 to 200 m. In the base flow regimes, places with sediment erosion occurred in front of the reservoir (~50 m upstream). As flow increased to medium flow regime, sediment erosion occurred farther upstream (> 100 m) due to the increased backwater effect. As the flow increased to high flow regime, sediment erosion occurred in the reservoir. Meanwhile, for sediment > 32 mm, the shortest distance between AST and dam ranged from 170 to 500 m. Sediment erosion did not occur in or near the reservoir. Therefore, 32 mm was chosen as threshold and the following analyses discuss sediment erosion for grains < 32 mm.

3.5.2 Sediment erosion with topographic controls

Spatially, topographic constrictions significantly increased sediment erosion in the narrowed channel while reducing sediment erosion upstream and downstream of TPC2 (Figure 3.7A). In the base and medium flow regimes, TPC2 cross sections were fully eroded, indicated by the full coverage of AST (>90%). Meanwhile, AST coverage upstream of TPC2 dropped from 75% to zero due to the increased backwater effect caused by TPC2. Downstream of TPC2, AST coverage reduced from 60% to zero compared with that in the same area in H1. The oversized cross-section between TPC1 and TPC2 acted as a buffer zone to stop sediment from entering TPC1. As inflow increased, the areal coverage of AST in TPC2 increased and expanded to its upstream until connected to the other AST patch while area downstream of the oversized cross-section was not

eroded until MYR reached the high flow regime (Figure 3.7B Q1 = 83 m^3/s).

As for the shortest distance between the dam and AST, adding TPCs ponded sediment upstream during base and medium flow regimes while reduced distance in high flow regime (Table 2 in supplementary document I). In the base flow regime, AST occurred in front of the reservoir in both H1 and H2. Adding TPCs had limited impact on the distancing of sediment erosion to the dam. In the medium flow regime, adding TPCs reduced sediment erosion near the dam. The distance between AST and dam was increased averagely by 66 m. As flow keeps increasing, sediment erosion near the reservoir was largely increased. The distance in H2 was averagely reduced by 97 m. This indicates that the mechanism is flow-dependent, which is meaningful for carefully designing topographic steering to obtain whatever outcome is desired for each flow.
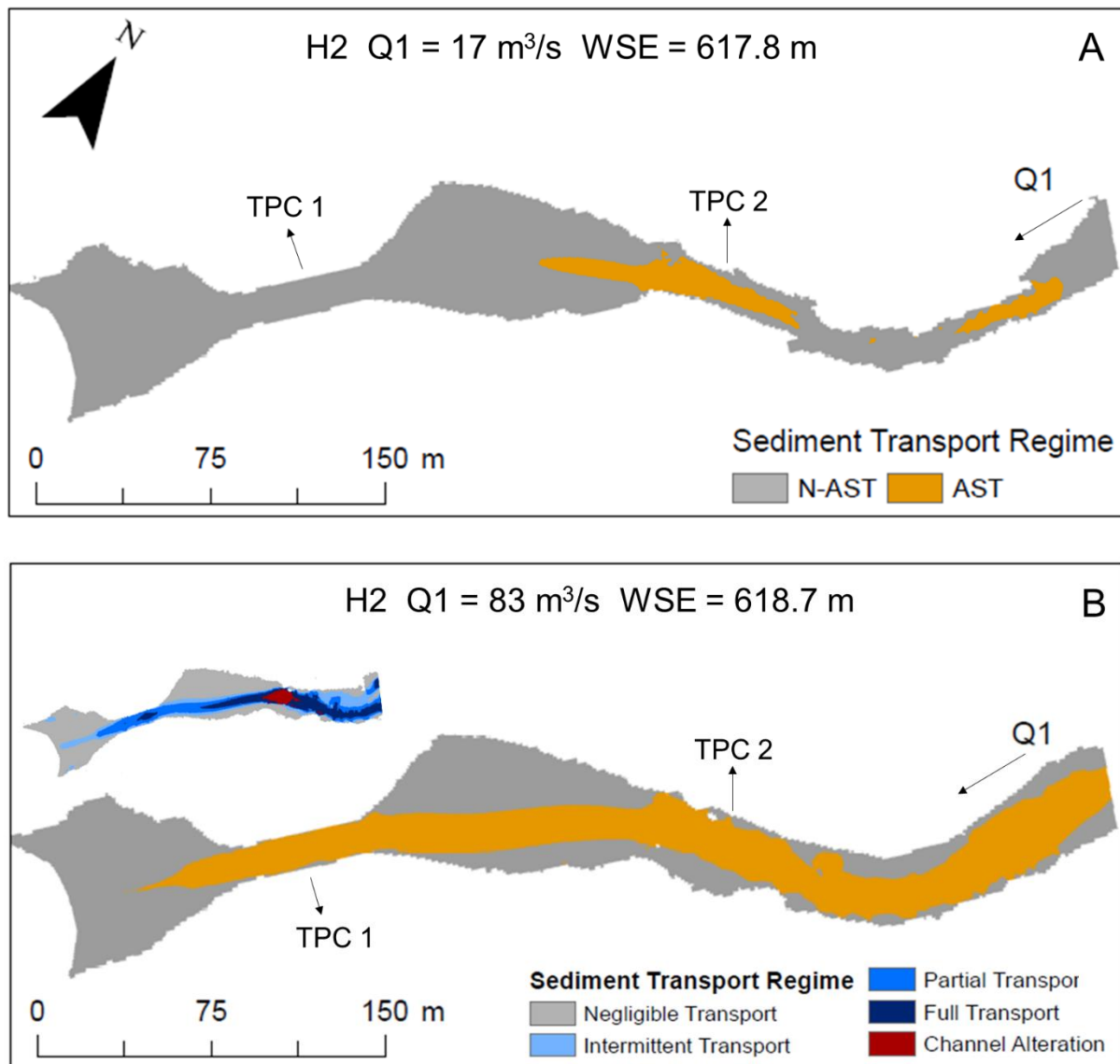
Figure 3.7. Spatial distribution of the sediment transport regimes of medium and high flow regimes in H2.

3.5.3 Sediment erosion with topographic control and WSE adjustment

Compared with H2, reducing reservoir WSE (H3-1) enhanced sediment erosion in TPC1 while the area near TPC2 was not affected. During base flow, no AST coverage was observed in TPC1 in H3-1. During medium flow, AST was observed near TPC1. As upstream flow increases within the

regime, areal coverage of AST in TPC1 was enhanced, expanding from the TPC1 center to its upstream and downstream. When the upstream inflow Q1 increased to high flow regime, the TPC1 was fully activated (Figure 3.8). The impact of stage drawdown on sediment erosion in TPC1 was positively related to the reduction of water level. Similarly, in H3-3, AST occurred at the end of TPC1 close to reservoir in the base flow regime. Then the erosion zone expanded upstream as the MYR inflow increased. TPC1 was fully activated during medium flow in H3-3.

In H3-2, increasing WSE slightly reduced sediment erosion in TPCs compared with that in H2. Therefore, comparison of AST to infer the increase of WSE was conducted between H3-1 and H3-2 due to the similar alteration in WSE. Increasing WSE by 0.6 m had limited impacts on AST coverage in the base flow regime due to the low AST coverage. During medium flow, AST in TPC2 shrank to its center while disappeared in TPC1. As upstream inflow increased to the high flow regime, increasing WSE did not change the AST coverage significantly, but the proportion of AST changed significantly (Figure 3.8). The original channel alteration zone in TPC1 in H3-1 downgraded to the full transport regime in H3-1. Meanwhile, in TPC2, the coverage of the channel alteration regime also reduced but with smaller change.

Minor WSE adjustment ($< 1m$) had limited impact ($< 5\%$) on the distance between AST and dam for all flow regimes. However, reducing WSE by ¼ of the adjustable range (2.9m) had a significant impact on the distance between AST and dam. On average, reducing WSE by 2.9m reduced the distance by 66%. During both base and medium flow regimes, distance variance caused by WSE adjustment was similar. Meanwhile, the distancing variance was lowest (23%) during the high flow regime for all scenarios.

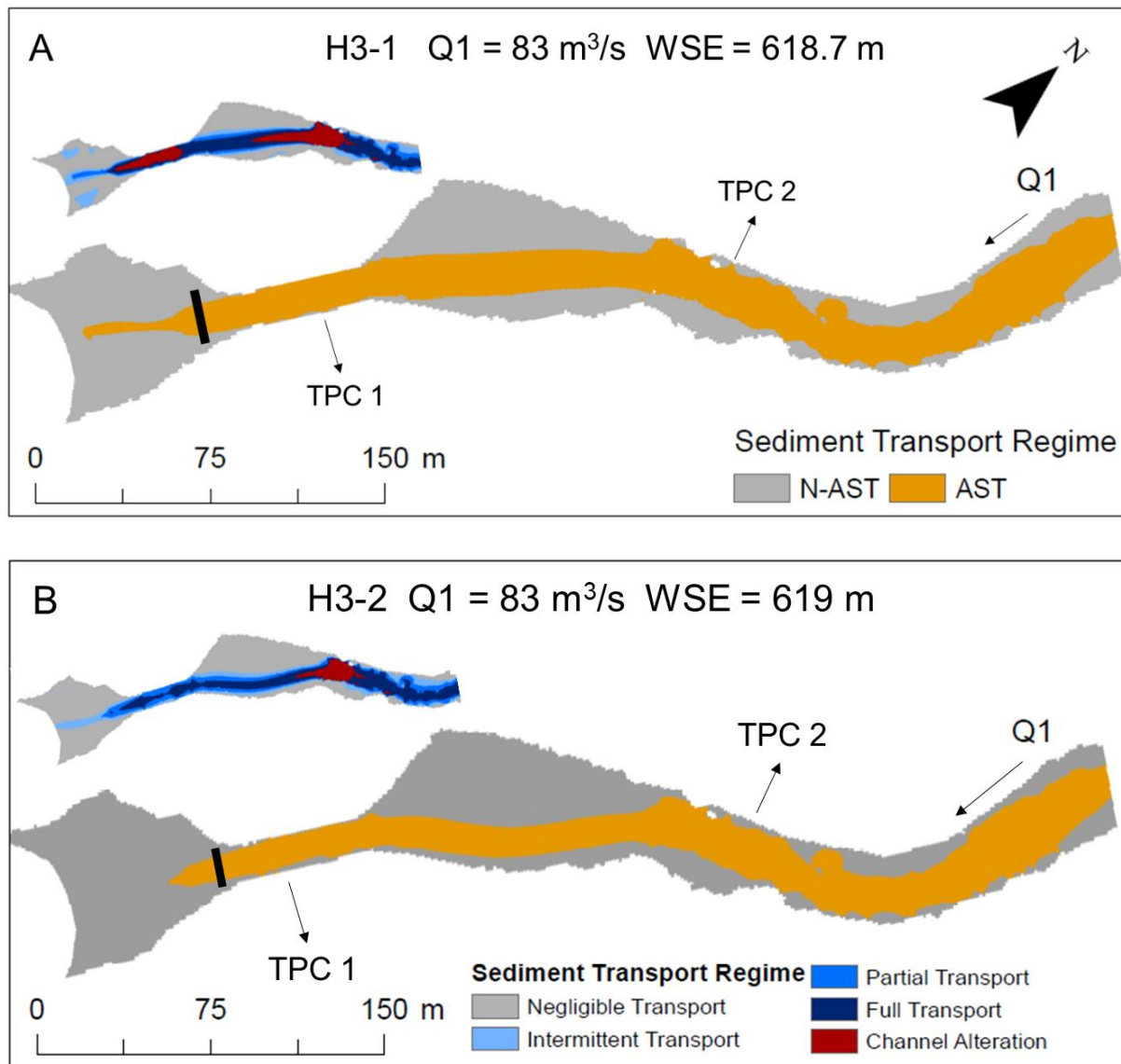Figure 3.8. Spatial distribution of sediment transport regimes of medium flow regime in H3-1 and H3-2. Q1 is Middle Yuba River inflow. The black rectangle indicates the starting point of the distance between the dam and AST cross section.

3.6   Discussion

3.6.1   Question 1: Impacts of topographic constrictions

Adding topographic constrictions to the channel enhanced the area of sediment erosion during high

in-channel flows while reducing it during lower flows (Figure 3.9). In the base flow regime, difference in AST among scenarios were negligible. The difference in AST between scenario H1, H2, H3-1 and H3-2 was small. The difference in AST between TPCs scenario and reference scenario was ≤ 5%. The potential reason for the small change is that the upstream inflow was too small to transport sediment. Thus, neither adjusting topography or hydrology altered sediment erosion significantly for low flows. In the medium flow regime, AST coverage with topographic constrictions, except for scenario H3-3, was lower than that of H1. The AST coverage in H2 was around 40% lower than that in H1. As discharge increased, AST coverage in topographic-control scenarios overpassed that in the reference scenario (AST in H2 was 29% higher than H1). The oversized cross-section acted as a buffer zone to reduce sediment erosion upstream of it in the low and medium flow. When in the high flow regime, TPC2 was submerged, and the ponding effect was defeated by the high inflow. Therefore, the narrowed channel width of TPC1 accelerated the flow velocity and thus increased sediment erosion greatly.
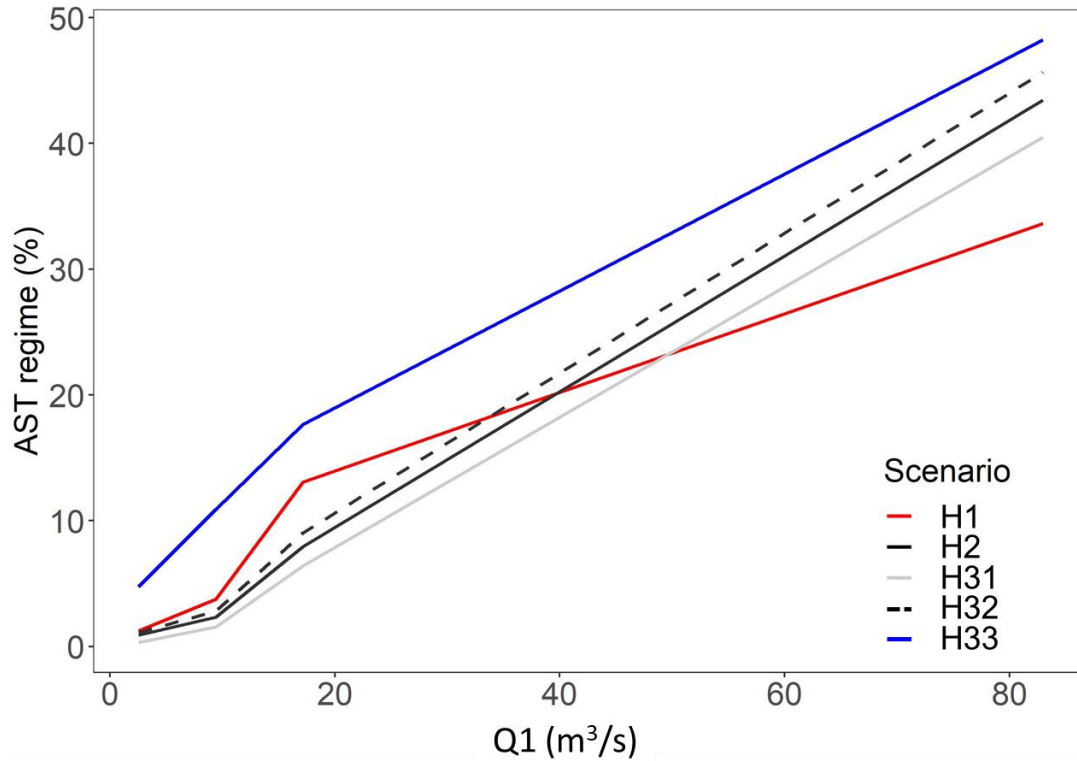
Figure 3.9. Areal percentage of AST of four scenarios along with upstream inflow-MYR.

Spatially, adding TPCs ponded sediment upstream in the base and medium flow regimes while reduced distance in high flow regime (Table 3.4). Due to the low flow and relatively high backwater effect, the current version of TPCs was able to pond sediment upstream of TPC2 to reduce sediment erosion near the dam. In this way, hydraulic or mechanic excavation can be set in this location to constantly remove new incoming sediment. However, instead of reducing sediment erosion near the dam, TPCs in high flow acted as accelerators of sediment transport. The distance between sediment erosion area and dam was largely reduced. If holding sediment erosion away from the dam is the key, the depth of the oversized cross section between TPCs should be increased to increase its ponding effect. If increase sediment erosion to have sediment transport over/through the dam is the goal, the current version of TPCs would be a good example for other rivers.

Table 3.4. Distance variance among scenarios. H2 ~ H1 is the comparison between H2 and H1. HX ~ H2 is the comparison between HX and H2. HX is H31, H32 and H33.

Q1 (m³/s)	H2 ~ H1	H31 ~ H2	H32 ~ H2	H33 ~ H2
2.5	-0.02	-0.02	0.05	-0.81
9.4	0.12	-0.02	0.03	-0.81
17.2	-0.30	-0.02	0.04	-0.82
83.0	0.71	0.00	0.08	-0.23

3.6.2   Question 2: Impacts of topographic constriction with WSE adjustment

Area affected by minor WSE adjustment ≤ 1m was in the vicinity of TPC2 (Table 3.4). Reducing reservoir WSE would increase sediment erosion near TPC2 and route more sediment through TPC2 into the oversized cross-section. Increasing WSE tends to pond sediment upstream of TPC1, reducing sediment erosion in both TPC1 and the oversized cross section. Compared with H2, reducing WSE by 0.3 m increased the coverage of unstable river bed by 17% during medium flow regime. And this 17% mainly occurred in TPC2.

However, reducing WSE significantly would fully activate TPC2 but also trigger sediment erosion in TPC1. The ponding effect of the oversized area had zero AST coverage during base and medium flow which implies little sediment would be routed to TPC2. But sediment already deposited in TPC1 would be eroded and transported to the front of reservoir even during the base flow.

In addition, the performance of WSE adjustment is flow dependent. The highest variance of AST caused by WSE adjustment always occurred during the base flow. As the flow increase, the AST variance decreased. The reason why this result happened was because during high flow, sediment was highly eroded even the WSE was high. Therefore, adjusting WSE in high flow regime led to a relatively small variance in AST.

3.6.3 Question 3: Optimal hydrologic conditions for topographic constriction

The medium flow with a minor WSE adjustment is recommended as the optimal range of hydrologic condition for TPCs for regular sedimentation management. Even though AST coverage in TPCs scenarios was lower than that in the reference scenario, sediment erosion occurred in the designated area TPC2 for hydraulic/mechanical excavation. The reduction in AST occurred in the oversized area which was originally covered by AST. This reduction of AST was expected by the hypothesis. Difference in AST between TPCs scenarios and the reference scenario was small (<5%) during the base flow because the base flow was too small to entrain sediment, not to mention having TPCs function. While during high flow, the AST coverage in TPCs scenarios overpassed that in the reference scenario, TPCs can lead more sediment erosion near the dam due to the narrowed channel width of TPC1. Besides the excessive sediment erosion near the dam, the high flow outweighed the impact of minor WSE adjustment on the distance of AST to the dam. To control the distance of sediment erosion to the dam, large WSE adjustment is needed.

3.7 Conclusions

This study experimentally tested the performance and topographic controls in assisting the sedimentation management of sand and gravel fraction bedload at the upstream end of the reservoir. Sediment transport regimes were divided into stable and unstable river bed by the

reference value of non-dimensional shear stress 0.03. The areal coverage and location of unstable river bed were analyzed to evaluate the redistribution of deposited sediment triggered by topographic constriction. The extent of backwater effect was detected by the Pettit test to infer the mechanistic chain triggered by water transfer. The results found that topographic constriction and expansion performed well at redistributing the sediment erosion. In the medium flow regime, the unstable river bed coverage was reduced averagely by 18% with topographic control. Adjusting water stage can effectively altering sediment erosion near the reservoir. Reducing WSE can enhance sediment erosion and can have more sediment erosion in the oversized cross section downstream, while increase WSE can enhance the backwater effect so that more sediment tends to stay upstream of TPC2. In the high flow regime, unstable river bed coverage was significantly increased (18%) due to topographic steering process in two constricted cross sections. However, topographic controls investigated here on a theoretical basis appear to be useful as a supplementary strategy for hydraulic and mechanic excavation. The reason is that topographic steering does not remove sediment when the flow is low or the valve is closed, eventually necessitating excavation and/or more topographic contouring. Although this study used OHD as the starting point for exploration of topographic control, the results are still at the conceptual status at this time.

3.8   References

Anim, D.O., Fletcher, T.D., Pasternack, G.B., Vietz, G.J., Duncan, H.P. and Burns, M.J., 2019. Can catchment-scale urban stormwater management measures benefit the stream hydraulic environment?. Journal of environmental management, 233, pp.1-11.

Blanckaert, K., 2011. Hydrodynamic processes in sharp meander bends and their morphological implications. Journal of Geophysical Research: Earth Surface, 116(F1).

Brandt, S.A., 2000. Classification of geomorphological effects downstream of dams. Catena, 40(4), pp.375-401.

Brown, R.A. and Pasternack, G.B., 2014. Hydrologic and topographic variability modulate channel change in mountain rivers. Journal of hydrology, 510, pp.551-564.

Brown, R. A., et al. 2016. "The Topographic Design of River Channels for Form-Process Linkages." Environ Manage 57 (4):929-42. doi: 10.1007/s00267-015-0648-0.

Chow, V.T., 1959. Open-channel hydraulics. McGraw-Hill civil engineering series.

Coleman, J.M. 1976. Deltas-Processes of Deposition and Models for Exploration: Continuing Education Publication Company, Champaign, IL.

Dettinger M. 2011. Climate change, atmospheric rivers, and floods in California – a multimodel analysis of storm frequency and magnitude changes. Journal of American Water Resources Association 47(3): 514–523. Doi: 10.1111/j.1752-1688.2011.00546.x.

EPA. 2020. "United States Environmental Protection Agency. Napa River Restoration: Basis of Design: Oakville to Oak Knoll Reach, working version 4." Prepared for County of Napa. https://www.epa.gov/sfbay-delta/napa-river-restoration-project-oakville-oak-knoll-reach-group-c-site-14 (Accessed 12 2020).

ESSA.   2019.   River   Bathymetry   Toolkit   (RBT). https://portal.opentopography.org/tools/viewTool?toolId=81. (Assessed 01 2019).

Fryirs, K., u2013. (Dis) Connectivity in catchment sediment cascades: a fresh look at the sediment delivery problem. Earth Surface Processes and Landforms, 38(1), pp.30-46.

Gore, J., Pasternack, G.B. and Wiener, J., 2016, December. Analysis and classification of topographic flow steering and inferred geomorphic processes as a function of discharge in a mountain river. In AGU Fall Meeting Abstracts (Vol. 2016, pp. EP53D-1016).

Hotchkiss, R. H. 1990. Reservoir sedimentation and sediment sluicing: experimental and numerical analysis.

Hotchkiss, R.H. and Parker, G., 1991. Shock fitting of aggradational profiles due to backwater. Journal of Hydraulic Engineering, 117(9), pp.1129-1144.

Hooke, J., 2003. Coarse sediment connectivity in river channel systems: a conceptual framework and methodology. Geomorphology, 56(1-2), pp.79-94.

Jackson, James R, et al. 2015. "Virtual manipulation of topography to test potential pool–riffle maintenance mechanisms." Geomorphology 228:617-627.

Julien, P.Y., 2010. Erosion and sedimentation. Cambridge university press.

Kjaran, S.P., Hólm, S.L. and Myer, E.M., 2004. Lake circulation and sediment transport in Lake Myvatn. Aquatic Ecology, 38(2), pp.145-162.

Lewis, D.J., Singer, M.J., Dahlgren, R.A. and Tate, K.W., 2006. Nitrate and sediment fluxes from a California rangeland watershed. Journal of environmental quality, 35(6), pp.2202-2211.

Litschert, S.E. and MacDonald, L.H., 2009. Frequency and characteristics of sediment delivery pathways from forest harvest units to streams. Forest Ecology and Management, 259(2), pp.143-150.

Liro, Maciej. 2015. "Gravel-bed channel changes upstream of a reservoir: The case of the Dunajec River upstream of the Czorsztyn Reservoir, southern Poland." *Geomorphology* 228:694-702. doi: 10.1016/j.geomorph.2014.10.030.

Liro, Maciej. 2016a . "Development of sediment slug upstream from the Czorsztyn Reservoir (southern Poland) and its interaction with river morphology." *Geomorphology* 253:225-238. doi: 10.1016/j.geomorph.2015.09.018.

Liro, M., 2019. Dam reservoir backwater as a field-scale laboratory of human-induced changes in river biogeomorphology: A review focused on gravel-bed rivers. Science of the Total Environment, 651, pp.2899-2912.

Liro, M., Ruiz-Villanueva, V., Mikuś, P., Wyżga, B. and Castellet, E.B., 2020. Changes in the hydrodynamics of a mountain river induced by dam reservoir backwater. Science of The Total Environment, 744, p.140555.

Lisle, T.E., Nelson, J.M., Pitlick, J., Madej, M.A. and Barkett, B.L., 2000. Variability of bed mobility in natural, gravel‐bed channels and adjustments to sediment load at local and reach scales. Water Resources Research, 36(12), pp.3743-3755.

MacWilliams Jr, M.L., Wheaton, J.M., Pasternack, G.B., Street, R.L. and Kitanidis, P.K., 2006. Flow convergence routing hypothesis for pool-riffle maintenance in alluvial rivers. Water Resources Research, 42(10).

Morris, G.L. and Fan, J., 1998. Reservoir sedimentation handbook: design and management of dams, reservoirs, and watersheds for sustainable use. McGraw Hill Professional.

Maselli, V., Pellegrini, C., Del Bianco, F., Mercorella, A., Nones, M., Crose, L., Guerrero, M. and Nittrouer, J.A., 2018. River morphodynamic evolution under dam-induced backwater: an example from the Po River (Italy). Journal of Sedimentary Research, 88(10), pp.1190-1204.

Nelson, A. and Dubé, K., 2016. Channel response to an extreme flood and sediment pulse in a mixed bedrock and gravel-bed river. Earth Surface Processes and Landforms, 41(2), pp.178-195.

Olsen, W.H., Wagenbrenner, J.W. and Robichaud, P.R., 2021. Factors affecting connectivity and sediment yields following wildfire and post‐fire salvage logging in California's Sierra Nevada. Hydrological Processes, 35(1), p.e13984.

Pasternack, G. B., Baig, D., Weber, M. D., & Brown, R. A. (2018). Hierarchically nested river landform sequences. Part 1: Theory. Earth Surface Processes and Landforms, 43(12), 2510-2518.

Pasternack, G. B., Baig, D., Webber, M., Brown, R. 2018. Hierarchically nested river landform sequences. Part 2: Bankfull channel morphodynamics governed by valley nesting structure. Earth Surface Processes and Landforms. DOI: 10.1002/esp.4410.

Pasternack, G. B., Gore, J., & Wiener, J. (2021). Geomorphic covariance structure of a confined mountain river reveals landform organization stage threshold. Earth Surface Processes and Landforms.

Ralph FM, Neiman PJ, Wick GA, Gutman SI, Dettinger MD, Cayan DR, White AB. 2006. Flooding on California's Russian River: role of atmospheric rivers. Geophysical Research Letters 33: L13801. doi: 10.1029/2006GL026689.

Sawyer, A.M., Pasternack, G.B., Moir, H.J. and Fulton, A.A., 2010. Riffle-pool maintenance and flow convergence routing observed on a large gravel-bed river. Geomorphology, 114(3), pp.143-160.

Schumm, S.A., 1985. Patterns of alluvial rivers. Annual Review of Earth and Planetary Sciences, 13(1), pp.5-27.

Shotbolt, L. A., Thomas, A. D., and Hutchinson, S. M. 2005. The use of reservoir sediments as environmental archives of catchment inputs and atmospheric pollution. Progress in Physical Geography: Earth and Environment, 29, 337-361.

Strom, M.A., Pasternack, G.B. and Wyrick, J.R., 2016. Reenvisioning velocity reversal as a diversity of hydraulic patch behaviours. Hydrological Processes, 30(13), pp.2348-2365.

SW. 2020. Sonoma Water. Dry creek habitat enhancement project 2018. https://www.sonomawater.org/drycreek (Accessed 09 2020).

Thorne, C., Hey, R. and Newson, M., 2005. Applied fluvial geomorphology for river engineering and management. John Wiley and Sons Ltd.

Thornton, K. W., Kimmel, B. L., & Payne, F. E. (1990). Reservoir limnology: ecological perspectives. John Wiley & Sons.

Toone, J, et al. 2014. "Spatial discontinuity and temporal evolution of channel morphology along a mixed bedrock-alluvial river, upper Drôme River, southeast France: Contingent responses to external and internal controls." Geomorphology 205:5-16.

Wheaton, J. M., Brasington, J., Darby, S., Merz, J. E., Pasternack, G. B., Sear, D. A., Vericat, D. 2010. Linking geomorphic changes to salmonid habitat at a scale relevant to fish. River Research and Applications 26:469-486, DOI: 10.1002/rra.1305.

Wilcock, P.R., Kondolf, G.M., Matthews, W.G. and Barta, A.F., 1996. Specification of sediment maintenance flows for a large gravel‑bed river. Water Resources Research, 32(9), pp.2911-2921.